Title
A meteorological overview of the Pacific Exploratory Mission (PEM) Tropics period

Journal
Journal of Geophysical Research, 104(D5)

ISSN
0148-0227

Authors
Fuelberg, Henry E
Newell, Reginald E
Longmore, Scott P
et al.

Publication Date
1999-03-20

DOI
10.1029/98jd01215

JOURNAL OF GEOPHYSICAL RESEARCH, VOL. 104, NO. D5, PAGES 5585–5622, MARCH 20, 1999

A meteorological overview of the Pacific Exploratory Mission (PEM) Tropics period

Henry E. Fuelberg,[1] Reginald E. Newell,[2] Scott P. Longmore,[1] Yong Zhu,[2] David J. Westberg,[3] Edward V. Browell,[4] Donald R. Blake,[5] Gerald L. Gregory,[4] and Glen W. Sachse[4]

Abstract. NASA's Pacific Exploratory Mission-Tropics (PEM-T) experiment investigated the atmospheric chemistry of a large portion of the tropical and subtropical Pacific Basin during August to October 1996. This paper summarizes meteorological conditions over the PEM-T domain. Mean flow patterns during PEM-T are described. Important circulation systems near the surface include subtropical anticyclones, the South Pacific Convergence Zone (SPCZ), the Intertropical Convergence Zone (ITCZ), and middle latitude transient cyclones. The SPCZ and ITCZ are areas of widespread ascent and deep convection; however, there is relatively little lightning in these oceanic regions. A large area of subsidence is associated with the subtropical anticyclone centered near Easter Island. PEM-T occurred during a period of near normal sea surface temperatures. When compared to an 11 year climatology (1986–1996), relatively minor circulation anomalies are observed during PEM-T. Some of these circulation anomalies are consistent with much stronger anomalies observed during previous La Nina events. In general, however, the 1996 PEM-T period appears to be climatologically representative. Meteorological conditions for specific flights from each major operations area are summarized. The vertical distribution of ozone along selected DC-8 flights is described using the DIAL remote sensing system. These ozone distributions are related to thermodynamic soundings obtained during aircraft maneuvers and to backward trajectories that arrived at locations along the flight tracks. Most locations in the deep tropics are found to have relatively small values of tropospheric ozone. Backward trajectories calculated from global gridded analyses show that much of this air originates from the east and has not passed over land within 10 days. The deep convection associated with the ITCZ and SPCZ also influences the atmospheric chemistry of these regions. Flights over portions of the subtropics and middle latitudes document layers of greatly enhanced tropospheric ozone, sometimes exceeding 80 ppbv. In situ carbon monoxide in these layers often exceeds 90 ppbv. These regions are located near, and especially south of Tahiti, Easter Island, and Fiji. The layers of enhanced ozone usually correspond to layers of dry air, associated with widespread subsiding air. The backward trajectories show that air parcels arriving in these regions originate from the west, passing over Australia and even extending back to southern Africa. These are regions of biomass burning. The in situ chemical measurements support the trajectory-derived origins of these ozone plumes. Thus the enhanced tropospheric ozone over the central Pacific Basin may be due to biomass burning many thousands of kilometers away. Middle-latitude portions of the PEM-T area are influenced by transient cyclones, and the DC-8 traversed tropopause folds during several flights. The flight area just west of Ecuador experiences outflow from South America. Thus the biomass burning that is prevalent over portions of Brazil influences this area.

1. Introduction

The Pacific Exploratory Mission-Tropics (PEM-T) was conducted between August to October 1996 as part of NASA's Global Tropospheric Experiment (GTE) [*McNeal et al.*, 1984]. The goal of PEM-T was to investigate the impact of human activity on the tropospheric chemistry of the Pacific Basin, especially its tropical portions [*Hoell et al.*, this issue]. This remote region of the world has traditionally been considered to be relatively free from the impacts of human activity. However, the air quality of the tropical Pacific is increasingly experiencing the effects of long-range transport from expanding population centers around the fringes of the basin, for example, South America, Southeast Asia, and Australia.

One of the objectives of PEM-T was to provide baseline data for gases that are important in controlling the oxidizing power of the atmosphere, including ozone (O_3) and its precursors [*Hoell et al.*, this issue]. A second objective was to understand the factors controlling the concentrations of these gases, and to assess the resulting sensitivity of the oxidizing power of the atmosphere to anthropogenic and natural perturbations. Three secondary

[1]Department of Meteorology, Florida State University, Tallahassee, FL
[2]Department of Earth, Atmospheric, and Planetary Sciences, Massachusetts Institute of Technology, Cambridge, MA
[3]Science Applications International Corp., Hampton, VA
[4]NASA Langley Research Center, Hampton, VA
[5]Department of Chemistry, University of California, Irvine, CA

Paper number 98JD01215.
0148-0227/99/98JD-01215$09.00

objectives were to survey the concentrations of aerosols and their precursors, investigate sulfur gas-to-particle formation, and to provide detailed latitude-altitude transects of long-lived gases for use in evaluating global tropospheric models.

PEM-T employed two NASA aircraft, the DC-8 based at Ames Research Center, California, and the P-3B based at the Wallops Flight Facility, Virginia. These two aircraft sampled an area stretching from Hawaii to the tip of Antarctica and from the west coast of South America to near New Guinea (Figure 1). *Hoell et al.* [this issue] provide a complete description of the various chemical species measured by the two aircraft. They include ozone, carbon monoxide, hydrocarbons, halocarbons, sulfur, nitrates, acids, peroxides, and aerosols.

This paper presents a general overview of meteorological conditions over the South Pacific Basin during PEM-T (August 14 to October 6, 1996). Section 2 describes our data and methodologies. Section 3 describes large-scale flow patterns, while section 4 examines their departures from climatology. The remaining sections highlight weather conditions encountered on selected flights from each base of operations and relate these conditions to observed chemical features. The general overview presented here will be elaborated in subsequent papers examining the atmospheric chemistry and meteorology of the PEM-T area.

2. Data and Methodologies

We utilized global gridded meteorological analyses prepared by the European Centre for Medium-Range Weather Forecasts (ECMWF) [*Bengtsson*, 1985; *Hollingsworth et al.*, 1986]. These analyses were obtained from the National Center for Atmospheric Research (NCAR). The ECMWF analyses are dynamically consistent, having been prepared using data assimilation techniques. The data were available twice daily (0000 and 1200 UTC) on a 2.5° × 2.5° latitude-longitude grid for the period 1986–1996. We used the lowest 13 isobaric surfaces in our computations (1000, 925, 850, 700, 500, 400, 300, 250, 200, 150, 100, 70, and 50 hPa).

Ten-day backward trajectories were calculated using a kinematic model, that is, employing the u, v, and w wind components from the ECMWF analyses. A cubic spline procedure was used to vertically interpolate the gridded data from the 13 initial levels to

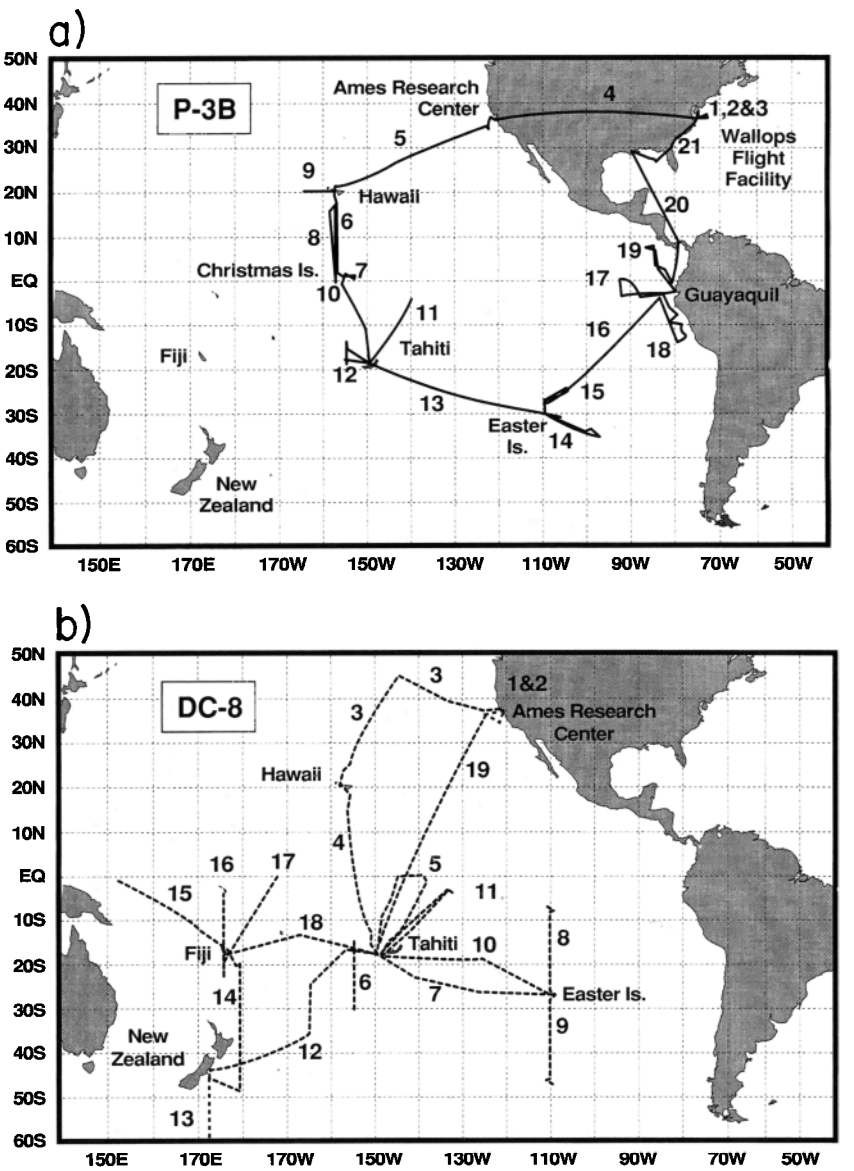

Figure 1. (a) Flight tracks for the P-3B during PEM-T.(b) Flight tracks for the DC-8 during PEM-T.

190 levels at 5-hPa intervals between 1000 and 50 hPa. Linear interpolation provided values within these 5-hPa intervals and at the parcel's precise horizontal locations. Linear interpolation also was used to temporally interpolate at 5-min time steps. Parcels that intersected the 1000 hPa surface were terminated at that location. Similarly, all trajectory locations were checked against a topographic field obtained from the United States Geological Survey. Parcels that intersected the topographic surface (e.g., the Andes) were terminated at that point. Additional details about the trajectory model, along with a comparison between kinematic and isentropic trajectories, are given by *Fuelberg et al.* [1996a].

Trajectories are subject to several limitations, some of which are described by *Stohl et al.* [1995]. First, the Pacific Basin is a relatively data sparse area. Thus the ECMWF analyses may position circulation features less accurately over the PEM-T domain than in more data rich areas. Second, the 2.5° and 12 hourly resolution of our ECMWF data means that small scale features will not be faithfully depicted. For example, winds associated with individual convective storms will not be resolved, although the aggregate effects of storm areas will be included. Finally, the trajectory model itself contains numerical limitations. These various limitations produce trajectories whose accuracy deteriorates with increasing time. Nonetheless, trajectories of 7 days duration or longer are relatively common in the literature, for example, *Rood et al.* [1997] (7 days), *Thompson et al.* [1996] (8 days), *Garstang et al.* [1996] (10 days), *Swap et al.* [1996] (10 days).

We calculated over 24,000 ten-day backward trajectories along the various PEM-T flight tracks as part of our research. In spite of the limitations described above, most of these trajectories showed reasonable conservation of their potential temperatures, without arbitrarily imposing the isentropic assumption. Specifically, at 5 days back, 83% (98%) of the trajectories experienced less than a 5° (10°) C change in their potential temperatures over 24 hour periods. At 10 days back, 73% (96%) of the trajectories had less than a 5° (10°) C change in potential temperatures over 24 hour periods.

In situ O_3 measurements were made using a chemiluminescent detector (nitric oxide plus O_3) (G.L. Gregory, personal communication, 1998). This instrument has been used in many GTE flights onboard the DC-8. For the PEM-T measurements, the system was configured for a 2 Hz response time, with a lower detection limit of <1 ppbv. Absolute accuracy is approximately 3% (or 2 ppbv), with a precision of 1% (or 0.8 ppbv).

Carbon monoxide (CO) measurements were made with a differential absorption diode laser sensor described by *Sachse et al.* [1987, 1991]. CO sensitivity is the greater of 1 ppbv or 1%, and time resolution is less than 5 s. Some in situ chemical measurements were obtained from whole air samples collected in evacuated 2 L stainless steel canisters that were pressurized to 40 psi. Samples were collected every 4 min, but increased to one per minute during some vertical profiles. The canisters then were returned to the laboratory at the University of California-Irvine where their contents were assayed for selected nonmethane hydrocarbons, halocarbons, and alkyl nitrates. A detailed description of the analytical apparatus and procedure is given by *Blake et al.* [1996].

Vertical profiles of O_3 were obtained along the flight track of the DC-8 using the differential absorption lidar (DIAL) instrument [*Browell*, 1989, 1991]. The DIAL system has been used in many previous field experiments to study distributions of aerosols and O_3 in the troposphere and to relate them to chemical and dynamical processes [e.g., *Browell et al.*, 1994, 1996; *Fuelberg et al.*, 1996b]. Simultaneous zenith and nadir lidar measurements of O_3 were made from a range of about 750 m above the aircraft to above the tropopause in the zenith case, and from about 750 m below the aircraft to about 300 m above the surface in the nadir case. The nadir and zenith data, together with the in situ O_3 measurements, were combined to produce the images that are shown here. This procedure is described by *Browell et al.* [1996]. The O_3 measurement accuracy is within 10%, unless the measured amount is less than 20 ppbv, when the accuracy is 2 ppbv. The precision is better than 5% or 1 ppbv [e.g., *Browell et al.*, 1996]. The vertical resolution is 300 m in the nadir and 450 m in the zenith, with a horizontal resolution in both cases of about 70 km. Optically thick clouds can blind the DIAL because they scatter much of the energy of the lidar beam. O_3 measurements can be made through thin cirrus; however, altocumulus, cumulus, and cirrus all are problematic.

3. Large-Scale Conditions

Streamlines representing time averaged large-scale flow patterns during the PEM-T period are shown in Figure 2. These fields were obtained by averaging the twice daily ECMWF wind analyses between August 14 and October 6, 1996. Atmospheric transport is not accomplished by the mean flow, but by the actual winds that vary both in time and space. Nonetheless, meteorological systems in the tropics do exhibit less variability than those in the middle latitudes. Furthermore, these "time-averaged" flow fields provide valuable information about large-scale conditions occurring during PEM-T.

Several prominent circulation features are present in the mission-averaged streamlines at 1000 hPa (Figure 2a). Subtropical anticyclones are located over both the North and South Pacific Oceans, one between Hawaii and the mainland United States, and the second near Easter Island in the South Pacific (28°S, 110°W). The northeasterly and southeasterly trades winds associated with these anticyclones converge near 10°N to form the Intertropical Convergence Zone (ITCZ). This convergence is strongest just west of Central America and becomes weaker farther west. Figure 3a shows locations of the ITCZ on the 21 days on which flights were conducted during PEM-T. These locations are based on the 1000 hPa divergent wind derived from the ECMWF data. The ITCZ exhibits relatively little day-to-day latitudinal variation at locations east of the date line. However, the strength of the convergence did vary on a daily basis, with a double convergence zone apparent on some days. Several PEM-T flights traversed the ITCZ (Figure 1).

General low pressure and confluent flow are present near Southeast Asia at 1000 hPa during the PEM-T period (Figure 2a). These features are associated with the summer monsoon. A monsoon trough and associated area of confluent flow also extend southeastward from near the coast of China. The ITCZ blends into this trough at approximately 15°N. A zone of confluent flow then stretches southeastward from the monsoon trough into the southern hemisphere to near Tahiti (18°S, 150°W). This feature, called the South Pacific Convergence Zone (SPCZ), has been reviewed in a recent paper by *Vincent* [1994]. The SPCZ is best defined during the austral summer months of January and February, not during the springtime PEM-T period.

Locations of the SPCZ on individual PEM-T flight days are shown in Figure 3b. Several of the PEM-T flights from Tahiti and Fiji (Figure 1) were influenced by the nearby SPCZ. As noted previously, the westernmost segments of the SPCZ and ITCZ usually merge together into a single convergence zone. That

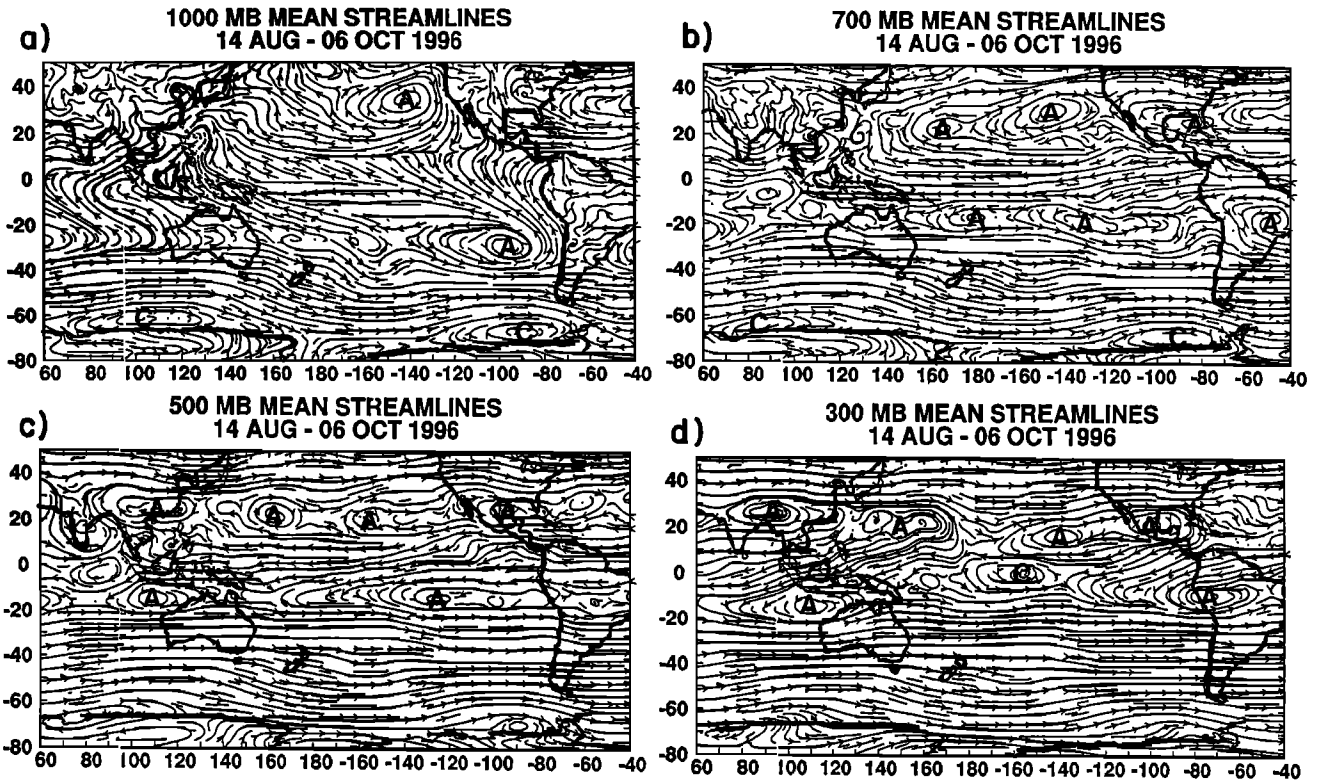

Figure 2. Mean streamlines during PEM-T (August 14 to October 6, 1996) for (a) 1000, (b) 700, (c) 500, and (d) 300 hPa. Major cyclonic and anticyclonic circulation centers are indicated as "C" and "A," respectively.

single zone is shown in both Figures 3a and 3b. The SPCZ shows little day-to-day variation near 0°–5°S; however, there is more variability at locations farther southeast. These spatial fluctuations occur because this segment of the SPCZ is influenced by nearby cyclone activity. Specifically, transient middle-latitude cyclones move from west to east over the South Pacific Basin [e.g., *Merrill*, 1989; *Sinclair*, 1994]. Their individual cyclonic circulations are not evident in Figure 2a because of the temporal averaging. The cold fronts associated with these systems advance in a generally northeasterly direction, eventually becoming stationary near latitudes 15°–20°S. The temperature contrast across the fronts diminishes during their northward transit, such that only a convergent zone remains. These frontal remnants appear to be responsible for maintaining the southeastern portion of the SPCZ [*Vincent*, 1994] and producing its variations in location between 10° and 20°S. We have arbitrarily terminated the SPCZ near 150°W (Figure 3b) because convergence farther southeast usually is associated with frontal-related temperature gradients.

Mean flow patterns at 700 hPa (~3 km mean sea level (msl), Figure 2b) during the PEM-T period are dominated by broad subtropical anticyclones. These anticyclones are centered near 20°N and 20°S, with the northern hemispheric (summer) anticyclones being best defined. Ridge axes that extend east-west from the anticyclone centers span virtually the entire North and South Pacific Basins. These anticyclones and ridge lines produce major wind shifts across the PEM-T domain. Specifically, there is westerly flow north of ~20°N and south of ~20°S, that is, the prevailing westerlies. However, easterly winds dominate the tropical latitudes that lie in between. Several PEM-T flights crossed these wind shift lines (Figure 1), documenting impressive changes in atmospheric chemical concentrations and associated meteorological variables. Section 9 describes one of these cases (DC-8 flight 16). Convergence associated with the ITCZ and SPCZ is not evident at 700 hPa since that convergence is confined to the low levels (e.g., Figure 2a).

Flow patterns at 500 hPa during PEM-T (~5.5 km, Figure 2c) are similar to those at 700 hPa. Although the anticyclonic circulation centers are not as well defined as in the lower levels, the east-west oriented ridge lines in the northern and southern hemispheres (near 20°) remain prominent. These ridge lines separate westerly middle latitude flow from the tropical easterlies.

Mean conditions at 300 hPa (~9 km, Figure 2d) show several well defined subtropical anticyclone centers in each hemisphere. The major new feature is the weak cyclonic circulation near 0°, 160°W. As a result, the tropical upper troposphere does not exhibit simple easterly flow, but there are areas of northerly and southerly winds as well.

Mean isotach analyses for 300 and 200 hPa during the PEM-T period are shown in Figure 4. The southern hemispheric subtropical jet stream is located at ~30°S. Several PEM-T flights traversed this region of strong winds (Figure 1). Since the subtropical jet does not exhibit large day-to-day changes in location or intensity, it is clearly depicted in the average field. Maximum mean speeds exceed 40 m s^{-1} (50 m s^{-1}) at 300 (200) hPa over southwestern Australia. Speeds along the jet axis diminish toward the east. Speeds also decrease both north and south of jet axis, with much of the tropical Pacific having speeds less than 10 m s^{-1}. The polar jet stream is poorly defined in the composite PEM-T

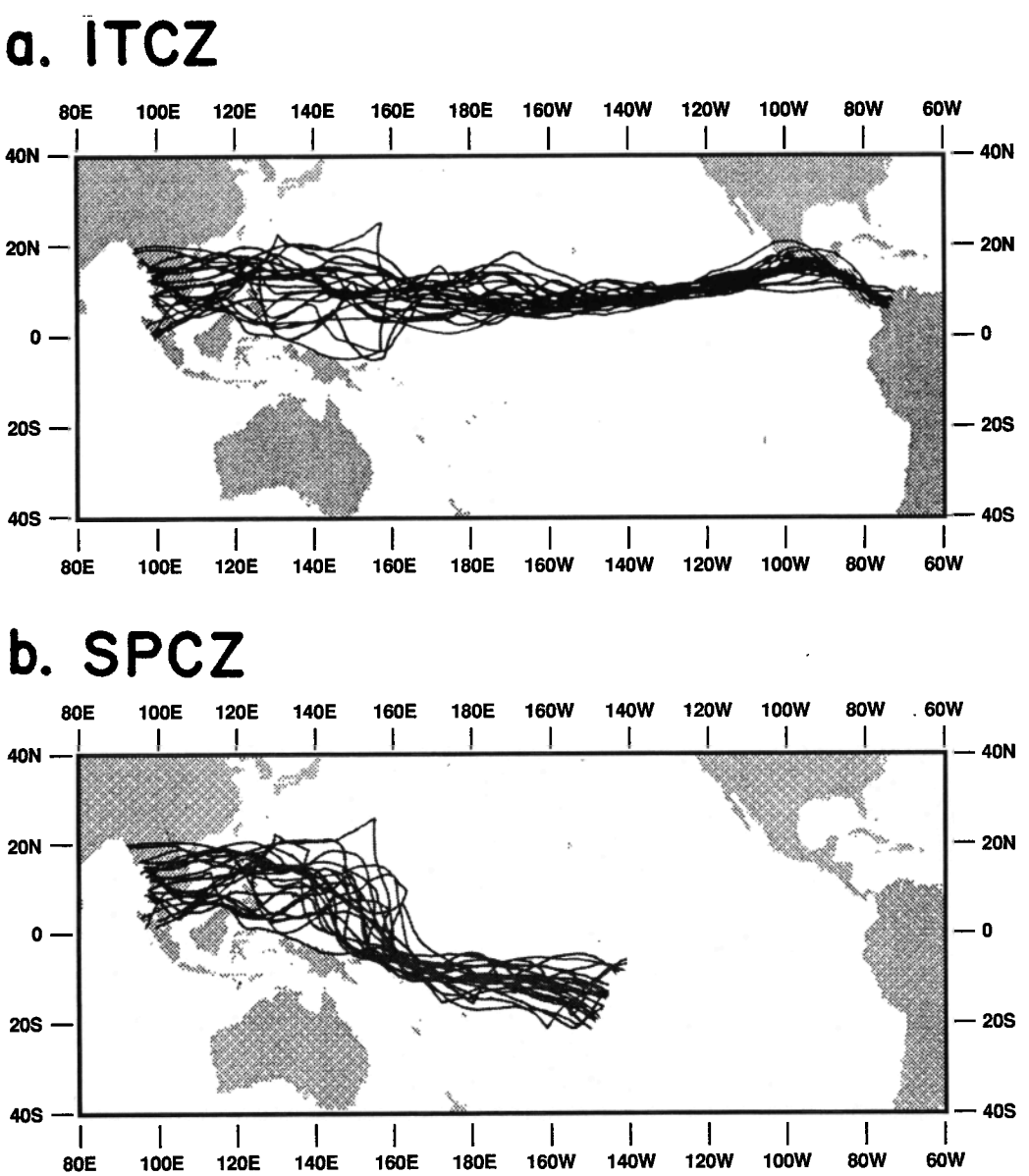

Figure 3. (a) Positions of the ITCZ on flight days during PEM-T. (b) Positions of the SPCZ on flight days during PEM-T.

analysis (Figure 4). This is common over the South Pacific Basin [e.g., *Chen et al.*, 1996] since the polar jet does undergo major day-to-day variability in both location and wind speed. Thus temporal averaging tends to filter it more than the subtropical jet.

It is informative to consider the distances covered by air parcels traveling at typical wind speeds during PEM-T. For example, a parcel at 20°S, traveling due east at a constant speed of 20 (30) m s^{-1}, will travel ~83° (~124°) longitude during a 5-day period. These numbers indicate that long-range transport can occur over relatively short time intervals.

Three north-south cross sections of the mean zonal wind during PEM-T are given in Figure 5. They indicate that the mean altitude of the subtropical jet stream is near 200 hPa (~11.7 km) and that maximum mean zonal speeds decrease toward the east, consistent with Figure 4. Easterly (negative) zonal components are prominent in the tropics. Specifically, the region of negative mean values extends to near 30°S at the lowest altitudes, but has the smallest southward penetration between 200 and 100 hPa. In fact, the cross section at 180° shows no easterly flow between 200 and 100 hPa. The strong easterly flow over the tropics at the highest levels corresponds to the tropical easterly jet stream.

The mean circulation during PEM-T also can be examined by dividing the wind into its divergent and rotational components, as done for PEM-West A and B [*Newell et al.*, 1996a] where the appropriate equations are discussed. The time-averaged velocity potential and divergent wind components for the PEM-T period are shown in Figure 6 for 1000 and 200 hPa. For the purposes of this discussion, surface topography has been ignored, but its effects were included in the original ECMWF analyses. At 1000 hPa (Figure 6b), there is strong convergence at ~15°N near the Philippines, and over the eastern Pacific Ocean and Central America. There is strong divergence over the southeast Pacific and off California. At 200 hPa (Figure 6a), there is compensating convergence over the southeast Pacific, with divergence over the

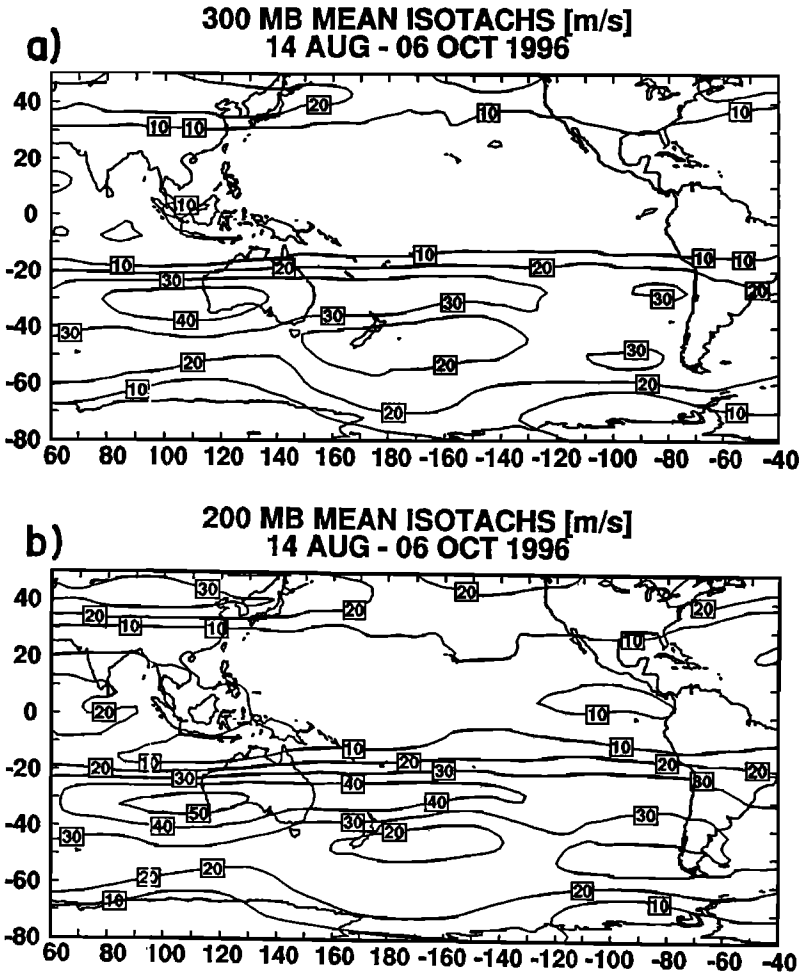

Figure 4. Mean isotachs (m s^{-1}) at (a) 300 and (b) 200 hPa during PEM-T (August 14 to October 6, 1996).

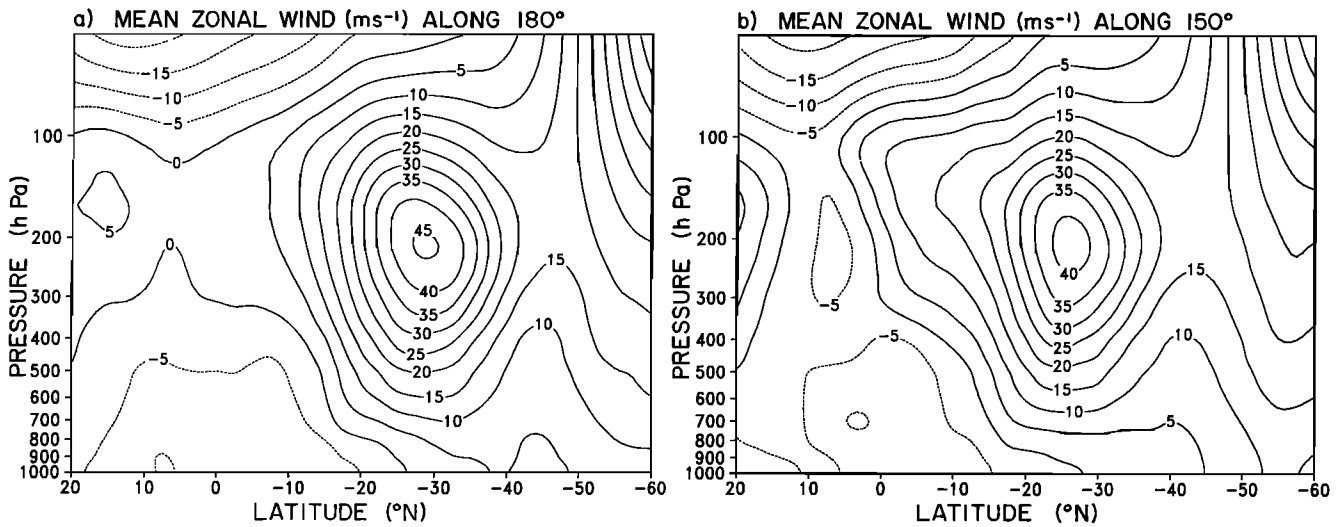

Figure 5. Cross sections of mean zonal wind (m s^{-1}) during PEM-T (August 14 to October 6) along (a) 180°W, (b) 150°W, and (c) 110°W.

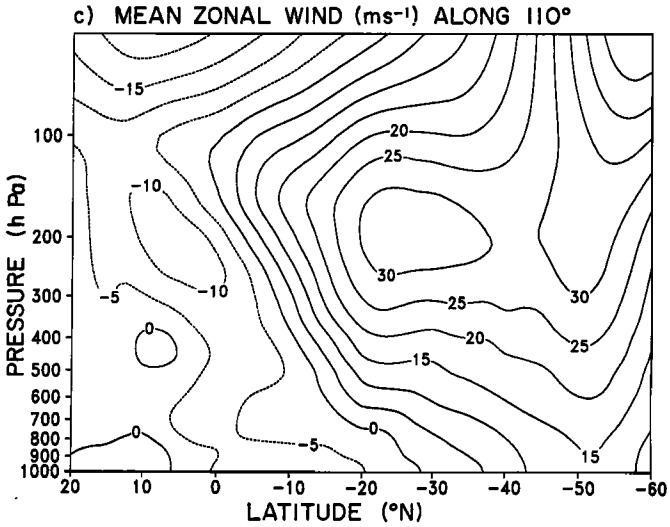

Figure 5. (continued)

western Pacific. The ITCZ is clearly indicated at 1000 hPa from Central America westward across the central Pacific, where it crosses the date line at ~11°N, before forming the Philippines convergent maximum. The SPCZ extends from north of New Guinea, east southeastward to ~140°W. It is much less defined than the ITCZ. The rising motion that connects the various areas of low-level convergence and upper level divergence appears in the day-to-day cloud patterns, which are shown in satellite imagery within later sections of this paper.

Mean stream function and rotational wind analyses for PEM-T at 1000 and 200 hPa are shown in Figure 7. When magnitudes of the divergent (Figure 6) and rotational wind vectors are compared, it is clear that the rotational component generally is greatest. Over the Pacific, both hemispheres are dominated by large anticyclonic systems at 1000 hPa (Figure 7b). The rotational wind at 200 hPa also shows large anticyclonic features (Figure 7a), with some evidence of interhemispheric flow over the southern Indian Ocean. This suggests a possible transport of biomass burning material between Borneo, Indonesia, and the southern hemisphere middle-latitude jet stream. Likewise, similar material from the northern South American continent moves westward out over the Pacific. These points will be confirmed in sections 5–11 using backward trajectories.

Atmospheric vertical motion is important because it influences the transport of chemical species, affects the humidity and stability of the atmosphere, and influences the formation of clouds and precipitation. Vertical motions provided with the ECMWF data sets were averaged over the PEM-T period, with the mean analy-

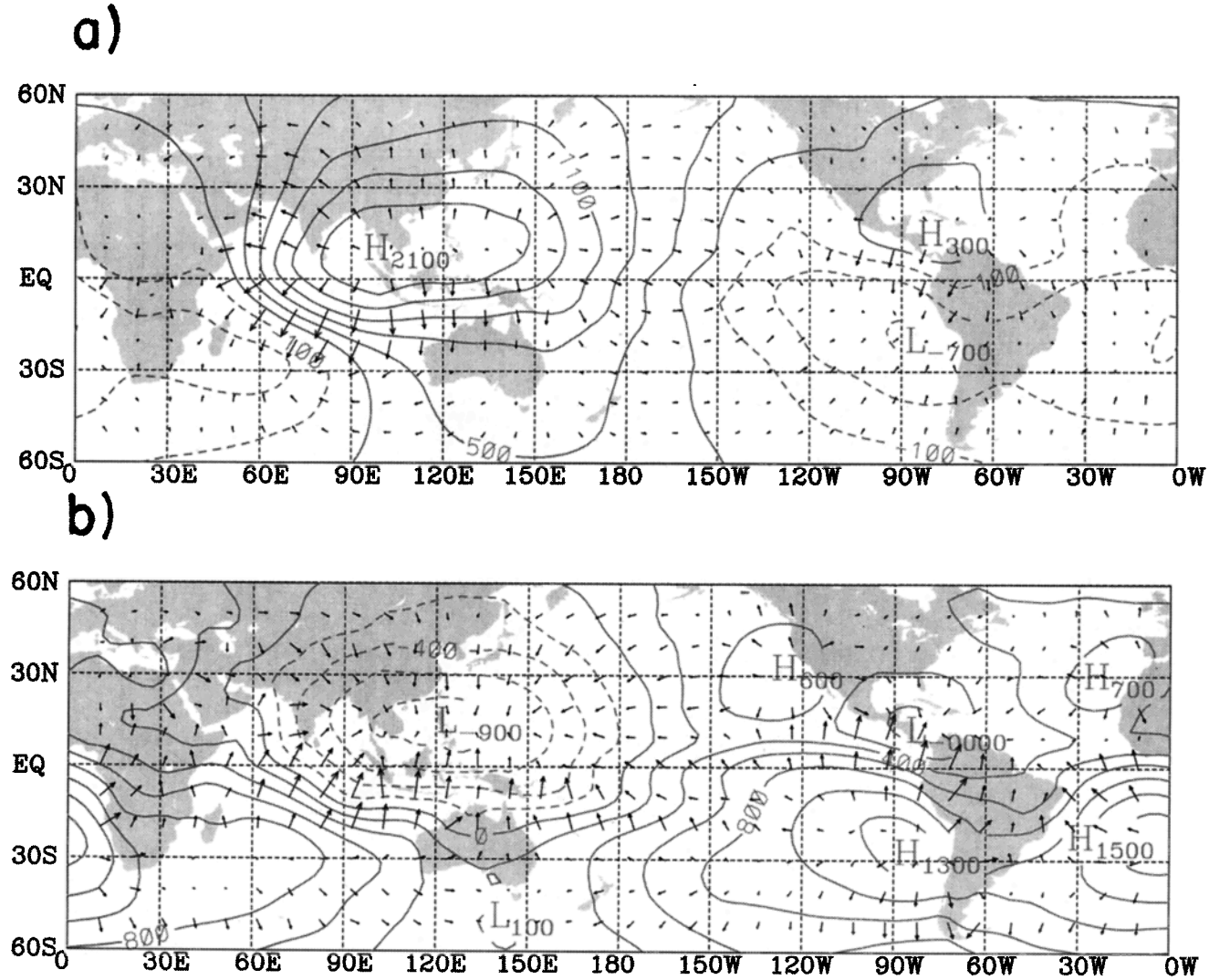

Figure 6. Mean velocity potential (isolines, 10^4 m^2 s^{-1}) and divergent wind component (vectors, m s^{-1}) at (a) 200 and (b) 1000 hPa during PEM-T (August 14 to October 6). The maximum vector is (a) 8.6 m s^{-1}, and (b) 5.5 m s^{-1}.

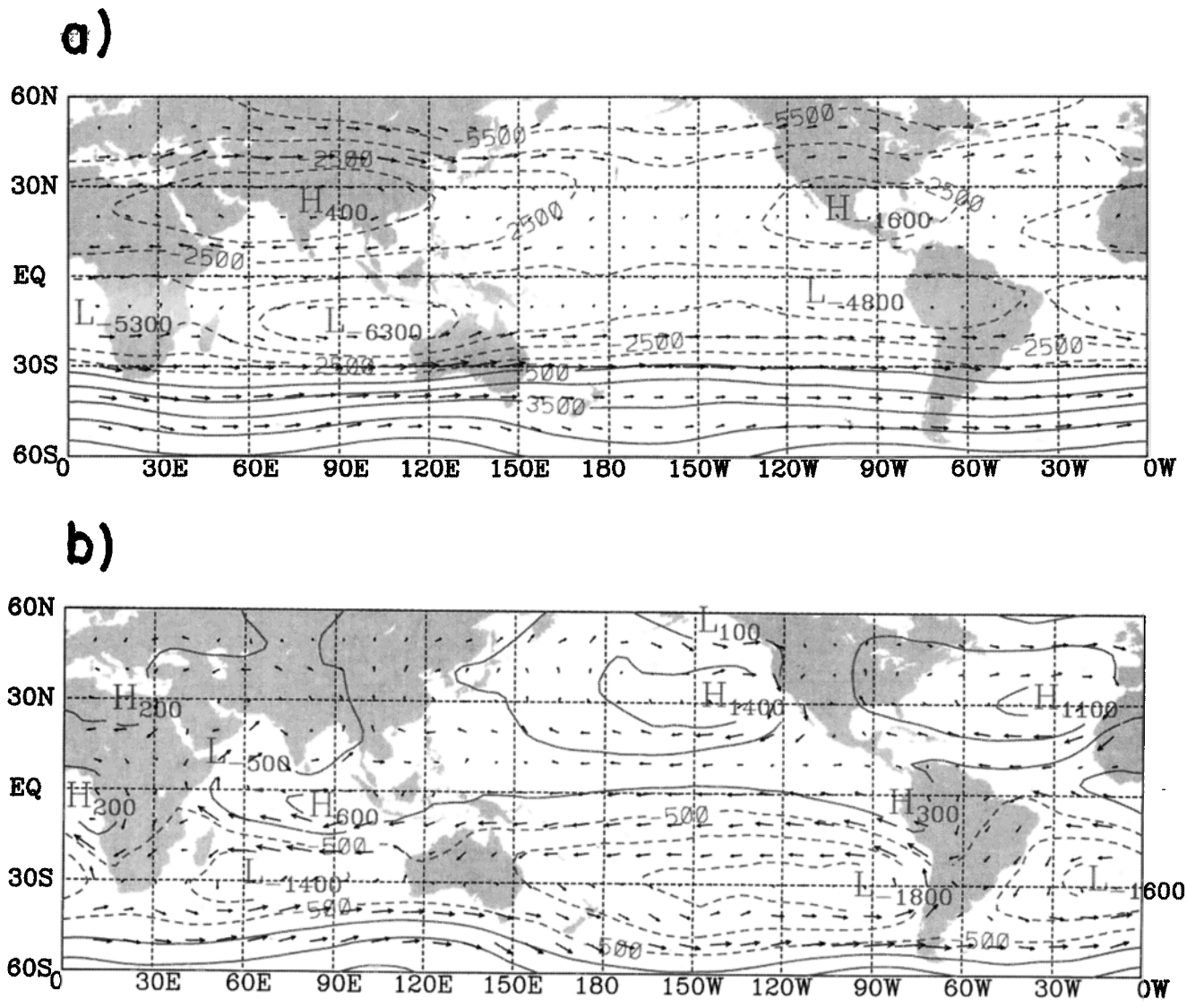

Figure 7. Mean streamfunction (isolines, 10^4 m^2 s^{-1}) and rotational wind component (vectors, m s^{-1}) at (a) 200 and (b) 1000 hPa during PEM-T (August 14 to October 6). The maximum vector is (a) 48.1 m s^{-1}, and (b) 11.1 m s^{-1}.

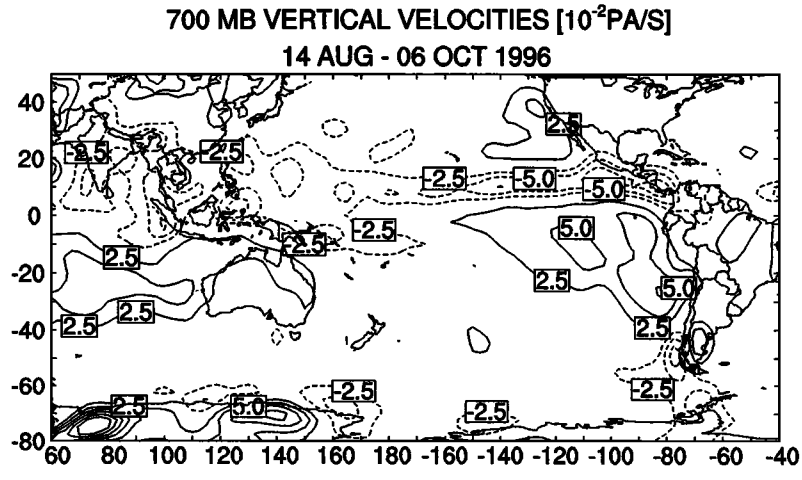

Figure 8. Mean vertical motion (10^{-2} Pa s^{-1}) at 700 hPa during PEM-T (August 14 to October 6). Negative values (dashed) indicate ascent. The zero isoline has been omitted for clarity.

sis for 700 hPa (~3.0 km) shown in Figure 8. The zero isopleth has been omitted for clarity. The area of strongest mean ascent (negative values) occurs along the eastern half of the ITCZ, near 10°N. Weaker ascent extends westward along the ITCZ to Southeast Asia and India. The southward extension of the ascent region near the date line is attributed to the SPCZ. Each of these areas of rising motion is associated with widespread multiple layered cloudiness (see later satellite imagery), including deep convection.

There are two major regions of persistent sinking motion (positive values) over the PEM-T domain (Figure 8). The strongest, located just west of South America, is attributed to the semipermanent anticyclone over the region (Figure 2). PEM-T flights out of Easter Island and Guayaquil were affected by this subsidence (see sections 7 and 10). The area north of Easter Island tended to be relatively cloud free, with well developed low-level temperature inversions. On the other hand, there was abundant low level cloudiness just west of South America because of the cold, northward moving ocean currents in the area. However, there was very little middle and upper level cloudiness. The second area of persistent subsidence is located over Australia and parts of the Indian Ocean. Air parcels traveling eastward through this region toward the PEM-T flight area experience the effects of this subsidence (see section 6).

There are few centers of vertical motion over middle-latitude portions of Figure 8. This occurs because the region is dominated by transient eastward moving cyclonic and anticyclonic systems. The associated ascent and descent tend to cancel during the temporal averaging. Thus the middle latitudes experience periods of widespread clouds and precipitation, followed by clearing skies.

It is useful to supplement the mean vertical motion patterns at 700 hPa (Figure 8) by considering the mass balance in atmospheric columns with horizontal dimensions of 30° × 30°. The procedure here is similar to that carried out in studies of Hurricane Mireille [*Newell et al.*, 1996b]. Specifically, the mass balance is evaluated from the divergent wind component, using 100 hPa intervals up to 300 hPa, and 50 hPa intervals between 300 and 100 hPa. The mass balance was adjusted internally to be zero at 100 hPa. Figure 9 shows the resulting profiles of vertical motion at four locations: the convergence region near Panama (15°N, 85°W), the SPCZ (5°S, 160°E), the Easter Island anticyclone (25°S, 85°W), and the sinking motion near Australia (15°S, 130°E). The greatest values in Figure 9 are associated with subsidence near the Easter Island anticyclone (Figure 9b). They numerically exceed values of ascent near Panama and the SPCZ where there is widespread convection (Figure 9a). Although much stronger ascent is associated with individual convective elements within these regions, that convection occupies only a small portion of the larger areas used in these calculations. The ascent or descent that occurs within these four regions is consistent from the surface to 100 hPa (~16.5 km).

Lightning is associated with deep convection and is a source of nitrogen oxides in the atmosphere [e.g., *Lawrence et al.*, 1995]. Plate 1 shows lightning discharges during September 1996 based on data from the Optical Transient Detector (OTD) that was launched into polar orbit during April 1995. The OTD detects cloud to ground, cloud to cloud, and intracloud lightning events during both daytime and nighttime [*Christian et al.*, 1989, 1992; NASA Optical Transient Detector World Wide Web site available at http://wwwghcc.msfc.nasa.gov/otd.html]. However, the satellite does not provide continuous coverage; thus some lightning is not detected. The plate shows relatively little lightning over the Pacific Ocean during September 1996, and this is confirmed by measurements taken onboard the DC-8. *Orville et al.* [1997] discuss possible reasons why lightning activity over the tropical oceans is so scarce. There are large concentrations of lightning over the fringes of the Pacific Basin, for example, Central and South America, Southeast Asia, eastern Australia, and Indonesia. There also is abundant lightning over tropical Africa. OTD results for September 1995 (not shown) indicate approximately 50%

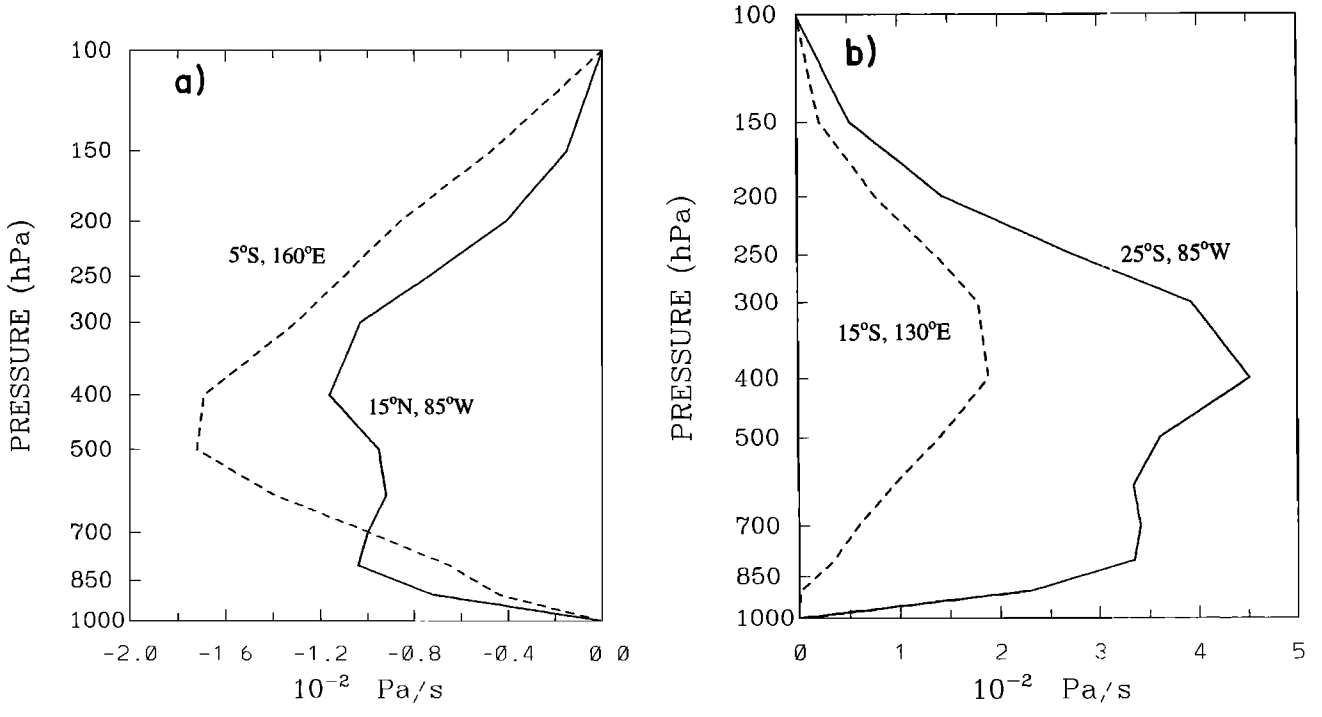

Figure 9. Profiles of vertical motion (10^{-2} Pa s^{-1}) at (a) 15°N, 85°W (solid) and 5°S, 160°E (dashed) and at (b) 25°S, 85°W (solid) and 15°S, 130°E (dashed). See text for computational details.

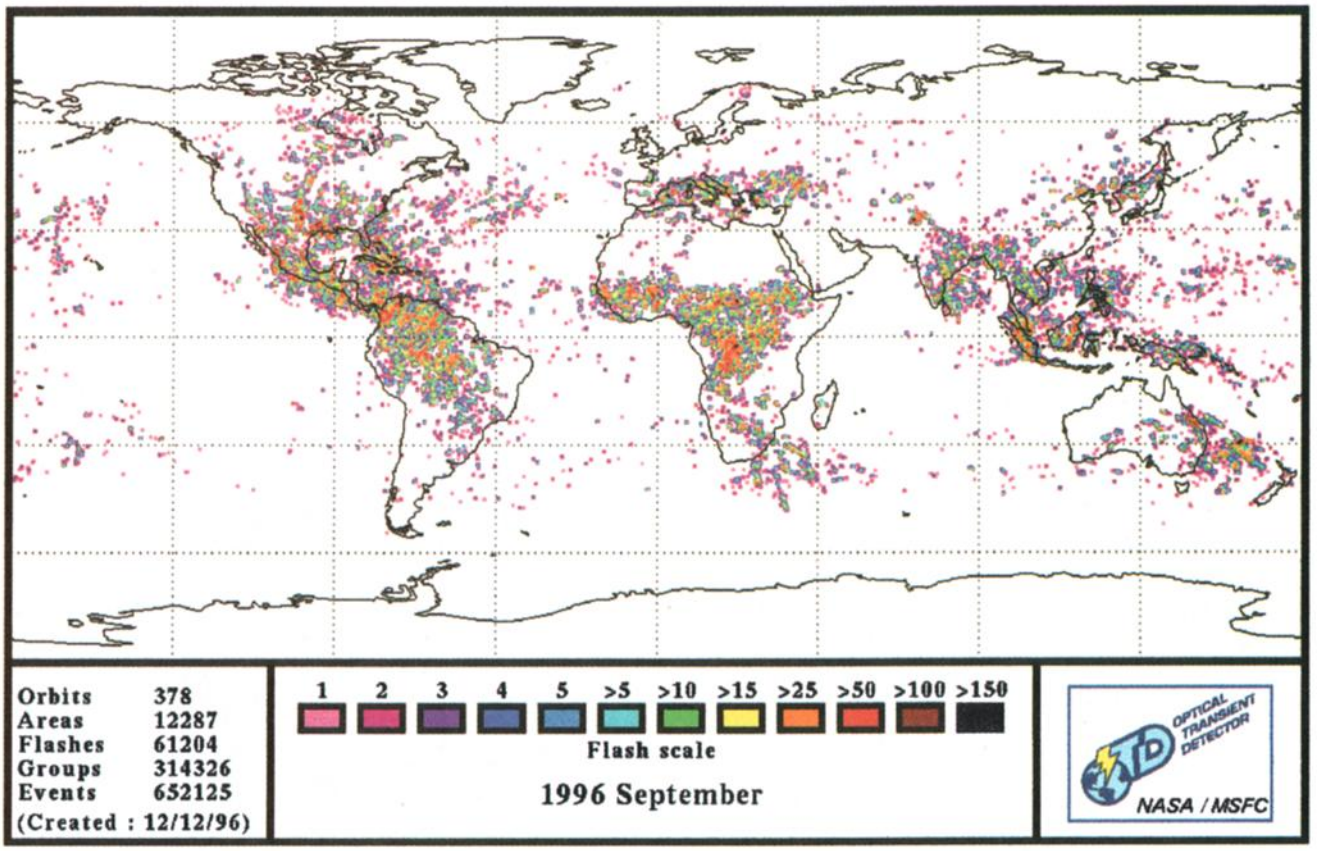

Plate 1. Lightning data for September 1996 detected by the Optical Transient Detector. Data provided by NASA Marshall Space Flight Center from their Web site at http://wwwghcc.msfc.nasa.gov.

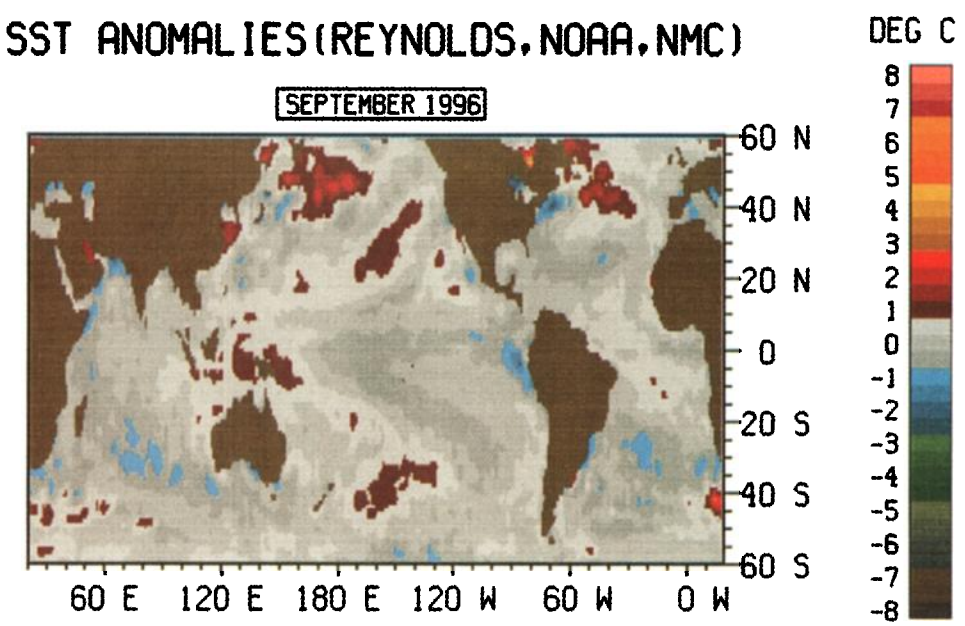

Plate 2. Sea surface temperature anomalies (in degrees Celsius) for September 1996.

more lightning than during September 1996 (Plate 1). The streamline charts (Figure 2) suggest that these areas of lightning are upwind of specific PEM-T flights at particular altitudes. This will be confirmed by trajectory analyses in sections 5–11. However, *Schultz et al.* [this issue] concluded that contributions from soil emissions and lightning were unlikely to produce enough O_3 to explain the observations during PEM-T.

4. Representativness of the PEM-T Period

It is important to determine whether the 1996 PEM-T period was anomalous or representative of a typical August/October. The El Nino (EN) phenomenon of the tropical Pacific Ocean and its associated Southern Oscillation (SO) of the Southern Hemispheric atmospheric circulation (together called ENSO) are major factors leading to interannual atmospheric variability in the tropics. Survey descriptions of ENSO are provided by *Philander and Rasmusson* [1985], *Philander* [1990], and *Trenberth* [1997]. The years 1990–1994 were an extended period of comparatively warm sea surface temperatures (SSTs) in the tropical Pacific, that is, El Nino events. On the other hand, during September 1996, Plate 2 shows few areas of relatively warm SST departures from the 16 year mean between 1981 and 1996. Conversely, the waters just west of Ecuador are the only portion of the Pacific Ocean with SST departures colder than 1°C during this period. Although SST anomalies are small, the Southern Oscillation Index [*Trenberth*, 1976; *Horel and Wallace*, 1981], based on sea level pressure differences between Darwin and Tahiti, is consistent with weak cold phase (La Nina) conditions. Thus there is some debate as to whether 1996 should be considered a neutral period or a weak La Nina event (J.J. O'Brien, personal communication, 1998).

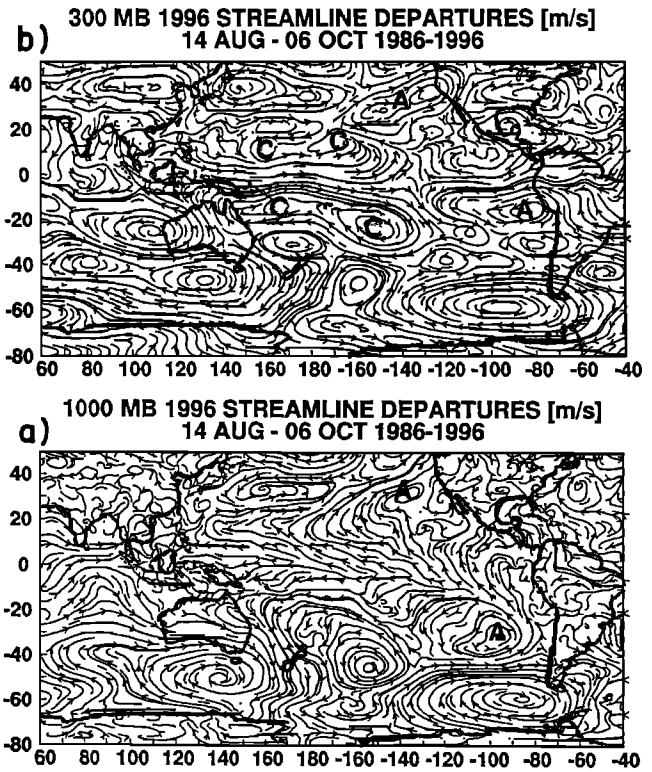

Figure 10. Streamlines of the vector departure of winds during PEM-T with those during a corresponding period between 1986 and 1996 at (a) 1000 hPa and (b) 300 hPa. Cyclonic and anticyclonic circulation anomalies discussed in the text are indicated by "C" and "A," respectively.

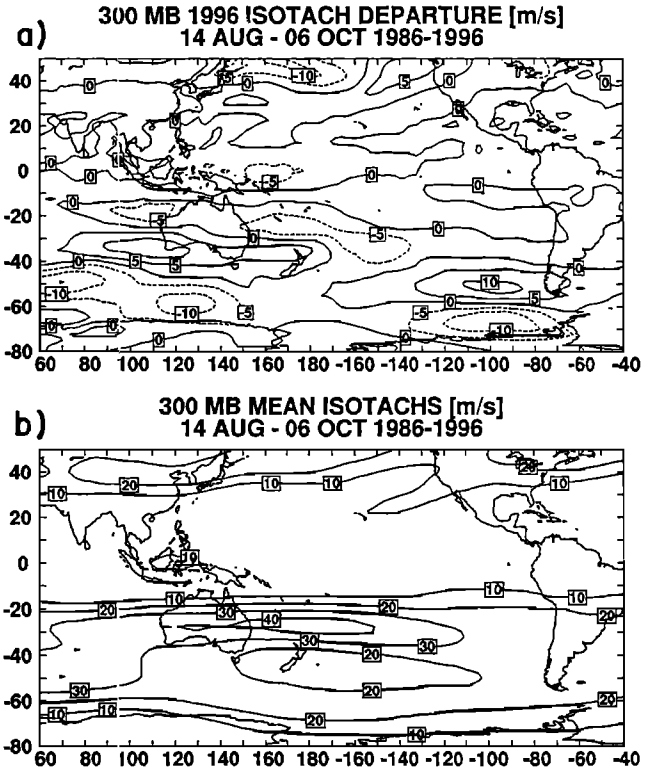

Figure 11. (a) Isotachs of the departure of 300 hPa wind speeds (m s^{-1}) during PEM-T with those during a corresponding period between 1986 and 1996 (in Figure 11b). (b) Isotachs of mean wind speeds (m s^{-1}) at 300 hPa during August 14 to October 6 of the years 1986–1996.

To examine the representativeness of PEM-T in greater detail, we calculated vector departures between mean winds during the 1996 PEM-T period and those of the corresponding 11 year mean (1986–1996) for which data were available. That is, the 11 year mean flow was subtracted from the mean during PEM-T. Figure 10 contains streamline analyses of these vector departures. During El Nino events, the low-level easterly trade winds become weaker, and may even shift to a westerly direction [e.g., *Philander*, 1990]. Conversely, the easterly trades are strengthened during La Nina events. Figure 10a shows that the 1000 hPa easterly trades during PEM-T are slightly stronger (westward pointing streamlines) than those of the 11 year mean, consistent with a cold phase. The subtropical anticyclones east of Hawaii and near Easter Island also are slightly stronger than average, again typical of a cold phase. Greater departures would be expected during more intense cold events. Circulation departures also are evident in the middle-latitude portions of Figure 10a, but their relation to the ENSO, if any, is unclear.

Streamlines of vector wind departures at 300 hPa (Figure 10b) also are consistent with cold phase conditions. Specifically, *Arkin* [1982] found an anomalous couplet of cyclonic circulation centers at 200 hPa during periods of relatively cold SSTs. The two circulation centers straddled the equator, that is, centers north and south of the equator. These are clearly evident during PEM-T over the central tropical Pacific. Conversely, during El Nino events, anomalous anticyclonic upper level couplets have been observed over the tropical Pacific [*Arkin*, 1982]. However, this is not observed during PEM-T. The upper level subtropical anticyclones over the eastern Pacific (Figure 10b) also are slightly stronger than average. The other circulation departures in

Figure 10b, mostly in the middle latitudes, have not been related previously to the ENSO.

Isotachs showing the departure of 300 hPa wind speeds during PEM-T from those of the 11 year mean are shown in Figure 11a. Specifically, the 11 year mean speeds (Figure 11b) were subtracted from those during 1996 (Figure 4a). Although the axis of the subtropical jet stream during PEM-T is near its 11 year mean position, the region of strongest speeds during PEM-T is somewhat displaced. Specifically, the jet streak during PEM-T is located west of its mean position. This is consistent with results of *Chen et al.* [1996] for cold phases. Maximum jet speeds during PEM-T (40 m s^{-1}) are similar to those of the longer-term mean. Finally, the polar jet stream is better defined during PEM-T than during the 11 year mean, at least off the southwestern tip of South America.

To summarize, wind directions and speeds during the 1996 PEM-T period do not exhibit major differences with those of the corresponding 11 year mean. Some of the wind departures occurring during PEM-T are consistent with those of a weak La Nina event. In general, however, we believe that flow patterns during PEM-T should not be considered anomalous, but fairly representative of this season.

5. Flights Near Christmas Island and Hawaii

The initial phase of PEM-T consisted of transit flights by both aircraft to Hawaii, the deployment of the P-3B from Hawaii to Christmas Island (2°N, 157°W), the return of the P-3B to Hawaii, a local flight by the P-3B from Hawaii, followed by both aircraft flying from Hawaii to Tahiti (Figure 1). These various flights investigated latitudinal gradients of atmospheric trace gases, their variations along the ITCZ, atmospheric photochemistry, and the sulfur oxidation cycle.

GOES-9 visible and infrared satellite imagery for the P-3B's local flight near Christmas Island (Flight 7) (Figure 12) illustrates cloud features that are typical of those encountered during other flights over the area. Deep convection associated with the ITCZ is located at approximately 10°N. The visible image (Figure 12a) shows a large region of broken cumulus and stratocumulus blanketing the central North Pacific east of Hawaii. The low clouds

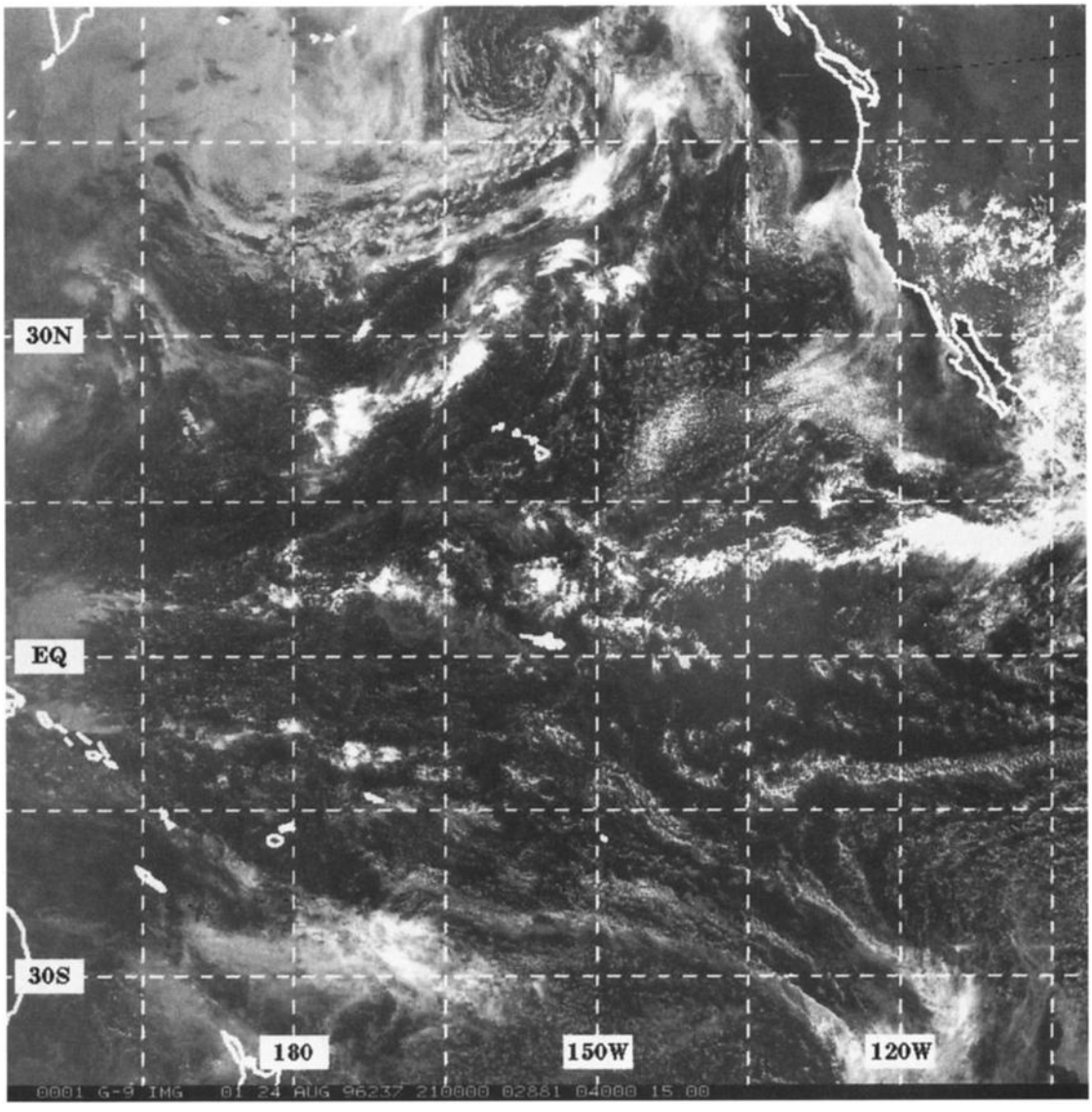

Figure 12. GOES-9 imagery for 2100 UTC August 24: (a) visible and (b) infrared. The track of P-3B flight 7 out of Christmas Island (2°N, 157°W) is superimposed.

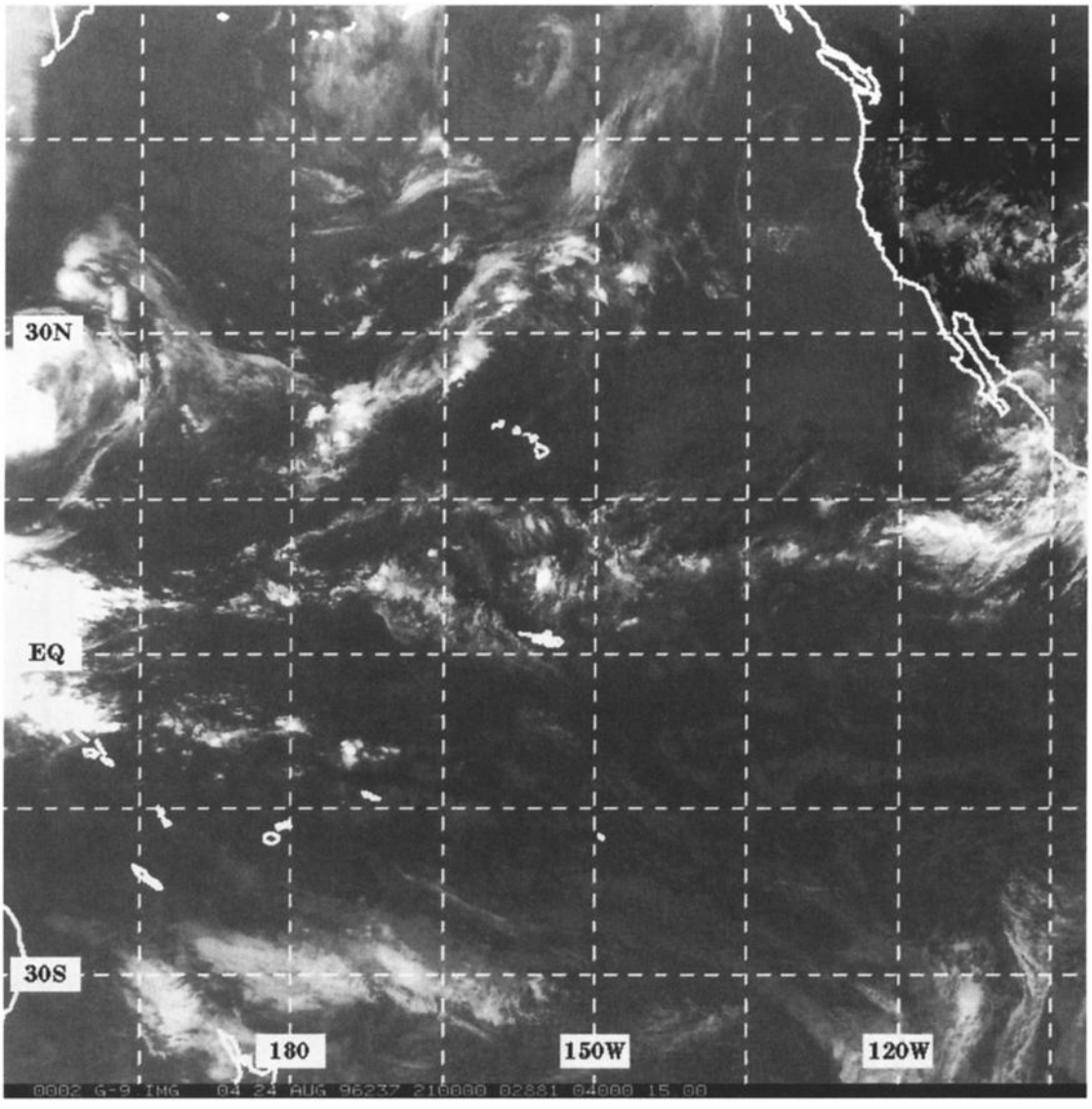

Figure 12. (continued)

just off the coast of California are a persistent feature that are associated with cold California ocean current.

Both PEM-T aircraft measured in situ temperature and humidity (dew point temperature) from which vertical profiles (soundings) could be obtained during maneuvers. The sounding derived from the P-3B's spiral ascent near 2°N, 155°W during flight 7 (Figure 13) is typical of those in the area. The lowest 50 hPa is well mixed, with a nearly dry adiabatic temperature profile and almost constant values of water vapor mixing ratio (not shown). This layer is overlain by a region of more stable and slightly drier air through 800 hPa, followed by a capping inversion centered at ~775 hPa. The driest air is located above 680 hPa.

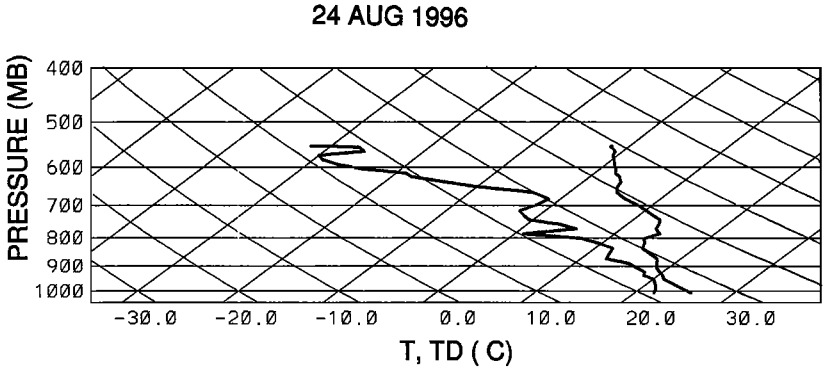

Figure 13. Vertical profile of temperature and dew point (in degrees Celsius) obtained by the P-3B on flight 7 (August 24) near 2°N, 155°W.

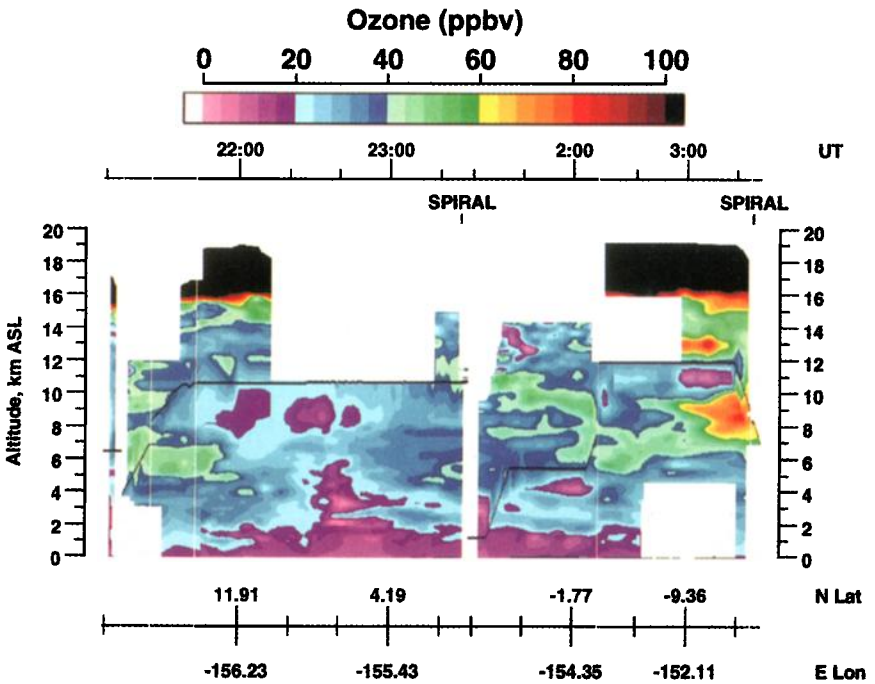

Plate 3. Cross section of DIAL-derived O_3 mixing ratio along DC-8 flight 4 from Hawaii to Tahiti on August 31, 1996 (Figure 1). The O_3 scale (ppbv) and time (UTC) are given at the top of the image, while latitude and longitude are given at the bottom. Locations of aircraft spirals are indicated. The black line through the image denotes the altitude of the DC-8.

Several papers in the current issue examine various chemical aspects of the marine boundary layer near Christmas Island [e.g., *Crawford et al.*, this issue; *Davis et al.*, this issue].

Both aircraft traveled from Hawaii to Tahiti on August 31, taking measurements along an ~40° range of latitudes that intersected the ITCZ. *Gregory et al.* [this issue] use in situ chemical measurements and trajectory data to characterize air on both sides of the ITCZ. Plate 3 shows the DIAL-derived vertical distribution of O_3 along the DC-8's flight track to Tahiti. Tropospheric O_3 mixing ratios north of the equator (left side) generally are less that 40 ppbv, with some regions near the surface and near 9 km having values less than 20 ppbv. Values of O_3 increase south of the equator (right side), exceeding 70 ppbv in the middle troposphere approaching Tahiti. This was the first of many observations of enhanced middle tropospheric O_3 over the south central Pacific Basin during PEM-T.

Ten-day backward trajectories arriving along the flight track at 700 hPa (~3 km, Figure 14a) show that air parcels have spent their entire 10 day histories over water. Since wind speeds are relatively light, the trajectories do not cover long distances. Although some trajectories might ultimately have a continental origin, this would have occurred much earlier than 10 days before arriving at the flight track. This "aged marine" character of the air is consistent with the relatively small values of O_3 seen in the DIAL image (Plate 3). Similar trajectory patterns are found at 850 hPa (not shown).

Trajectories arriving along the flight track at 300 hPa (~9 km, Figure 14b) exhibit a more complex behavior. Most arrivals along the northern half of the flight originate from the east, but they do not pass over land during their 10 day histories. This part of the flight track exhibits relatively small amounts of O_3 in the upper troposphere (Plate 3). Parcels arriving along the southern half of the flight track originate from the west since they are dominated by the prevailing westerlies. These parcels, especially the southernmost arrivals, travel relatively long distances, passing over portions of Indonesia, Australia, southern Africa, and South

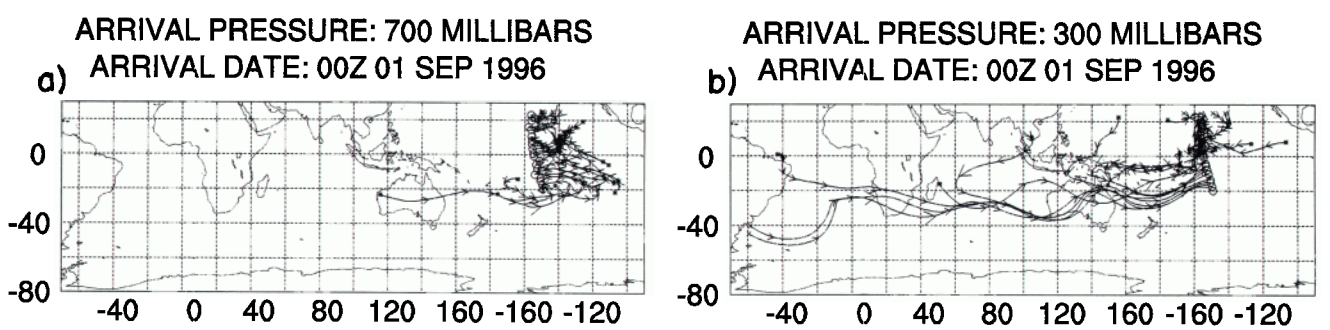

Figure 14. Ten-day backward trajectories arriving at (a) 700 hPa and (b) 300 hPa along DC-8 flight 4 at 0000 UTC September 1. Small arrows denote locations at daily intervals; large arrows denote locations at 5 day intervals.

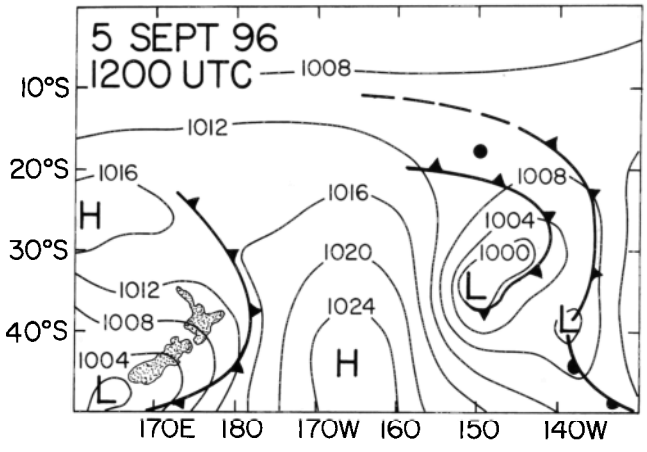

Figure 15. Surface analysis at 1200 UTC September 5 adapted from an original prepared by Meteo France in Tahiti. Tahiti is located at 18°S, 150°W.

America. The implications of these paths on observed chemical measurements are described in section 6.

6. Flights Near Tahiti

Tahiti (18°S, 150°W) was a major base of operations during PEM-T since it is centrally located in the tropical Pacific Basin. The DC-8 had three local flights in the area, while the P-3B had two (Figure 1). In addition, other flights either landed or departed Tahiti as part of transits to or from other operations sites.

Both the P-3B and DC-8 had local flights from Tahiti on September 5 (flights 12 and 6, respectively, Figure 1). Figure 15 shows the surface analysis derived from one prepared by the Tahiti office of Meteo France early on the day of these flights. Three middle-latitude frontal systems are moving from west to east across the area. Such systems typically passed near Tahiti at intervals of 3–4 days. The visible satellite image during the flights (0000 UTC September 6, Figure 16) shows the cloud bands associated with these fronts, as well as the less cloudy air between

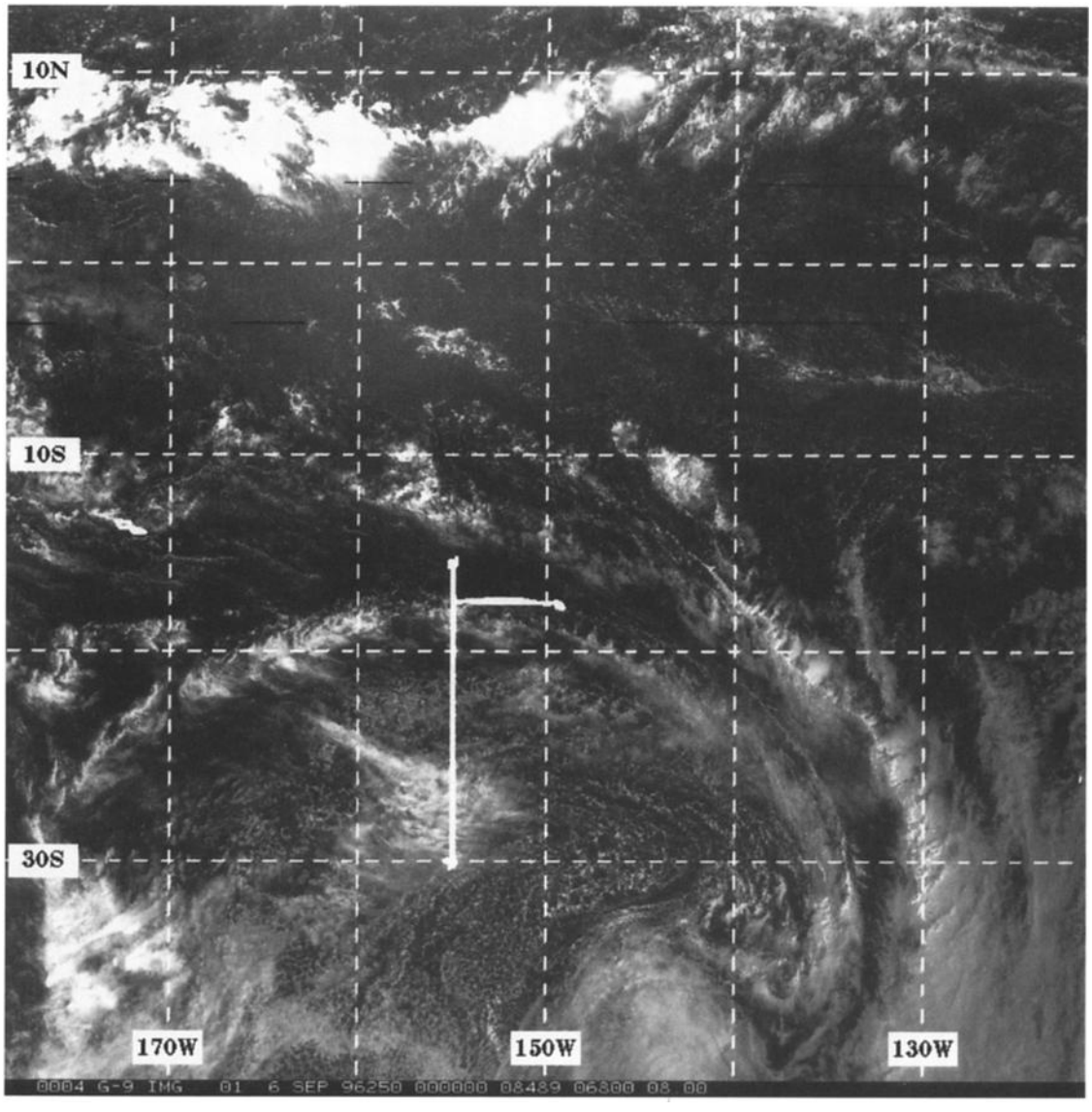

Figure 16. GOES-9 visible image at 0000 UTC September 6. The track of DC-8 flight 6 out of Tahiti (18°S, 150°W) is superimposed.

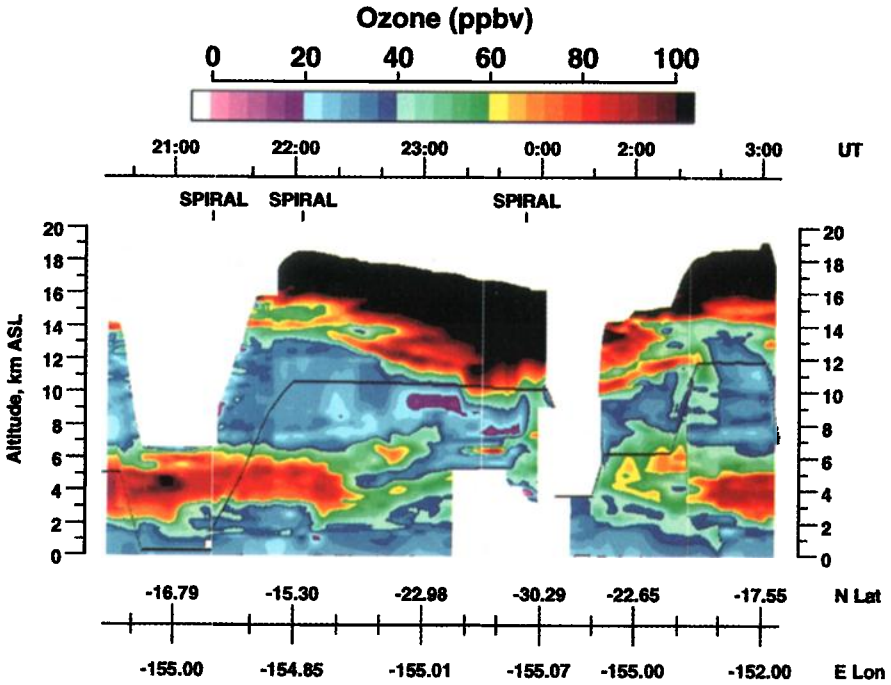

Plate 4. As in Plate 3, but for flight 6 out of Tahiti on September5 (Figure 1). The DC-8 flew west from Tahiti, then followed a north-south track along 155°W before returning.

them. As noted earlier, the fronts became diffuse as they approached Tahiti, loosing their horizontal temperature gradients, but maintaining zones of horizontal convergence which reinforced the SPCZ that extended northwest of the island (Figure 3).

The DC-8 flight on September 5 occurred just west of Tahiti (155°W) and was oriented north-south between 15°–30°S (flight 6 in Figure 1). The northern part of this track traversed the dissipating frontal system (Figure 15), while its southern part passed through the postfrontal air mass. The center portion of the DIAL O_3 image (between 2200–0000 UTC, Plate 4) depicts the south bound portion of this flight; the right segment (after ~0000 UTC) shows conditions during the return flight to Tahiti. A plume of O_3 enriched air is centered near 4.5 km altitude along the northern portion of the flight (i.e., prior to ~2230 UTC). Values in this region exceed 80 ppbv. The layer of enhanced O_3 becomes weaker farther south. At higher altitudes, there is a gradual lowering of largest O_3 values that corresponds to a lowering of the tropopause in the post-frontal region. There are several undulations in the O_3 pattern near 11 km.

The in situ temperature, dew point, and O_3 sounding (Figure 17) from the DC-8's spiral near 15°S, 155°W (~2200 UTC) contains several interesting features. This spiral

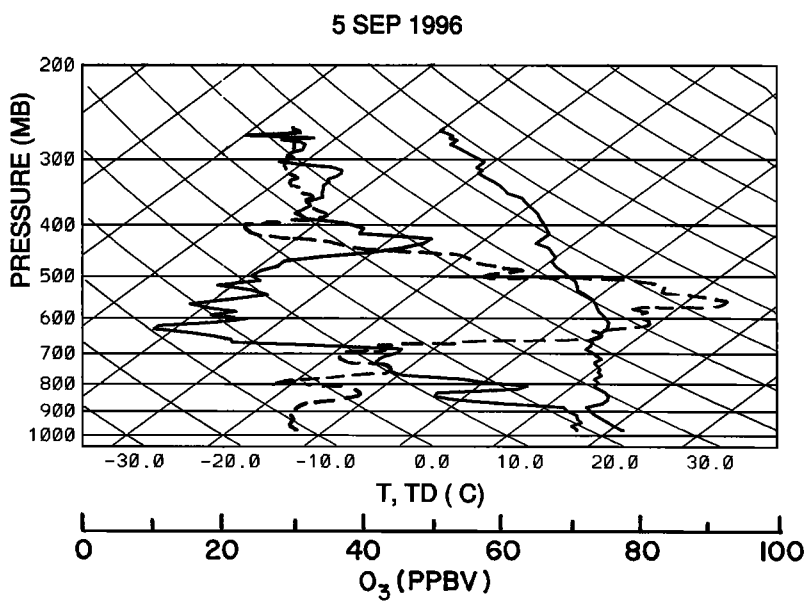

Figure 17. Vertical profile of temperature and dew point (solid, in degrees Celsius) obtained by the DC-8 on flight 6 (September 5) near 15°S, 155°W. The dashed line is in situ O_3 (ppbv).

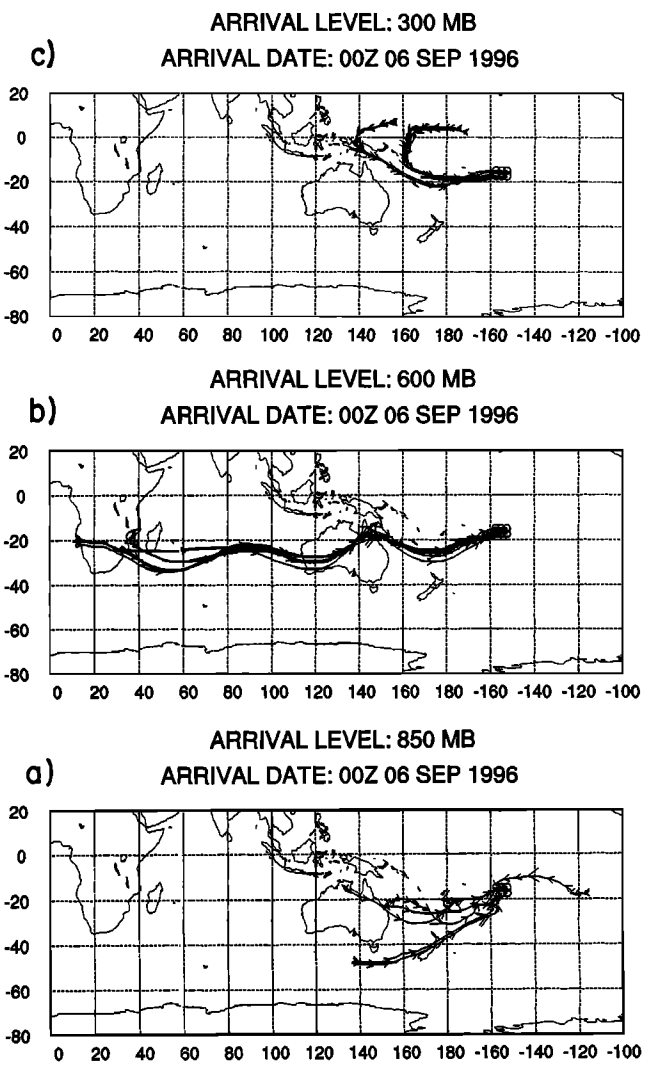

Figure 18. Ten-day backward trajectories arriving at (a) 850 hPa, (b) 600 hPa, and (c) 300 hPa near a spiral location of the DC-8 during flight 6 at 0000 UTC September 6. Small (large) arrows denote locations at 1 (5) day intervals.

passed through the region of enhanced O_3 centered near 4.5 km (~550 hPa) (Plate 4). The well mixed marine boundary layer, located below ~880 hPa, is capped by the trade wind inversion. The region above the inversion is very dry, suggesting subsidence, with coldest dew point temperatures occurring near 625 hPa. Other weaker stable layers are located throughout the sounding. The profile of in situ O_3 mixing ratio shows a well defined maximum of ~90 ppbv near 550 hPa that corresponds to the layer of very dry air.

Ten-day backward trajectories from the spiral location near 15°S, 155°W (Figure 18) are helpful in understanding the O_3 distribution (Figure 17, Plate 4). The cluster of six arrival locations about the spiral point acknowledges the limitations of the ECMWF data and trajectory model in interpreting chemical data at a specific location, especially for a 10 day period [e.g., *Merrill et al.*, 1985; *Kahl*, 1993; *Pickering et al.*, 1996b]. Most trajectories arriving at 850 hPa (~1.5 km, Figure 18a) originate from the west, with a few passing over the coast of Australia 8–10 days prior to reaching the DC-8's location. This aged marine air would be expected to contain relatively little O_3.

Trajectories arriving at 600 hPa near 15°S, 155°W (~4.2 km, Figure 18b) arrive near the center of the O_3 plume (Plate 4, Figure 17). Although these trajectories also originate from the west, they travel longer distances during the 10 day period. They pass over the east coast of Australia approximately 5 days before reaching the PEM-T flight location and extend to southern Africa 9–10 days prior to arriving at the flight location. Australia, southern Africa, Indonesia, and South America are locations of widespread biomass burning during the September–October period [e.g., *Hao and Liu*, 1994; *Hurst et al.*, 1996; *Elvidge and Baugh*, 1996; *Justice et al.*, 1996; *Fishman et al.*, 1996]. The uncertainties associated with long-range trajectories must be acknowledged; however, their origins over Australia and Africa are consistent with the large values of O_3 observed at this altitude (Figure 17, Plate 4). *Garstang et al.* [1996] and *Tyson et al.* [1996] found considerable recirculation of air over the biomass burning regions of southern Africa. They also noted the frequent exit of air from the east coast of southern Africa and into the Indian Ocean. Similarly, a month long trajectory climatology during much of October 1992 showed extensive eastward transport of air off the east coast of Africa [*Thompson et al.*, 1996].

In situ chemical measurements within the middle tropospheric O_3 plume (Plate 4, Figure 17) also suggest that it is due to biomass burning. During the DC-8's ascent through the plume near 2140 UTC, in situ O_3 reaches a maximum of ~90 ppbv (Figure 17), while CO increases to ~95 ppbv (not shown). Values of the ratio C_2H_2/CO are approximately 1 pptv/ppbv in the plume region, indicating that the air is aged approximately 5–7 days from its emission source [e.g., *Greenberg and Zimmerman*, 1984; *Greenberg et al.*, 1990; *Singh and Zimmerman*, 1992; *Gregory et al.*, this issue].

Several PEM-T studies have concluded that middle tropospheric O_3 plumes such as seen in Plate 4 are attributed to biomass burning. *Schultz et al.* [this issue] noted that plumes encountered near Tahiti were somewhat diluted or chemically degraded compared to those encountered farther west (closer to the assumed source region). *Talbot et al.* [this issue] examined regions of enhanced acidic trace gases during PEM-T and concluded that there was no correlation with industrial tracer compounds. Conversely, they found a general correlation with CH_3Cl, PAN, and O_3 which suggested photochemical and biomass

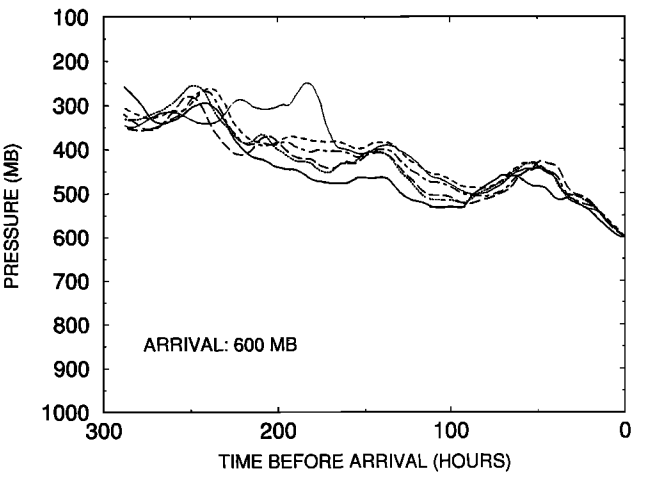

Figure 19. Time/altitude plot for the six 10-day backward trajectories arriving at 600 hPa in Figure 18b. Arrival at the flight track is indicated by time equal to 0.

burning sources. Similarly, *Vay et al.* [this issue] concluded that regions of enhanced CO_2 within the lower to middle troposphere were produced by biomass burning.

The relatively large values of CO within the plume (reaching ~95 ppbv) are not consistent with a stratospheric origin. Furthermore, values of potential vorticity (not shown) along the trajectories in Figure 18b remain less than commonly accepted stratospheric thresholds (see *Loring et al.* [1996] for a recent discussion of these thresholds).

The trajectories arriving at 600 hPa (Figure 18b) pass over Australia approximately 120 hours prior to reaching the aircraft. Their altitudes over Australia (Figure 19) are approximately 500 hPa (~5.5 km). The trajectories pass over southern Africa near the end of the 10 day period at altitudes near 300 hPa (~9 km). Considerable lightning occurred over southern Africa and southeastern Australia during PEM-T (Plate 1). Satellite imagery (not shown) also indicates intermittent deep convection over these regions during the period. Thus the convection may have transported burning by-products into the upper troposphere where they were transported rapidly eastward into the PEM-T domain [e.g., *Pickering et al.*, 1996b; *Thompson et al.*, 1996]. This hypothesis also is discussed by *Schultz et al.* [this issue].

Figure 19 shows that the trajectories arriving at 600 hPa (Figure 18b) descend several hundred hPa during their eastward journeys toward the DC-8 flight track. This subsidence is consistent with the extreme dryness that is observed in the sounding (Figure 17) and with the descent that is indicated along the paths of the trajectories (Figure 8). There are several prominent temperature inversions in the aircraft-derived sounding (Figure 17). Bases of these inversions are located near 880 hPa (~1.2 km), 680 hPa (~3.2 km), and 430 hPa (~6.7 km). As noted earlier, these inversions have the classic appearance of subsidence; that is, the dew point temperature decreases as the temperature increases. The top two inversions are located near the top and bottom of the middle tropospheric O_3 plume (Plate 4). Inversions are stable layers that limit vertical mixing. Therefore the subsidence-induced inversions may be important factors in explaining the strong vertical gradients in these O_3 plumes that are observed well away from their apparent emission source. Subsidence inversions are evident in many of the soundings that are presented in later sections.

Considering even higher altitudes, trajectories arriving at the spiral location (~2200 UTC) at 300 hPa (~9 km, Figure 18c) follow a somewhat different path, mostly remaining over the ocean, and only skirting portions of Indonesia. Their maritime history is consistent with the relatively small O_3 values that are observed at this altitude of the spiral (Figure 17, Plate 4).

Several ongoing studies are investigating in greater detail the chemical and meteorological aspects of the O_3 plumes during PEM-T. These include *J.A. Logan et al.* (manuscript in preparation, 1998) and *A.S. Board and H.E. Fuelberg* (manuscript in preparation, 1998). *W.R. Lusher and H.E. Fuelberg* (manuscript in preparation, 1998) are calculating forward trajectories from southern Africa and South America, to examine transport toward the PEM-T region.

DC-8 flight 5 on September 3 permitted an interesting phenomenon to be examined. During the planning for PEM-T, we frequently referred to "stalactites." This word was used to describe patches of air in the tropical upper troposphere that contained small water vapor content, as shown by the Microwave Limb Sounder (MLS) onboard the NASA Upper Atmosphere Research Satellite (UARS). Stalactites also exhibit large values of potential vorticity [*Newell et al.*, 1996a]. If such a phenomenon also contains large values of O_3, this would be evidence of a direct penetration of stratospheric air into the tropical upper troposphere. Such a direct exchange previously had not been considered possible.

A region of large potential vorticity was observed over the equator north of Tahiti on September 3–4 (Figure 20). Counterclockwise flow dominates the region between 130° and 160°W on the 350 K isentropic surface (~12.5 km altitude). Its

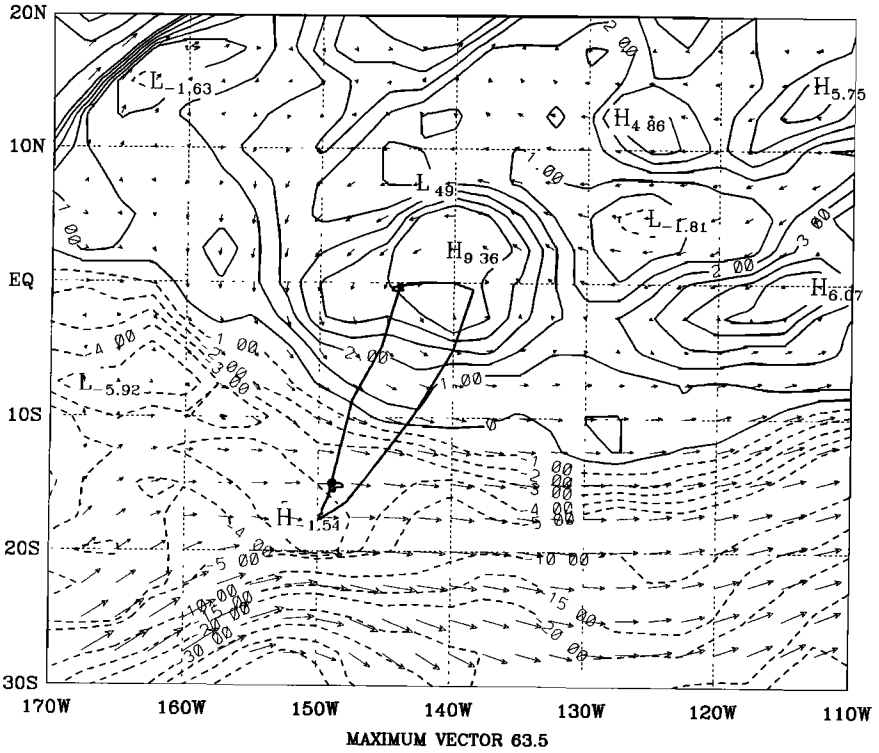

Figure 20. Analysis of potential vorticity (10^{-7} K m^2 (kg s)$^{-1}$) on the 350 K isentropic surface (~12.5 km) at 0000 UTC September 4. Wind vectors are superimposed; the maximum is 63.5 m s^{-1}. The track of DC-8 flight 5 is superimposed.

latitudinal extent is from 5°N–5°S, with the center at ~0°, 140°W. DC-8 flight 5 reached the equator at 2141 UTC September 5, the eastern extent of its track, and then flew westward, staying within 100 km of the equator until 2311 UTC. The DIAL O_3 image (Plate 5) shows an apparent connection between a region of large O_3 in a layer near 12–13.5 km (50–75 ppbv, colored green), and what appears to be stratospheric O_3 above. If this feature is not an artifact of differential horizontal advection, then it indicates that stratospheric air is being transferred directly into the tropical upper troposphere.

The cross section of potential vorticity from the ECMWF data (Figure 21) shows large values extending down to ~10 km near the equator, accompanied by a dip in the isentropes that denotes subsidence. Values of ECMWF-derived specific humidity in this area at 300 hPa are very small (<0.2 g kg^{-1}), again suggesting subsidence (Figure 22). Water vapor data at higher levels (from the MLS) were not available. The relatively large positive values of potential vorticity are consistent with both the actual flow and the backward trajectories (Figure 23). Although the air closest to the equator may have had a slightly different source than that farther south, the probability that this difference could account for the DIAL image seems small. The consistent picture given by the dry air and subsidence suggests that the connection of large O_3 centered at 2136 UTC is a "stalactite."

Suhre et al. [1997] recently reported similar features in the tropical upper troposphere based on measurements from commercial jet aircraft. The scales that they measured were in the 5–80 km range, with O_3 discontinuities up to 500 ppbv, well above the background level. In addition, these features were accompanied by positive water vapor anomalies, just opposite the earlier PEM findings [*Newell et al.*, 1996a]. As *Suhre et al.* pointed out, however, the process we have described may play a role in transferring stratospheric air several kilometers downward before a convective event moves it down to flight level. The fact that a stalactite apparently has been detected is certainly worthy of note and will encourage further searches in future expeditions.

7. Flights Near Easter Island

Both the DC-8 and P-3B conducted local flights out of Easter Island (28°S, 110°W) on September 10 and 11 (Figure 1). Easter Island is located near the major semipermanent anticyclone over the eastern Pacific (Figure 2), in a region of subsiding air (Figures 8 and 9). The northbound flights on September 10 penetrated deep into the tropics, with the DC-8 reaching ~7°S. The visible satellite image for 2100 UTC September 10 (Figure 24) indicates only scattered to broken shallow, cumuloform clouds in the area. The DIAL O_3 image from the DC-8 (Plate 6a) shows layers of enhanced O_3 centered near 3 km and near 9 km, with most values in these layers <60 ppbv. The sounding obtained during the DC-8's downward spiral at its northernmost location (Figure 25a) shows the moist marine boundary layer, with much drier air aloft. The greatest in situ O_3 (~60 ppbv) is located near the base of the second major temperature inversion, that is, ~650 hPa (~3.7 km). Smallest dew points occur between 500–600 hPa. These dry layers undoubtedly are due to the subsidence associated with the anticyclone in the region.

The portions of the DIAL O_3 image near Easter Island (extreme left and right sections of Plate 6a) reveal a broad region

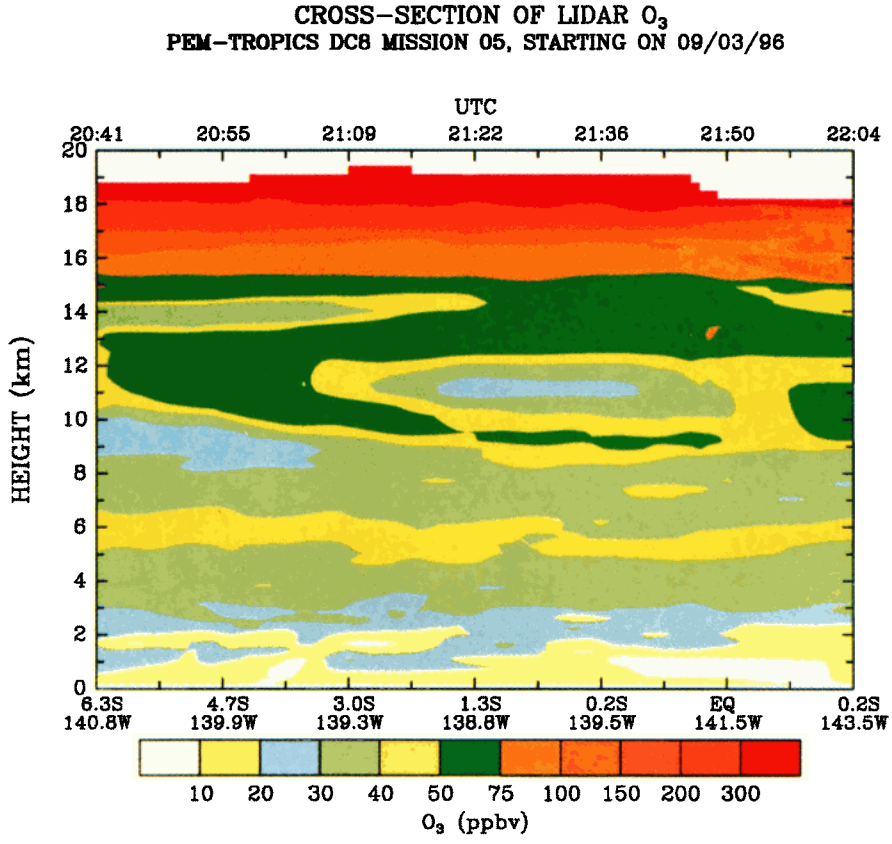

Plate 5. Cross section of DIAL-derived O_3 along a portion of DC-8 flight 5 on September 3 (Figures 1 and 20).

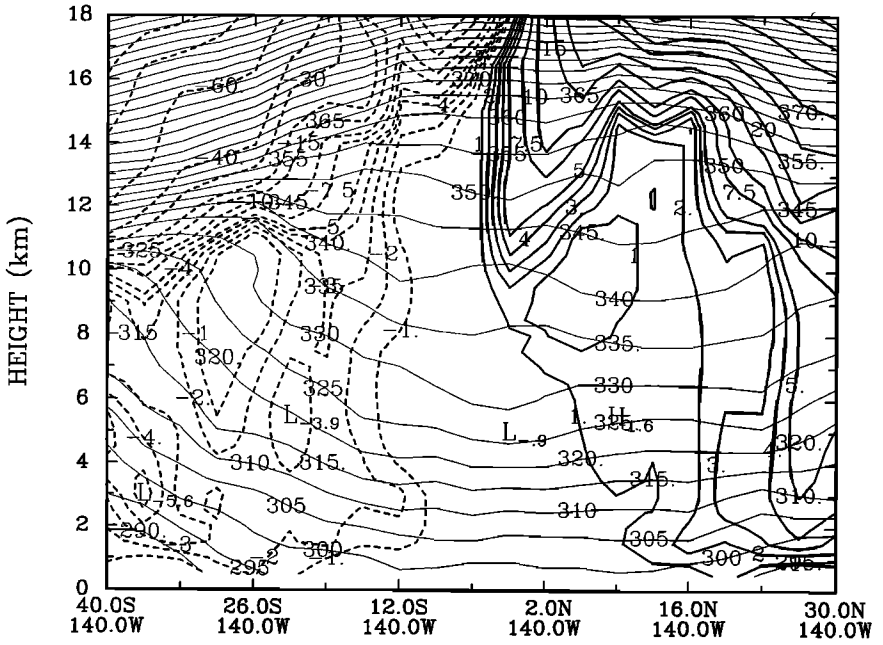

Figure 21. Cross section of potential vorticity (dashed, 10^{-7} K m^2 (kg s)$^{-1}$) and isentropes (solid, K) along a portion of DC-8 flight 5 at 0000 UTC September 4.

of values exceeding 80 ppbv at altitudes above ~9 km. The sounding obtained from the spiral descent approaching Easter Island (~1900 UTC, Figure 25b) shows an isothermal layer between 260 and 300 hPa in which dew points decrease to approximately −65°C. This layer corresponds to large in situ O_3 (~90 ppbv, Figure 25b), but relatively small in situ CO (~50 ppbv, not shown). This region probably represents a broad downward undulation in the tropopause. However, the magnitudes of these chemical data suggest that the aircraft did not penetrate far into the stratosphere.

The DC-8's southbound flight on September 11 traversed a middle-latitude frontal system at ~35°S that was associated with a broad band of multilayered clouds (Figure 24). The DIAL image (Plate 6b) shows a general lowering of maximum O_3 toward the south (right), corresponding to a lowering of the tropopause as the flight extends farther into the middle latitudes. Several downward

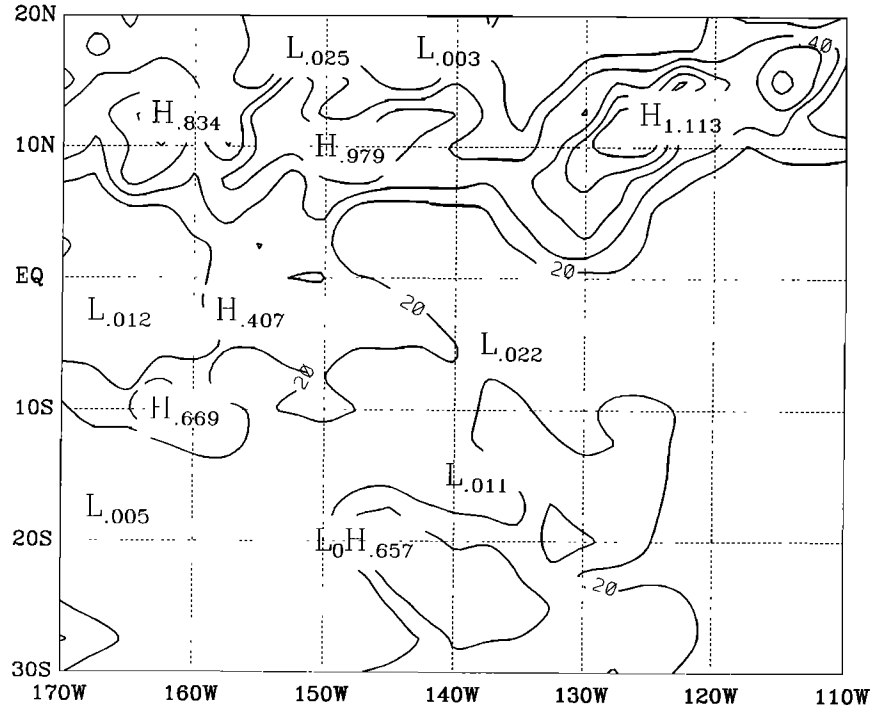

Figure 22. Analysis of specific humidity (g kg^{-1}) at 300 hPa for 0000 UTC September 4.

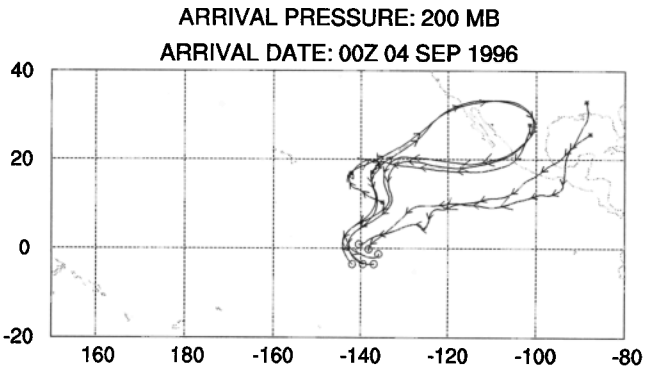

Figure 23. Six 10-day backward trajectories arriving near the "stalactite" at 200 hPa on 0000 UTC September 4. Small (large) arrows denote locations at 1 (5) day intervals.

distortions of enhanced O_3 are indicated. The DC-8 derived sounding at its southernmost point (~46°S, Figure 25c) indicates a temperature inversion beginning near 280 hPa that corresponds to a rapid increase in in situ O_3. Just before beginning the descent, the in situ O_3 is ~250 ppbv, and the in situ CO ~35 ppbv. These values indicate that the DC-8 was within the stratosphere at this location.

Ten-day backward trajectories arriving along 110°W (Figure 26) reveal the origins of the air encountered by the DC-8 during its two flights. These parcels arrive at 0000 UTC September 11, nearly in between the flights on September 10 and 11. Most parcels arriving north of Easter Island at 700 hPa (~3 km, Figure 26a) undergo considerable recirculation between the flight track and the coast of South America. Some of the northernmost arrivals penetrate the coasts of Peru and Ecuador. Conversely, arrivals south of Easter Island at 700 hPa originate from the west. Most of them remain over the Pacific during the entire 10 day period. The few that do pass over Australia did so ~7 days prior to arriving at the flight track. Thus most of the southern arrivals at 700 hPa have a long maritime history that is consistent with the small O_3 values at 3 km (Plate 6b).

The trajectories arriving along 110°W at 300 hPa (~9 km, Figure 26b) exhibit considerably different characteristics. The northernmost arrival originates near central America, but all others originate from the west. Many trajectories arriving between

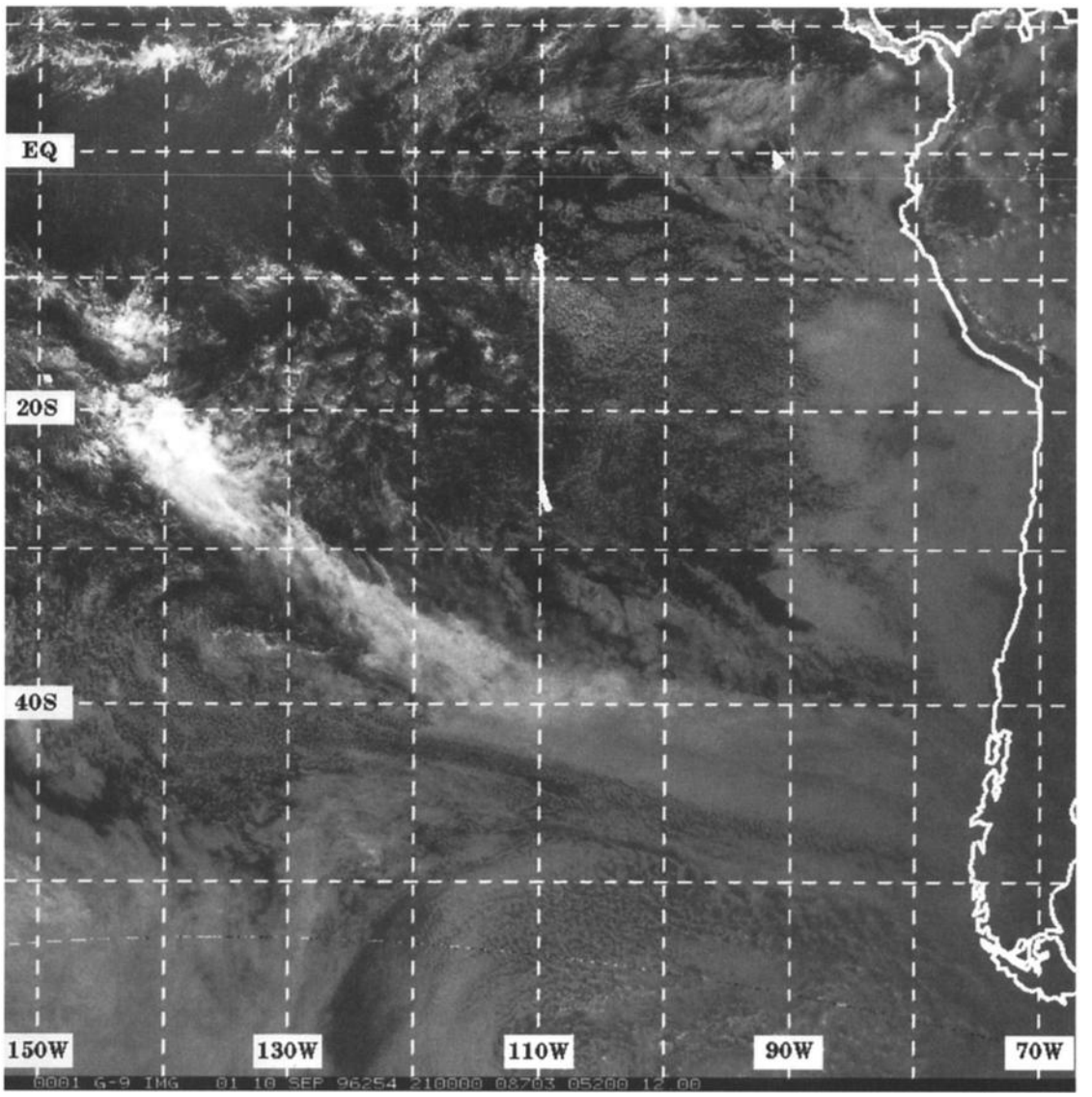

Figure 24. GOES-9 visible image at 2100 UTC September 10. The track of DC-8 flight 8 out of Easter Island (28°S, 110°W) is superimposed.

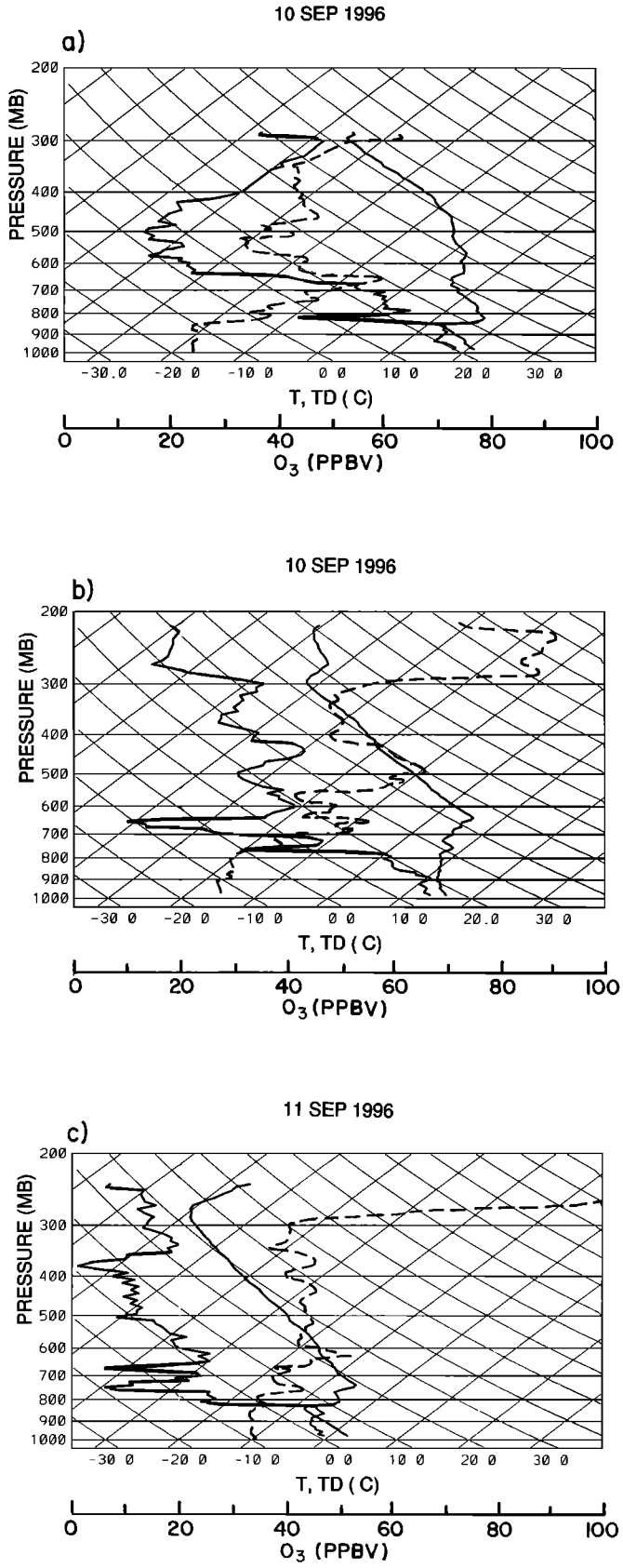

Figure 25. Vertical profiles of temperature and dew point (solid, in degrees Celsius) obtained by the DC-8 on flights 8 and 9 (September 10 and 11). In situ O_3 (ppbv) is superimposed (dashed). (a) Near 9°S, 110°W, (b) near 27°S, 110°W, and (c) near 46°S, 110°W.

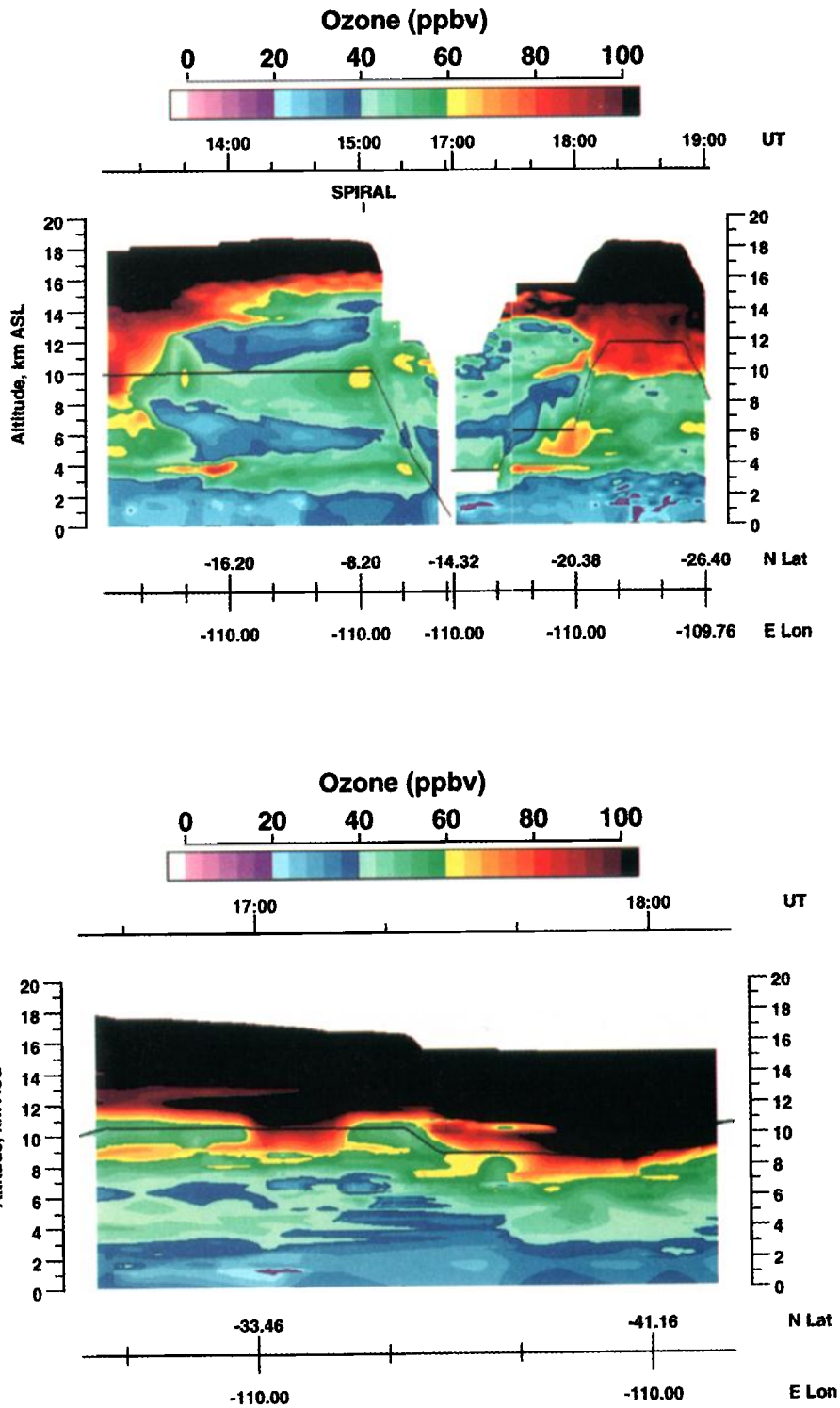

Plate 6. (a) As in Plate 3, but for DC-8 flight 8 northbound out of Easter Island on September 10 (Figure 1). (b) As in Plate 3, but for DC-8 flight 9 southbound out of Easter Island on September 11 (Figure 1).

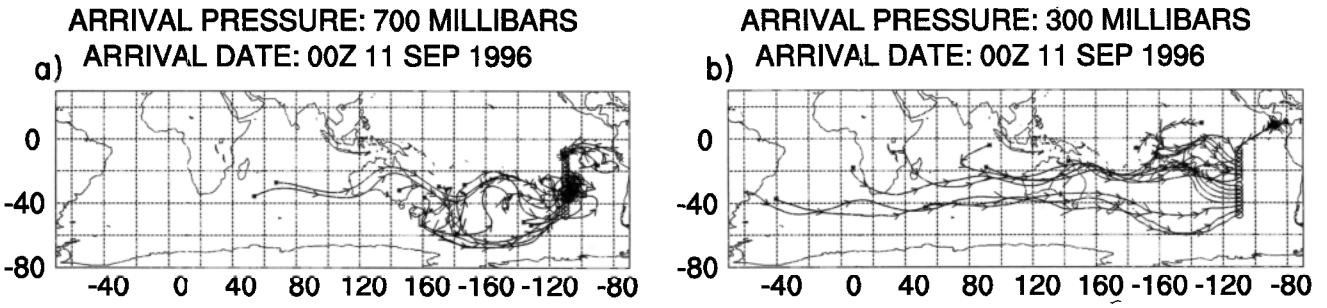

Figure 26. Ten-day backward trajectories arriving along 110°W at (a) 700 and (b) 300 hPa on 0000 September 11. Small (large) arrows denote locations at 1 (5) day intervals.

30° and 40°S pass over Australia ~5 days back and then extend into the Indian Ocean. Two of them pass over southern Africa near the end of the 10-day period. Trajectories arriving along the southernmost part of the diagram skirt the southern coast of Australia, pass south of Africa, and are near Brazil near day 10. Many trajectories arriving south of ~35°S at ~9 km either are in the stratosphere when arriving at the flight track or were in the stratosphere during the previous 10 days (based on values of potential vorticity). This stratospheric history is consistent with the in situ chemical data described above.

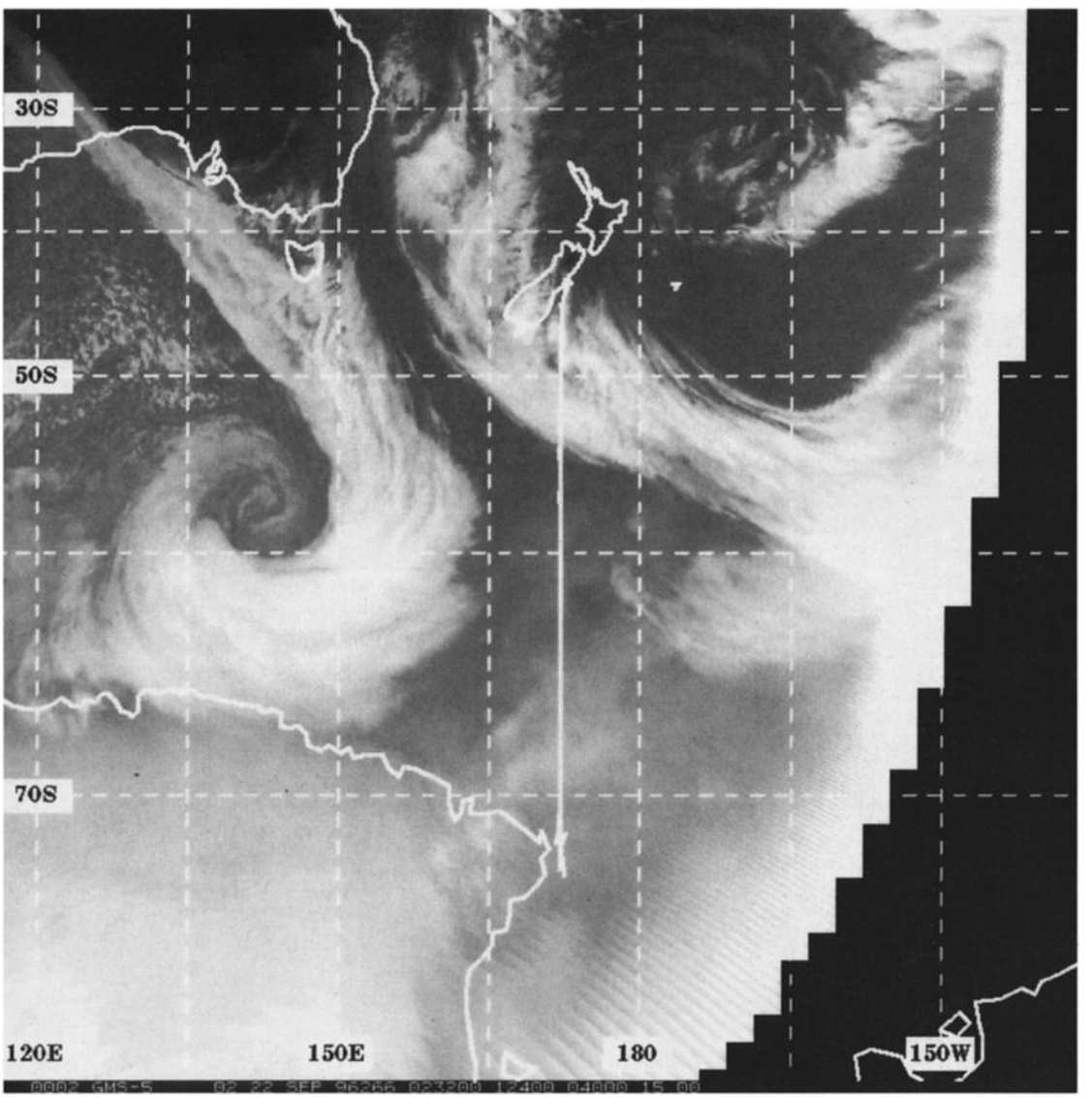

Figure 27. GMS-5 infrared image at 0232 UTC September 22. The track of DC-8 flight 13 from Christchurch to the coast of Antarctica is superimposed.

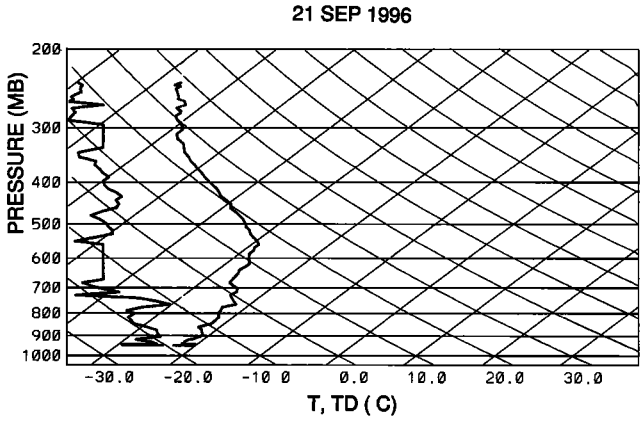

Figure 28. Vertical profiles of temperature and dew point (in degrees Celsius) obtained by the DC-8 on flight 13 (September 21) near 72°S, 172°E.

8. Flight to the Antarctic Coast

The DC-8 traveled from Tahiti to Christchurch, New Zealand (43°S, 172°E), on September 18, and then flew south to the coast of Antarctica on September 21 (flights 12 and 13, Figure 1). The major objective of these flights was to extend the latitudinal survey of PEM-T to its southernmost extent. Surface conditions on the morning of September 21 included high pressure centered over New Zealand, and two middle-latitude cyclones located southeast and southwest of the islands (not shown). Satellite imagery (Figure 27) shows the major cloud bands associated with these cyclones. The flight to the coast of Antarctica was along 172°E, between the two cyclones. This track traversed the polar jet stream at ~56°S where flight level winds (31,000 feet, ~9.1 km) were westerly at 157 kt, the strongest encountered by the DC-8. Sea ice first was observed near 63°S, and the sea was entirely frozen at the Antarctic coast (72°S, 172°E). The DC-8 then spiraled down to 1800 feet (~0.6 km), providing the sounding shown in Figure 28. The deep stable layer that extends from the surface to approximately 550 hPa is typical of polar regions. The tropopause is located near 300 hPa. There is a relatively large dew point depression throughout the troposphere.

The DIAL O_3 image for the southbound leg of the flight is shown on the left side of Plate 7. A region of enhanced O_3 (>90 ppbv) is located below the DC-8 (near 5 km altitude) just south of Christchurch (~51°S). Trajectories and chemical data described in the following paragraph suggest that this feature is due to biomass burning to the west of the flight track. The downward extension of enhanced O_3 to ~7 km between 53° and 61°S coincides with the location of the polar jet stream. In situ O_3 in this region reaches 210 ppbv, but in situ CO is as small as 35 ppbv. These values and the pattern of the DIAL image suggest that stratospheric O_3 is descending in the region, probably due to the transverse circulations and tropopause breaks that are associated with jet streams [e.g., *Carlson*, 1991]. Farther south, the altitude of greatest O_3 rises to between 9 and 10 km. Much of the troposphere south of 60°S contains O_3 mixing ratios less than 40 ppbv.

Ten-day backward trajectories arriving along the flight track are shown in Figure 29. Along the northern half of the flight, most of the 700 hPa (~3 km) arrivals either remain off the east coast of Australia or pass along the southern fringe of this continent. Some trajectories arriving near 50°S at 500 hPa (~5.5 km) pass over Australia and then extend to near the coast of southern Africa by the end of the ten day period. The DC-8 is approximately 1 km above the altitude of greatest O_3 centered near 5 km between 48° and 53°S (Plate 7). However, in situ O_3 at that altitude is ~90 ppbv, while in situ CO reaches 150 ppbv. Although the uncertainties of such long-range trajectories again must be acknowledged, their paths and the chemical data suggest that the region of enhanced O_3 near 5 km (Plate 7) is due to biomass burning. Along the southern half of the flight, the arrivals at both 700 and 500 hPa pass between Australia and Antarctica. These

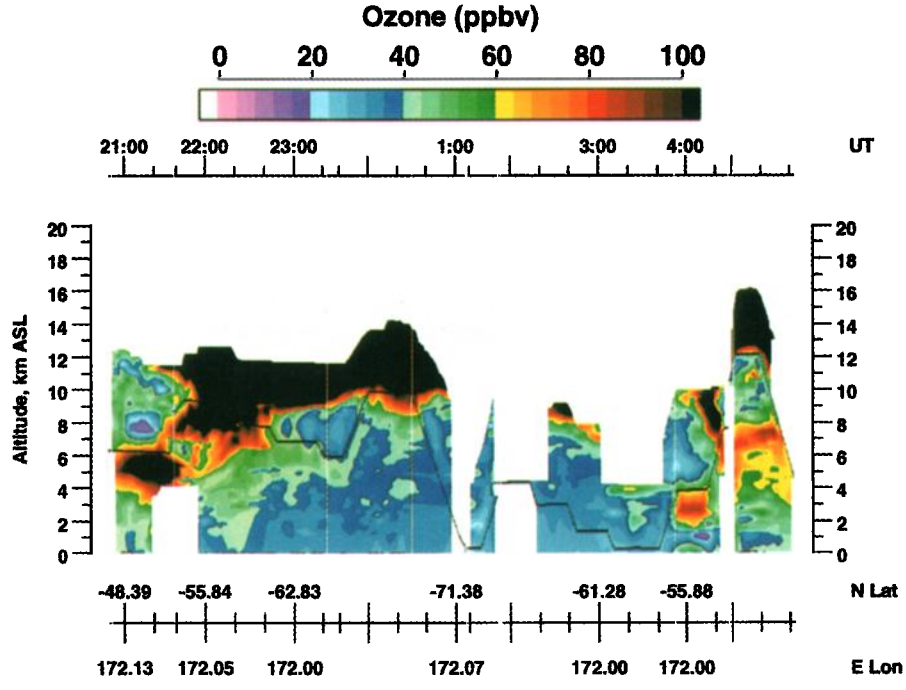

Plate 7. As in Plate 3, but for DC-8 flight 13 southbound out of Christchurch on September 21 (Figure 1).

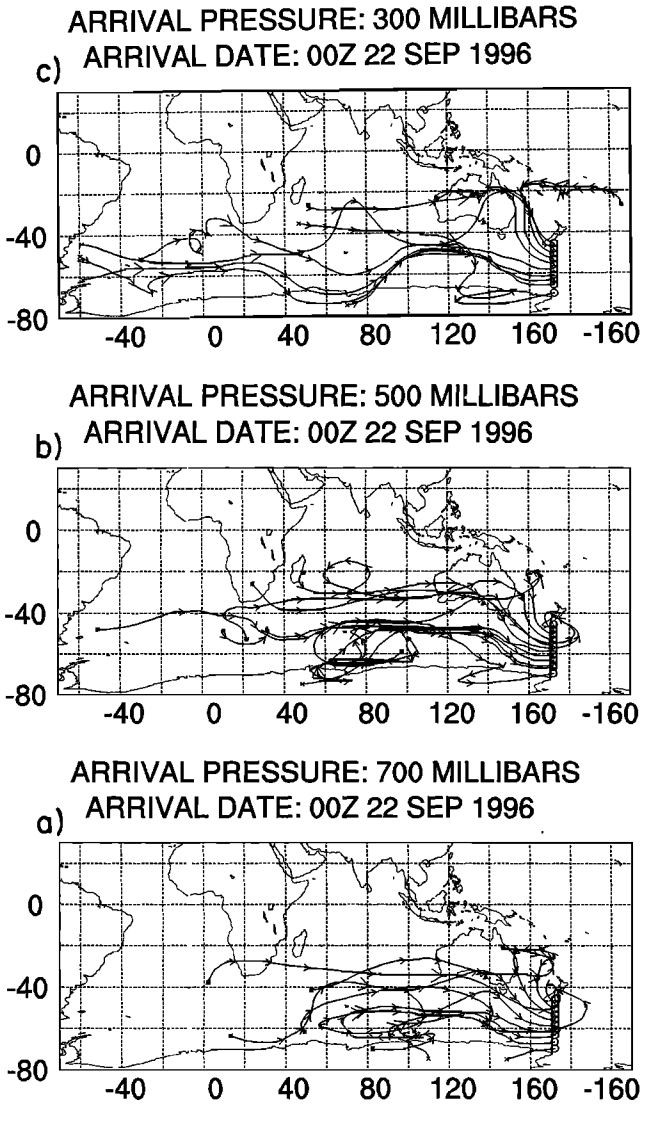

Figure 29. Ten-day backward trajectories arriving along DC-8 flight 13 at (a) 700 hPa, (b) 500 hPa, and (c) 300 hPa on 0000 UTC September 22. Small (large) arrows denote locations at 1 (5) day intervals.

tracks, covering areas of relatively little human activity, are consistent with the relatively small values of O_3 that are observed along the southern portion of the flight (Plate 7) Trajectory information south of ~60°S should be used with caution because of distortions that occur when ECMWF data are converted from spherical to Cartesian coordinates.

The chemical data cited above suggest that the tropopause and its undulations are major factors in explaining the O_3 pattern near 9 km (Plate 7) However, trajectories arriving along the flight track at 300 hPa (Figure 29c) do provide useful information. The northernmost arrivals originate over the waters northeast of New Zealand. This is consistent with the relatively small values of O_3 observed near 9 km altitude between 48° and 50°S (Plate 7). Farther south, potential vorticity calculations indicate that many of the trajectories either arrive at stratospheric altitudes or have stratospheric histories. Some of these arrivals pass over Australia and extend into the Indian Ocean. Finally, trajectories arriving along the remainder of the flight pass over the waters between Australia and Antarctica.

9. Flights Near Fiji

The DC-8 conducted three local flights out of Fiji (flights 15, 16, and 17, Figure 1). These flights were designed to sample the region of small O_3 over the warm waters near Indonesia (flight 15) and to obtain samples on either side of the SPCZ (flights 16 and 17). *Gregory et al.* [this issue] contrast the atmospheric chemistry on both sides of the SPCZ.

Flight 15 on September 26 headed northwest from Fiji, reaching 2°S, 153°E. This track was approximately parallel to, but just south of the SPCZ which extended from approximately 0°, 145°E to 10°S, 180°. There was widespread deep convection near much of the flight track (Figure 30), with many storm tops exceeding 30,000 feet (9.1 km). Most of this convection was oriented along the axis of the SPCZ; however, at times another broken line of storms was located just south of the main one. Sea surface temperatures near Fiji were near 26°C, but increased to approximately 31°C at the northwest corner of the flight.

The DIAL O_3 image (Plate 8) indicates an extensive, deep layer of values less than 20 ppbv, with portions of the lower troposphere having values less than 10 ppbv. Smallest O_3 is located along the northwest half of the flight (center of the image), while greatest values occur near Fiji (left and right sections of the image).

The aircraft-derived sounding (Figure 31) at the extreme northwest corner of the flight (2°S, 153°E) indicates the mixing that is associated with the widespread convection. Specifically, the temperature profile is approximately moist adiabatic between the surface and the tropopause. In addition, the dew point profile shows very moist conditions below ~500 hPa, with the driest air located in the upper troposphere. The superimposed profile of in situ O_3 shows that greatest values (only ~25 ppbv) correspond to this region of dry air.

Backward trajectories along this flight must be interpreted with considerable caution because of the extensive convection in the area. As noted earlier, the ECMWF data used to prepare the trajectories do not resolve individual convective elements, only their broadscale effects at a horizontal resolution of 2.5° latitude/longitude. Nonetheless, the trajectories (Figure 32) do provide insight into the very small O_3 values over the warm pool. Most arrivals at 700 hPa (~3 km, Figure 32a) originate from the east and show little motion during the 10 day period. This air is many days from any land mass. At the northwest corner of the flight, the in situ O_3 at 3 km is ~15 ppbv (Figure 31), while CO is ~50 ppbv (not shown). Trajectories arriving along the flight track at 300 hPa (~9 km, Figure 32b) exhibit considerably more motion during the period. Many of them have northern hemispheric origins, following broad, curving paths, originating near the Philippines or Indonesia, and then passing over Australia. In situ 9 km chemical measurements at the northwest corner indicate that O_3 is ~20 ppbv (Figure 31) and CO is ~55 ppbv (not shown). These values suggest that relatively clean air in the marine boundary layer may have been carried upward by the deep convection in the area. Conversely, deep convection may have transported upper level O_3 downward to altitudes where its destruction is more rapid [*Leliveld and Crutzen*, 1994]. Some trajectories arriving near Fiji follow a more westerly track, consistent with the greater O_3 in that area.

DC-8 flight 16 on September 28 was oriented north to south along 175°E, just west of Fiji (Figure 1). In the lower troposphere, this flight intersected the SPCZ and an associated dissipating frontal boundary between 10° and 15°S. In the middle troposphere, winds in this region exhibited a major shift due the

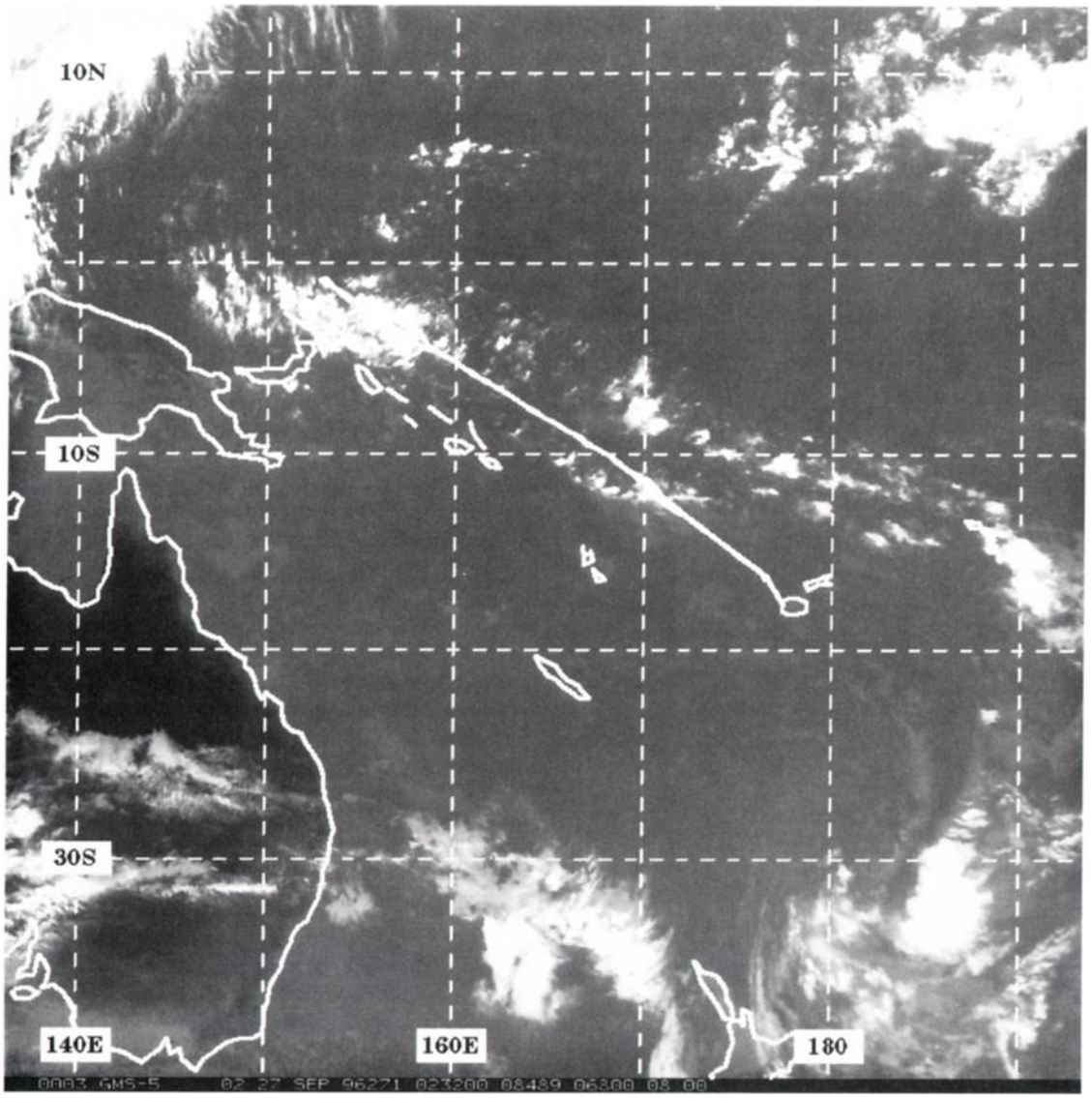

Figure 30. GMS-5 infrared image at 0232 UTC September 27. The track of DC-8 flight 15 out of Fiji (18°S, 177°E) is superimposed.

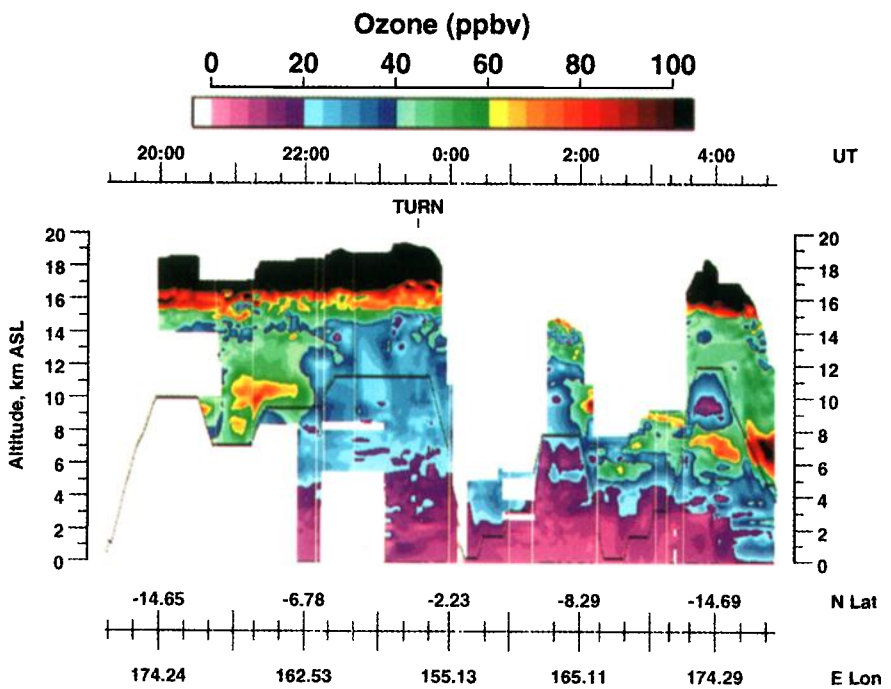

Plate 8. As in Plate 3, but for DC-8 flight 15 northwestward out of Fiji on September 26 (Figure 1).

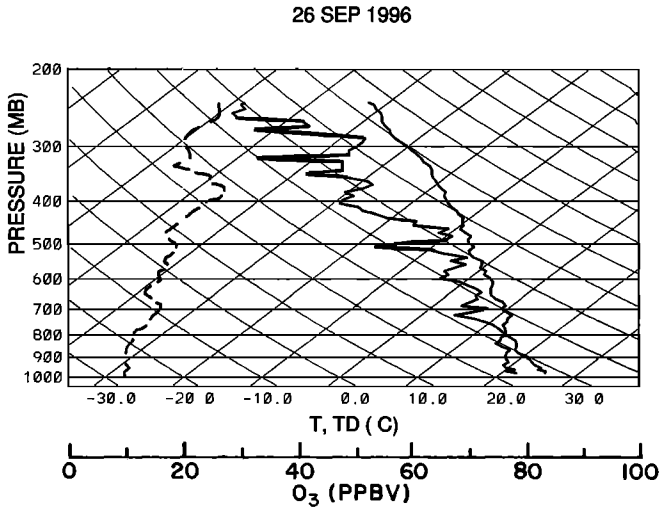

Figure 31. Vertical profiles of temperature and dew point (solid, in degrees Celsius) obtained by the DC-8 on flight 15 (September 26) near 2°S, 153°E. In situ O_3 (dashed, ppbv) is superimposed.

persistent ridge line that was described earlier in the climatological charts (Figures 2b–2c). Intense convection, with tops reaching 40,000 feet (12.2 km), was located near 12°S, along the SPCZ/upper level wind shift line (Figure 33).

The DIAL image shows a major horizontal O_3 gradient midway through the northbound leg of the flight (2230–0200 UTC in Plate 9). Specifically, much of the middle troposphere south of ~15°S contains O_3 values in excess of 60 ppbv. However, values north of this latitude are much smaller, for example, <40 ppbv. The gradient also is seen on the return (southbound) leg (~0400 UTC). Figure 34 contains soundings at 21°S, 175°E in the O_3-enriched air (Figure 34a) and at 4°S, 175°E in the area of reduced O_3 (Figure 34b). Both soundings exhibit major temperature inversions in the lower levels along with dry air aloft. However, the southernmost location (Figure 34a) has a deeper dry layer and a lower, more sharply defined temperature inversion. Both soundings suggest broadscale subsidence. The profiles of in situ O_3 show the major horizontal gradient seen in the DIAL image (Plate 9).

Backward trajectories and in situ chemical measurements help explain the strong horizontal O_3 gradient along flight 16. Parcels arriving along the flight track at 700 hPa (Figure 35a) exhibit a major change in direction that is associated with the SPCZ and the upper level ridge line. Specifically, arrivals along the southern portion of the flight originate from the west, passing over Australia, the Indian Ocean, and near southern Africa. These parcels travel long distances during the 10 day period since they are in the relatively strong westerly flow. At 21°S, in situ O_3 at 3km (~700 hPa) is ~60 ppbv (Figure 34a), with CO being ~100 ppbv (not shown). The enhanced CO and trajectories suggest that biomass burning to the west contributes to the large O_3 in the middle troposphere. The C_2H_2/CO ratio of ~1.1 pptv/ppbv indicates that the air has traveled ~1 week from its emission source. Parcels arriving along the northern part of the flight at 700 hPa

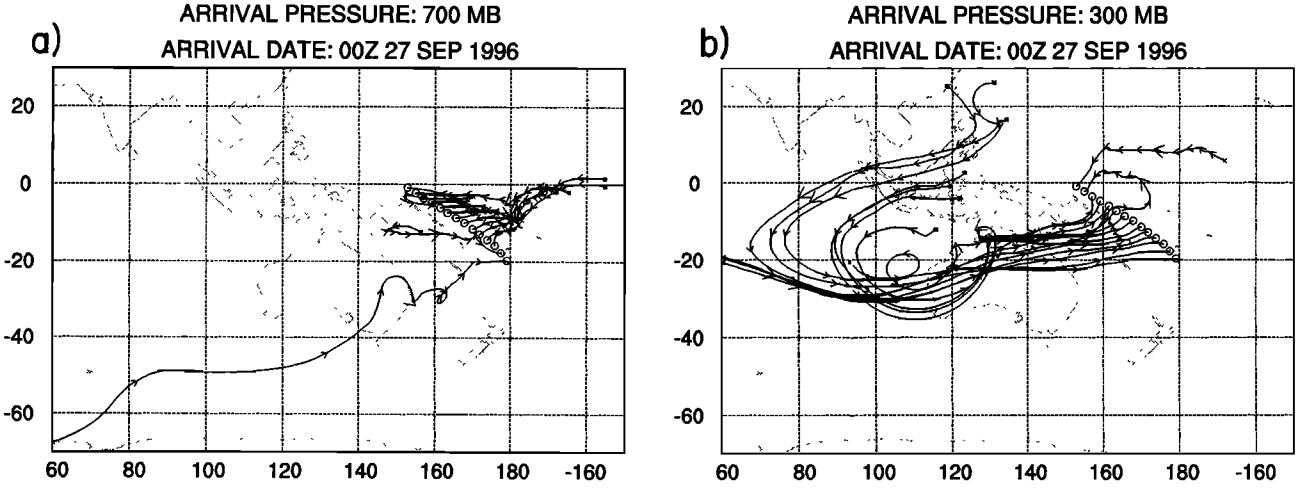

Figure 32. Ten-day backward trajectories arriving along DC-8 flight 15 at (a) 700 hPa and (b) 300 hPa on 0000 UTC September 27. Small (large) arrows denote locations at 1 (5) day intervals.

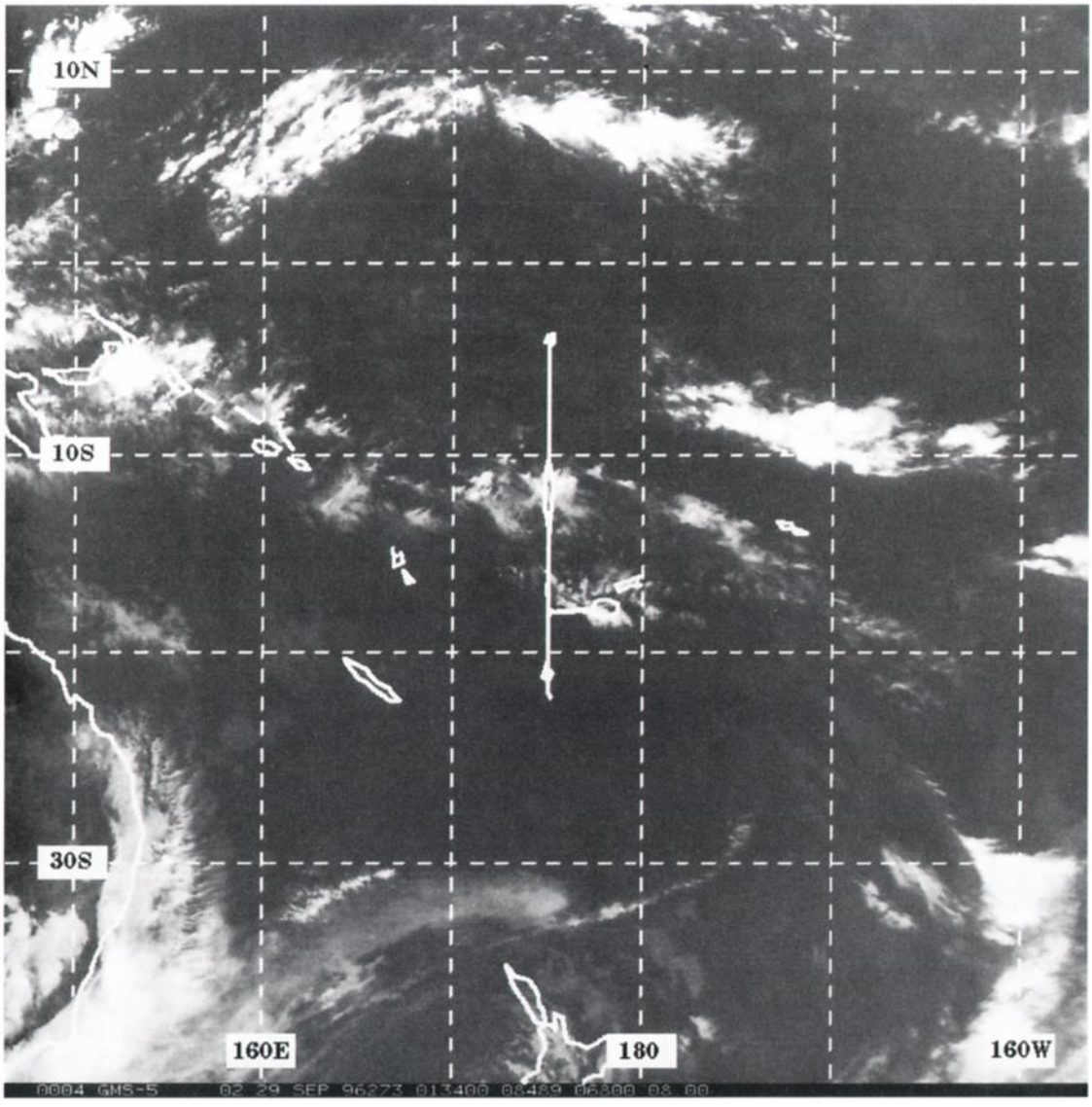

Figure 33. GMS-5 infrared image at 0134 UTC September 29. The track of DC-8 flight 16 out of Fiji (18°S, 177°E) is superimposed.

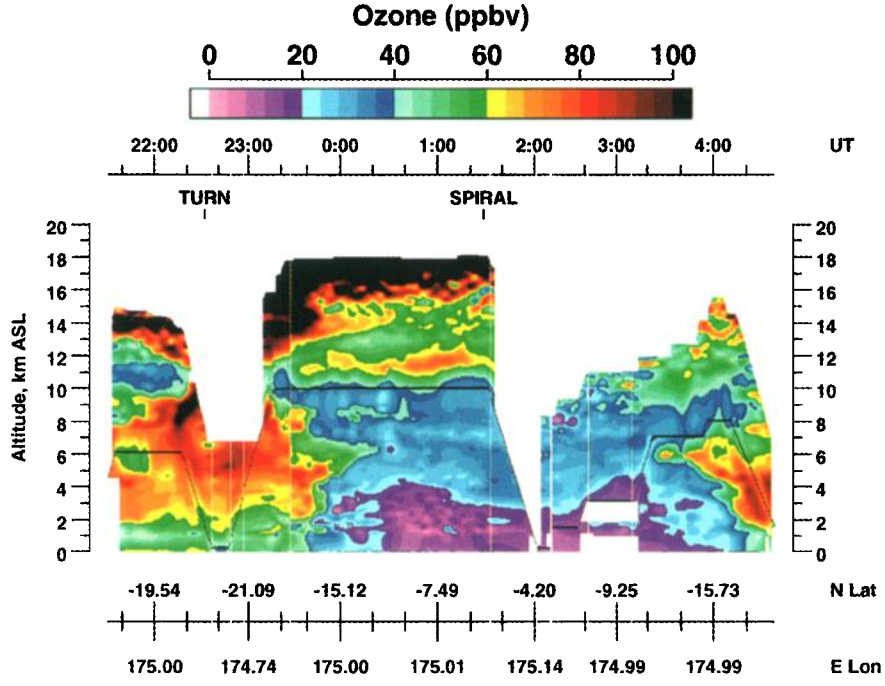

Plate 9. As in Plate 3, but for DC-8 flight 16, southbound then northbound out of Fiji on September 28 (Figure 1).

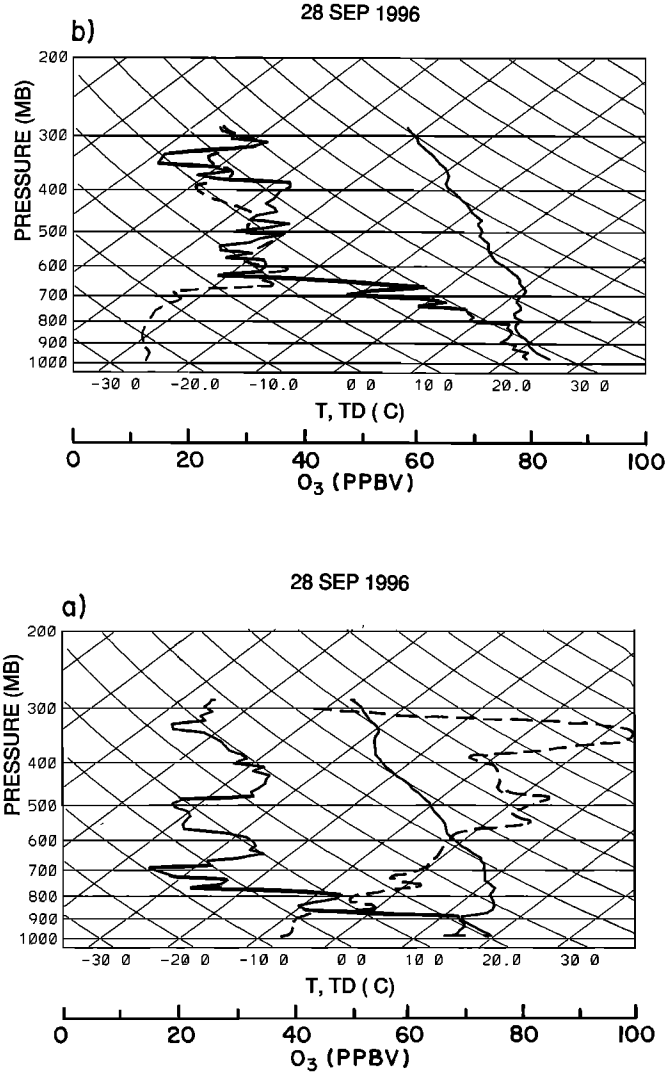

Figure 34. Vertical profiles of temperature and dew point (solid, in degrees Celsius) obtained by the DC-8 on flight 16 (September 28) near (a) 21°S, 175°E and (b) 4°S, 175°E. In situ O_3 (dashed, ppbv) is superimposed.

(Figure 35a) have followed a quite different path. They originate from the east and travel much shorter distances during the same time, spending a long period over the Pacific Ocean. Chemical characteristics at these arrival locations also are quite different from those farther south. At 4°S, in situ O_3 at 3 km (~700 hPa) is only ~20 ppbv (Figure 34b), and CO is reduced to ~55 ppbv (not shown). The ratio C_2H_2/CO is 0.2 pptv/ppbv, indicating a well aged air mass

Concerning arrivals at 300 hPa (Figure 35b), most pass over Australia within ~2 days. The more northern arrivals then continue to southeastern Asia. O_3 at 9 km (~300 hPa) is ~30 ppbv along the northern portion of the flight (Plate 9). Trajectories arriving along the southern portion of the flight track continue to the vicinity of southern Africa. The DIAL image shows that O_3 values at 9 km along the southern segment of the flight leg are much greater than those farther north.

10. Flights Near Guayaquil

The P-3B conducted three local flights out of Guayaquil, Ecuador, to investigate marine upwelling, the sulfur oxidation cycle, and continental outflow from South America. These flights occurred on September 18, 22, and 23 (flights 17–19, Figure 1). Streamline patterns near Guayaquil on the 3 flight days (not shown) are similar to those of the PEM-T mission average (Figure 2). That is, winds offshore of Guayaquil near the surface (~1000 hPa) are from the southeast, having spiraled out of the subtropical anticyclone near 30°S to form the southeast trade winds. Winds at higher altitudes are influenced by the anticyclone/ridge line located between 10° and 15°S, that is, easterly (offshore) at locations north of ~10°S and westerly (onshore) at locations farther south.

Persistent, low-level clouds blanket the Pacific waters west of South America, including the Guayaquil area (Figure 36). These clouds are due to the combined effects of the cold, northward moving ocean current together with subsidence associated with the subtropical anticyclone. To the north of Guayaquil, the clouds become more broken and then more convective in the vicinity of the ITCZ. Large complexes of thunderstorms are seen over interior South America.

Soundings from the P-3B show that the atmosphere's thermodynamic structure varies considerably over the flight area (Figure 37). At the southernmost sounding (12°S, 79°W, Figure 37a), the marine boundary layer is capped by an intense temperature inversion near 900 hPa (~1 km). This inversion greatly inhibits mixing between the boundary layer and higher altitudes. The overlying air is very dry, due to subsidence associated with the anticyclone. Farther north, at 2°S, 80°W (near Guayaquil, Figure 37b), the low-level inversion is weaker, and the

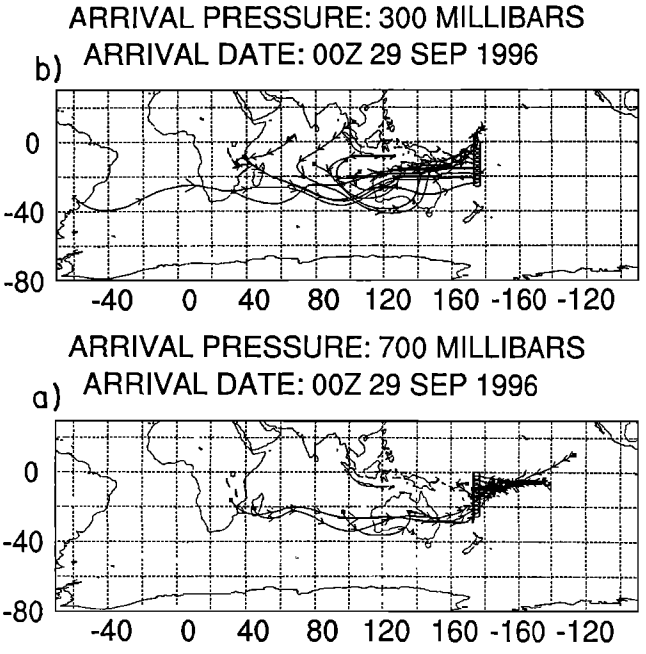

Figure 35. Ten-day backward trajectories arriving along DC-8 flight 16 at (a) 700 hPa and (b) 300 hPa on 0000 UTC September 29. Small (large) arrows denote locations at 1 (5) day intervals.

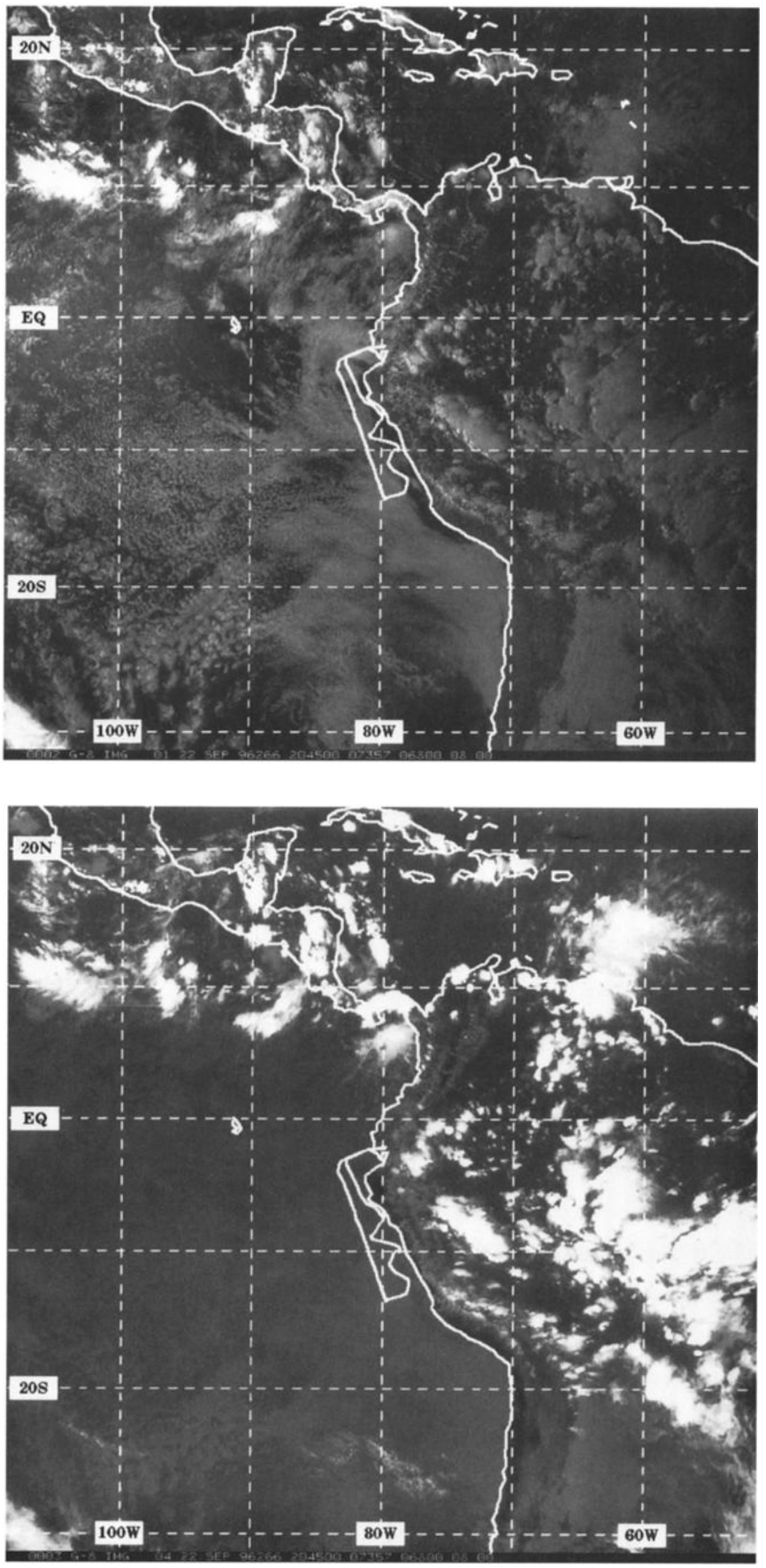

Figure 36. GOES-8 imagery at 2045 UTC September 22: (a) visible and (b) infrared. The track of P-3B flight 18 out of Guayaquil (2°S, 80°W) is superimposed.

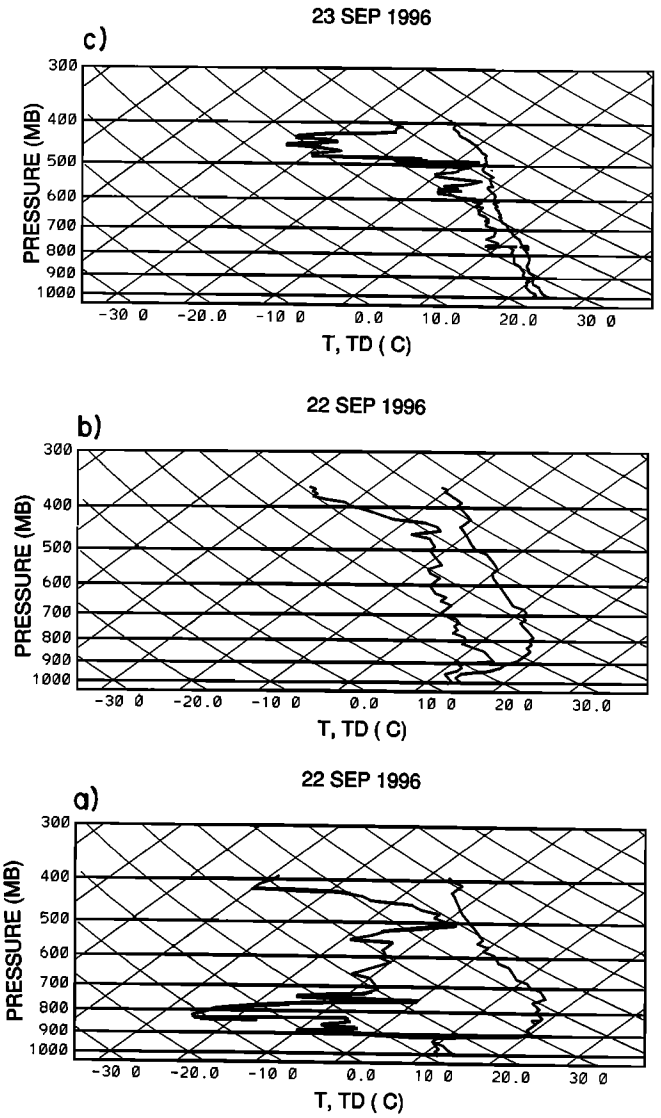

Figure 37. Vertical profiles of temperature and dew point (in degrees Celsius) obtained by the P-3B on flights 18 and 19 (September 22 and 23) near (a) 12°S, 79°W, (b) 2°S, 80°W, and (c) 8°N, 86°W.

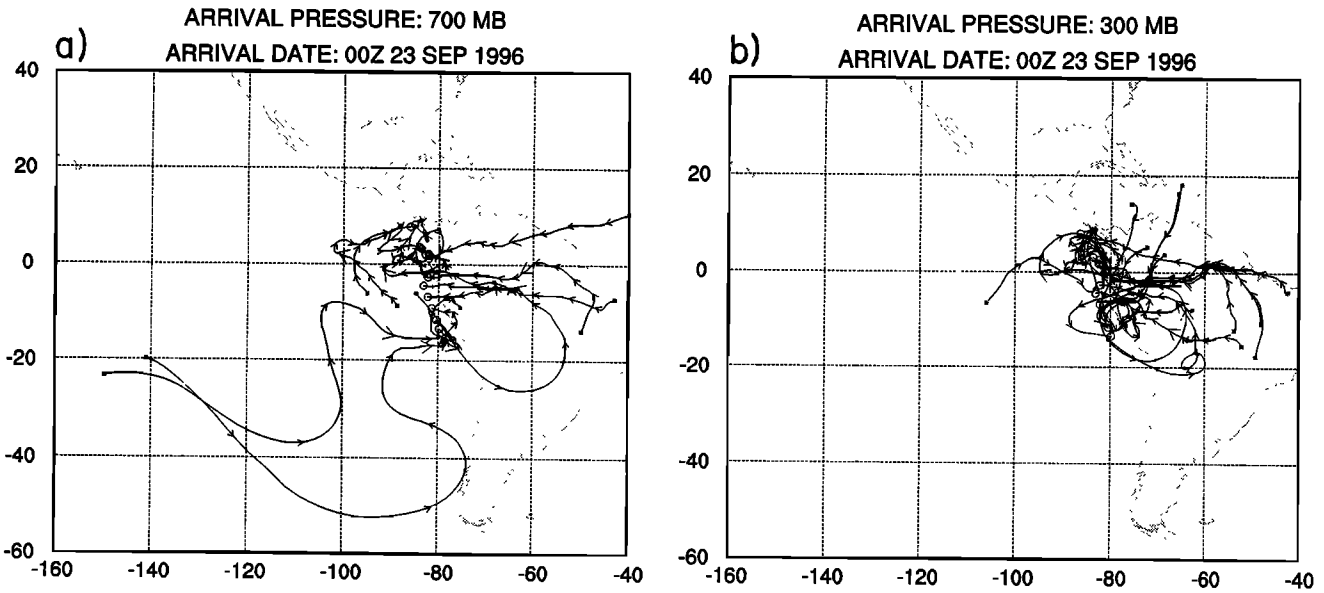

Figure 38. Ten-day backward trajectories arriving along P-3B flights 18 and 19 at (a) 700 hPa and (b) 300 hPa on 0000 UTC September 23. Small (large) arrows denote locations at 1 (5) day intervals.

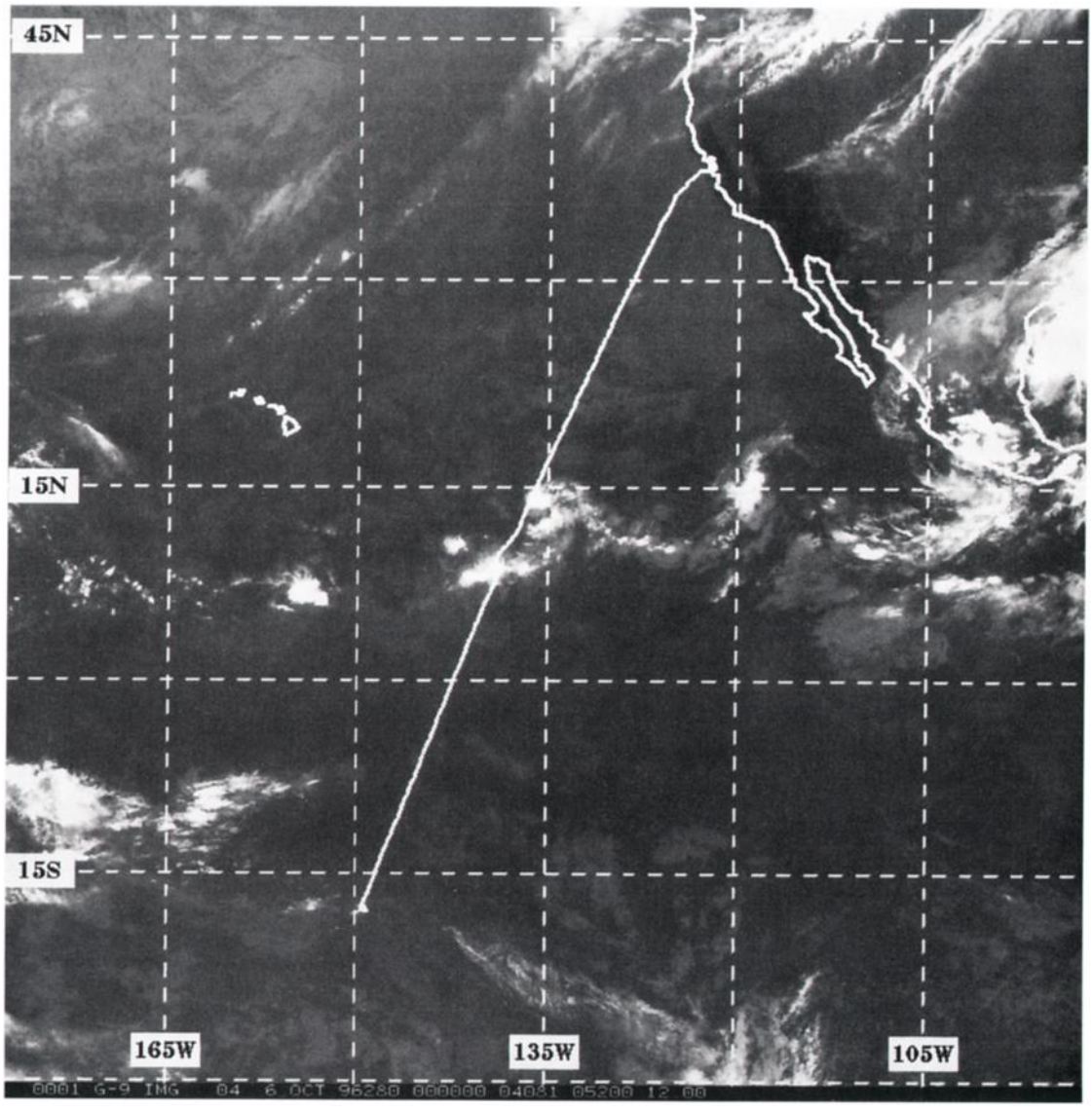

Figure 39. GOES-9 infrared image at 0000 UTC October 6. The track of DC-8 flight 19 from Tahiti (18°S, 150°W) to NASA Ames Research Center, California, is superimposed.

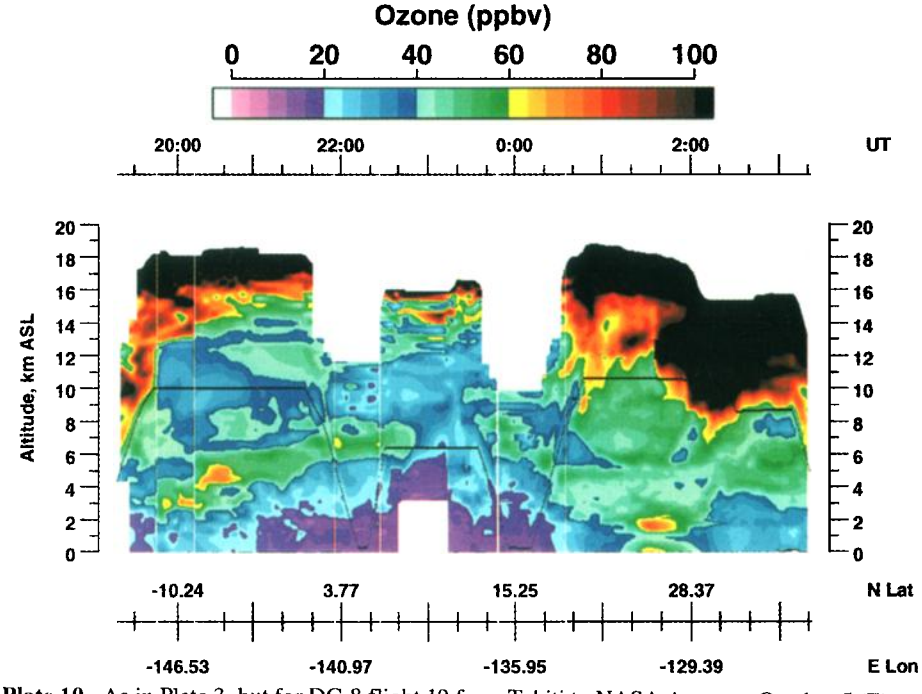

Plate 10. As in Plate 3, but for DC-8 flight 19 from Tahiti to NASA Ames on October 5 (Figure 1).

air above is considerably more humid. Finally, near the ITCZ (8°N, 86°W, Figure 37c), the sounding exhibits no major inversions and is quite moist between the surface and 500 hPa. This sounding is consistent with the convection that appears on the satellite imagery (Figure 36).

Ten-day backward trajectories for the combination of flights 18 and 19 (Figure 1) are shown in Figure 38. The southernmost arrivals at 700 hPa (~3 km, Figure 38a) travel the farthest during the 10 day period, originating over the central South Pacific Ocean. Many arrivals near the equator indicate outflow from South America. However, some trajectories arriving along the northern edge of the flight exhibit short, erratic tracks since they have traveled in a region of light and variable winds. Many trajectories arriving at 300 hPa (Figure 38b) follow counterclockwise paths as they travel around the upper level anticyclone (Figure 2) and pass over portions of South America. Others have short erratic paths near the coastline.

Biomass burning is widespread over portions of South America during September [e.g., *Fishman et al.*, 1996]. The trajectories in Figure 38 indicate that by products of this burning can be transported off the west coast of South America and into the PEM-T region. This occurs in both the lower and upper troposphere. (One should recall that trajectories were terminated if they intersected the Andes.) In the case of upper level flow, the burning by products can be carried upward by deep convection (e.g., Figure 36) and then transported westward by the large scale wind [e.g., *Pickering et al.*, 1996b; *Thompson et al.*, 1996].

11. Homeward Bound

The DC-8 traveled from Tahiti back to NASA Ames Research Center on October 6 (flight 19, Figure 1). The P-3B flew from Guayaquil to New Orleans on September 25 (flight 20, Figure 1) and then back to NASA Wallops Island on the following day. These flights sampled broad ranges of latitude on the eastern side of the PEM-T region.

The ITCZ was the major meteorological feature of interest during these return flights. Located at approximately 10°N, the ITCZ was associated with widespread deep convection (Figure 39). The DIAL O_3 image for the DC-8's flight (Plate 10) indicates that the convectively active ITCZ region is characterized by a relatively deep layer of values <20 ppbv. Values >60 ppbv extend down to ~8 km near 28°N (southwest of California). There appears to be considerably greater tropospheric O_3 north of the ITCZ than to its south.

Ten-day backward trajectories arriving along the DC-8's flight track at 850 hPa (~1.5 km, Figure 40a) clearly show the effects of the northeasterly and southeasterly trade winds that form the ITCZ near 10°N. Only the trajectories arriving at the most northern and southern portions of the flight track have westerly origins. Almost none of the trajectories has passed over land during the 10 day period, consistent with the small values of O_3 that are observed at 1.5 km (Plate 10).

Trajectory patterns at 500 hPa (~5.5 km, Figure 40b) generally are similar to those arriving at 850 hPa. Parcels originate from the east in the tropical regions, but from the west along the northern and southern portions of the flight. An important difference is that these parcels travel much farther during the 10 day period than those arriving at 850 hPa, especially those in the middle latitudes. For example, the two trajectories passing over Australia already have reached 100°E after only 5 days. Furthermore, some trajectories arriving between 20° and 35°N are near the Asian continent at the beginning of the 10 day period.

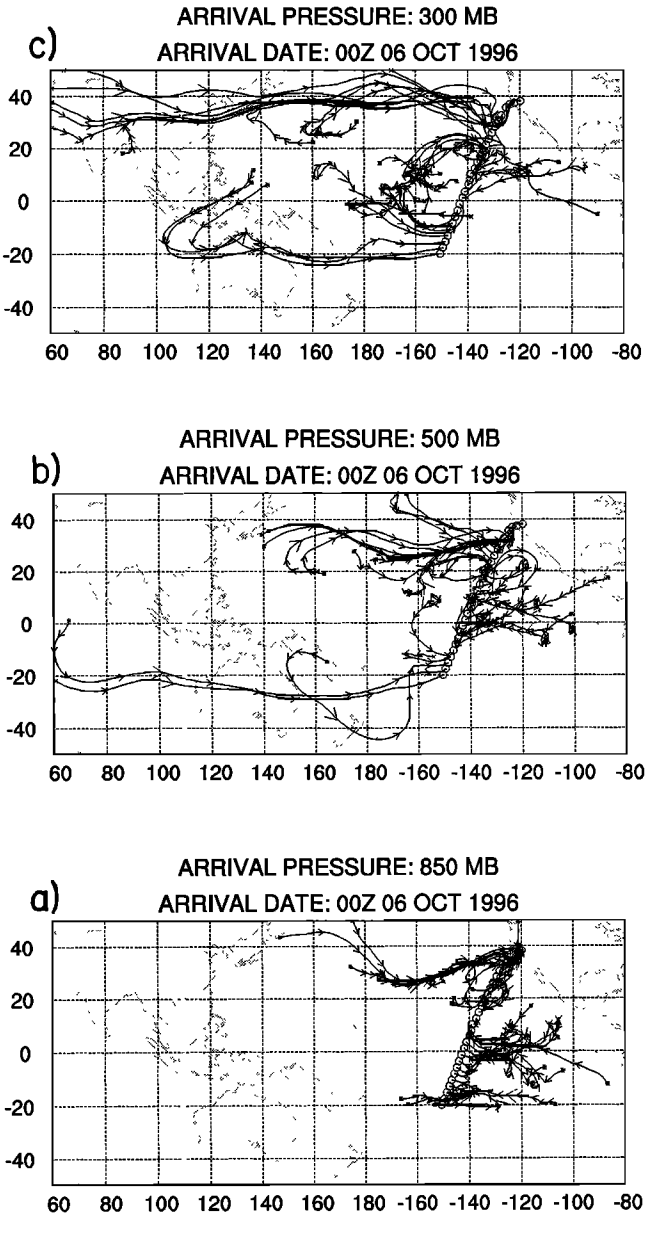

Figure 40. Ten-day backward trajectories arriving along DC-8 flight 19 at (a) 850 hPa, (b) 500 hPa, and (c) 300 hPa on 0000 UTC October 6. Small (large) arrows denote locations at 1 (5) day intervals.

Most trajectories arriving at 300 hPa (~9 km, Figure 40c) originate from the west. Only those arriving in a narrow band near 10°N have an eastern origin. Arrivals north of ~20°N exhibit the longest paths. These parcels have been over Asia within the previous 4–5 days. Although arrivals in this region have Asian origins, the downward extension of large O_3 near 28°N (Plate 10) represents a lowered tropopause. In situ O_3 at ~10 km is as great as 170 ppbv; however, CO values are the smallest of the entire flight, ~45 ppbv.

During the P-3B's flight from Guayaquil to New Orleans (flight 20, Figure 1), the ITCZ and associated convection again were major features (Figure 41). Trajectories arriving along the flight track at 850, 500, and 300 hPa exhibit several common characteristics (Figure 42). Most arrivals south of ~20°N originate from the east, passing over the Caribbean Sea and the north-

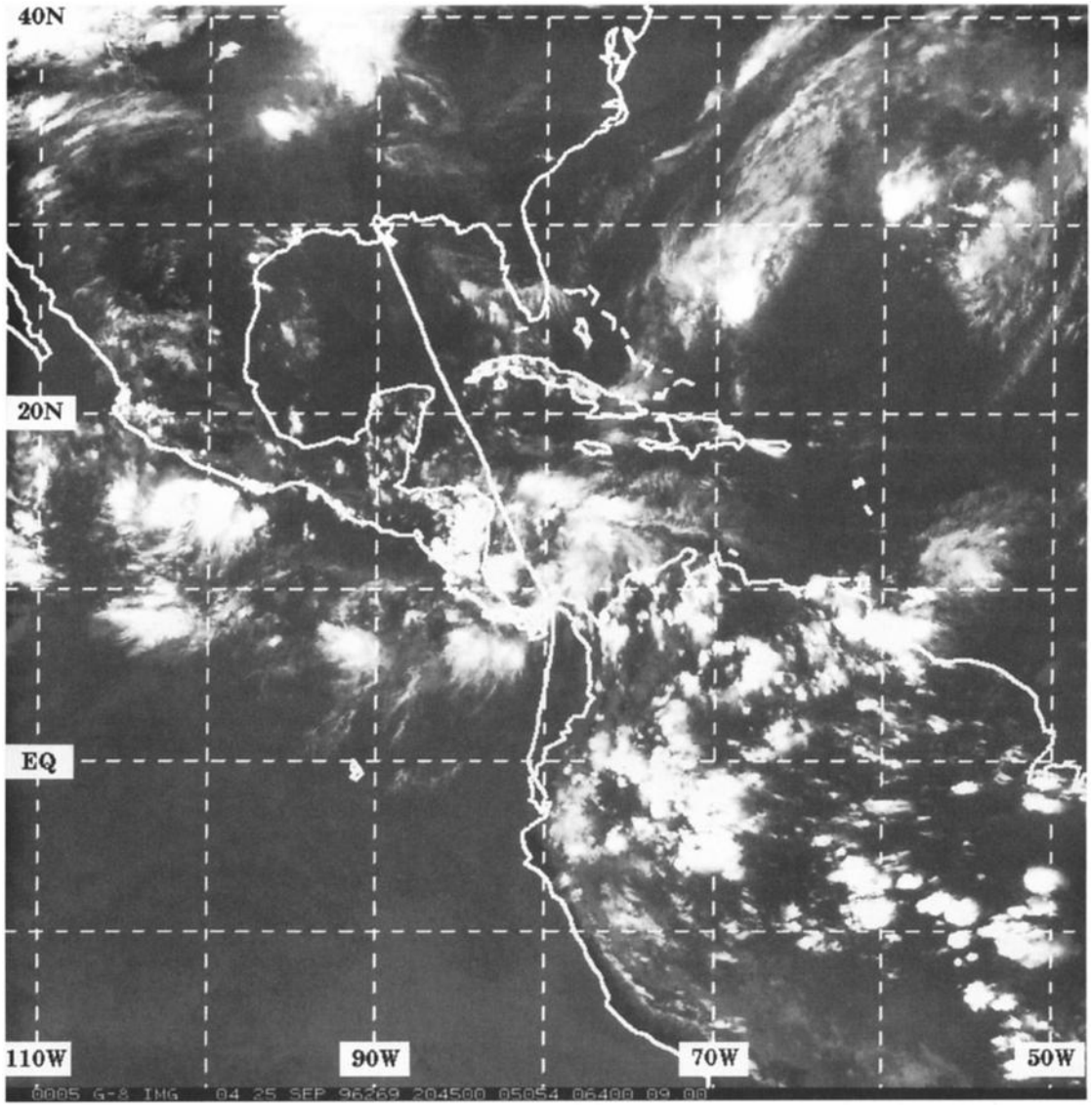

Figure 41. GOES-8 infrared image at 2045 UTC September 25. The track of P-3B flight 20 from Guayaquil (2°S, 80°W) to New Orleans, Louisiana, is superimposed.

ern parts of South America. Some extend beyond the data domain (40°W) before the end of the 10 day period. Farther north, parcels originate over the Pacific Ocean and then pass over the southwestern United States before arriving at the flight track.

12. Summary and Conclusions

NASA's PEM-T experiment investigated the atmospheric chemistry of a large portion of the tropical and subtropical Pacific Basin during August to October 1996. This paper has summarized meteorological conditions over the PEM-T domain. Important circulation systems near the surface included subtropical anticyclones, the South Pacific Convergence Zone, and the Intertropical Convergence Zone. Most of the deep tropical Pacific Basin exhibited easterly flow through the entire troposphere, whereas regions poleward of ~20° had westerly flow. The two convergence zones were areas of widespread ascent and deep convection; however, there was relatively little lightning associated with these storms. A large area of subsidence was associated with the subtropical anticyclone located near Easter Island. PEM-T was a period of near normal sea surface temperatures. When compared to an 11 year climatology, relatively minor circulation anomalies were observed during PEM-T. However, some of these anomalies were consistent with much stronger anomalies observed during previous La Nina events. In general, the 1996 PEM-T period appeared to be climatologically representative.

Meteorological conditions for specific flights from each major operations area were summarized. These included flights out of Hawaii/Christmas Island, Tahiti, Easter Island, Fiji, Guayaquil (Ecuador), and Christchurch (New Zealand). The vertical distribution of O_3 along the selected DC-8 flights was described using the DIAL remote sensing system. These O_3 distributions then were related to thermodynamic soundings obtained during aircraft maneuvers and to backward trajectories that arrived along the flight tracks.

Locations in the deep tropics generally had relatively small values of tropospheric O_3. The trajectories showed that much of this air had originated from the east and had not passed over land within 10 days. The deep convection associated with the ITCZ

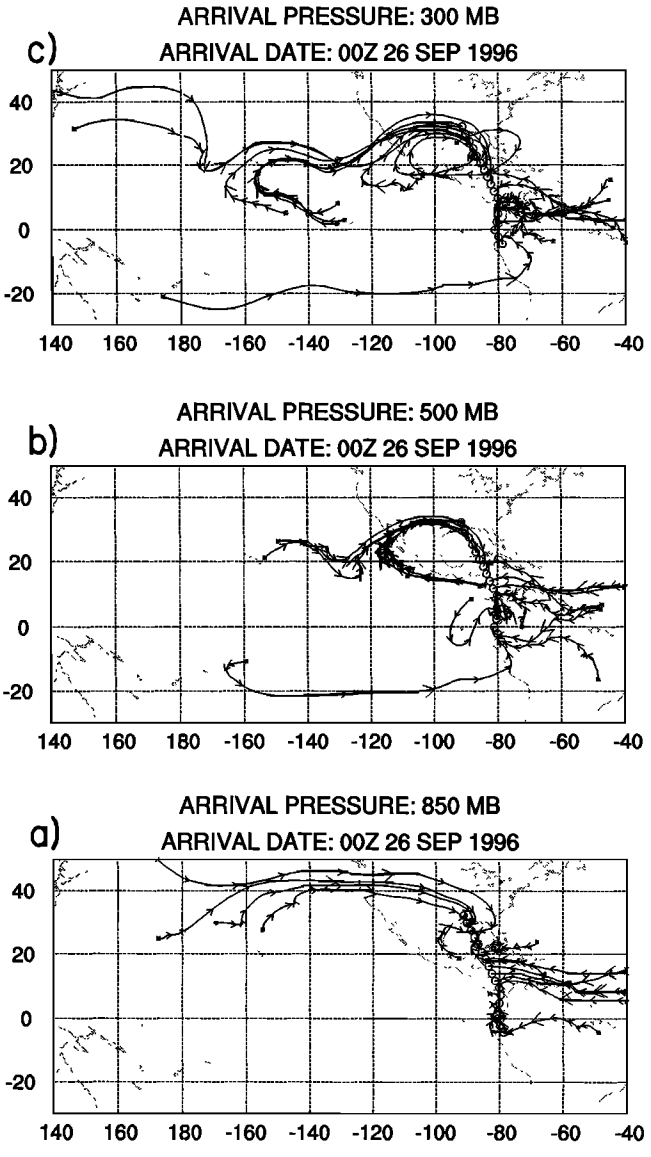

Figure 42. Ten-day backward trajectories arriving along P-3B flight 20 at (a) 850 hPa, (b) 500 hPa, and (c) 300 hPa on 0000 UTC September 26. Small (large) arrows denote locations at 1 (5) day intervals.

and SPCZ also influenced the atmospheric chemistry of these regions.

The situation was quite different over portions of the subtropics and middle latitudes. Many of these flights detected layers of greatly enhanced tropospheric O_3, sometimes exceeding 80 ppbv. These layers had relatively large values of CO, often exceeding 90 ppbv. The layers were located near, and especially south of Tahiti, Easter Island, and Fiji. The enhanced O_3 often corresponded to layers of dry air, indicative of widespread subsiding air. The backward trajectories showed that air parcels arriving in these regions had originated from the west. Many had passed over Australia and some extended to southern Africa near the end of the 10 day period. These are regions of widespread biomass burning during the months of PEM-T. Thus the enhanced values of O_3 in the central Pacific Basin may be due to this biomass burning many thousands of kilometers away. The importance of biomass burning during PEM-T is discussed in several papers of this issue [e.g., *Schultz et al., this issue; Talbot et al., this issue; Vay et al., this issue*].

The DC-8 lidar detected large values of O_3 in the equatorial upper troposphere on September 3 when the aircraft was vectored into a region of high potential vorticity at ~12 km altitude. One possible interpretation is that the high O_3 originated locally from the equatorial stratosphere. A detailed case study of these measurements is planned.

The middle latitudes also were influenced by middle-latitude transient cyclones. The DC-8 traversed tropopause folds during several flights. Finally, the flight area just west of Ecuador experienced outflow from South America. Thus the biomass burning that is prevalent over portions of Brazil influenced this area.

Acknowledgments. The PEM-T meteorological team expresses its deep appreciation to the staffs of the meteorological services at the locations from which PEM-T operated. These individuals provided valuable insight into local weather conditions. The services include the U.S. Air Weather Service at Hickham Field, Hawaii, Meteo France at Tahiti, Direccion Meteorologica de Chile at Easter Island, the Meteorological Service of New Zealand at Christchurch, and the Fiji Meteorological Service. Meteo France, through its regional office in French Polynesia and data distribution center in Toulouse, kindly provided ECMWF gridded data during the field phase. Patrick Simon and Isabelle Lulu in Tahiti were especially helpful in securing these data for us. Sonya Kulkarni at the Florida State University Center for Oceanic and Atmospheric Prediction provided sea surface data. The Global Hydrology and Climate Center at NASA Marshall Space Center provided the OTD lightning data through its web site. Rick Lusher, Ashley Board, and Jeff Cupo at Florida State assisted in the preparation of this manuscript. We gratefully acknowledge the efforts of the entire DIAL team in the acquisition and processing of the ozone data discussed in this manuscript. In particular, we recognize Bill Grant, Carolyn Butler, and Susan Kooi for their leadership in directing the DIAL data acquisition during the PEM-T field experiment, and Marta Fenn and Marian Clayton for their postmission DIAL ozone data processing. This research was sponsored by the NASA Tropospheric Chemistry Program. We appreciate the support of Joe McNeal, Jim Hoell, and Richard Bendura in helping with the many scientific, logistical, and managerial matters. Similarly, the crews and support staff of the DC-8 and P3-B aircraft always were most helpful during the preparations and deployments of PEM-T. We thank Mike Cadena and Fred Reisinger of the GTE Project Office for their assistance during all phases of the project.

References

Arkin, P.A., The relationship between interannual variability in the 200 mb tropical wind field and the southern oscillation, *Mon. Weather Rev., 110*, 1393–1404, 1982.

Bengtsson, L., Medium-range forecasting—The experience of ECMWF, *Bull. Am. Meteorol. Soc., 66*, 1133–1146, 1985.

Blake, D.R., T.-Y. Chen, T.W. Smith Jr., C.J.-L. Wang, O.W. Wingenter, N.J. Blake, F.S. Rowland, and E.W. Mayer, Three-dimensional distribution of NMHCs and halocarbons over the northwestern Pacific during the 1991 Pacific Exploratory Mission (PEM-West), *J. Geophys. Res., 101*, 1763–1778, 1996.

Browell, E.V., Differential absorption lidar sensing of ozone, *Proc. IEEE, 77*, 419–432, 1989.

Browell, E.V., Ozone and aerosol measurements with an airborne lidar system, *Opt. Photonics News, 2*, No. 10, 8–11, 1991.

Browell, E.V., E. Danielsen, S. Ismail, G. Gregory, and S. Beck, Tropopause fold structure determined from airborne lidar and in situ measurements, *J. Geophys. Res., 92*, 2112–2120, 1987.

Browell, E.V., M.A. Fenn, C.F. Butler, W.B. Grant, R.C. Harriss, and M.C. Shipham, Ozone and aerosol distributions in the summertime troposphere over Canada, *J. Geophys. Res., 99*, 1739–1755, 1994.

Browell, E.V., et al., Ozone and aerosol distributions and air mass characteristics over the South Atlantic Basin during the burning season, *J. Geophys. Res., 101*, 24043–24068, 1996.

Carlson, T.N., *Mid-Latitude Weather Systems*, 507 pp., HarperCollins, New York, 1991.

Chen, B., S.R. Smith, and D.H. Bromwich, Evolution of the tropospheric split jet over the South Pacific Ocean during the 1986–1989 ENSO cycle, *Mon. Weather Rev., 124*, 1711–1731, 1996.

Christian, H.J., R.J. Blakeslee, and S.J. Goodman, The detection of lightning from geostationary orbit, *J. Geophys. Res., 94*, 12329–13337, 1989.

Christian, H.J., R.J. Blakeslee, and S.J. Goodman, Lightning imaging sensor (LIS) for the Earth observing system, *NASA Tech. Memo. 4350*, 1992.

Crawford, J., D. Davis, G. Chen, R. Shetter, M. Muller, J. Barrick, and J. Olson, An assessment of cloud effects on photolysis rates coefficients: Comparison of experimental and theoretical values, *J. Geophys. Res.*, this issue.

Davis, D., et al., DMS oxidation in the equatorial Pacific: Comparison of model simulations with field observations for DMS, SO_2, H_2SO_4(g), MSA(g), MS, and NSS, *J. Geophys. Res.*, this issue.

Elvidge, C.D., and K.E. Baugh, Survey of fires in Southeast Asia and India during 1987, in *Biomass Burning and Global Change*, edited by J.S. Levine, pp. 663–670, MIT Press, Cambridge, Mass., 1996.

Fishman, J., J.M. Hoell Jr., R.D. Bendura, R.J. McNeal, and V.W.J.H. Kirchhoff, NASA GTE TRACE A Experiment (September-October 1992): Overview, *J. Geophys. Res., 101*, 23865–23879, 1996.

Fuelberg, H.E., R.O. Loring Jr., M.V. Watson, M.C. Sinha, K.E. Pickering, A.M. Thompson, G.W. Sachse, D.R. Blake, and M.R. Schoeberl, TRACE-A trajectory intercomparison, 2, Isentropic and kinematic methods, *J. Geophys. Res., 101*, 23927–23939, 1996a.

Fuelberg, H.E., J.D. VanAusdall, E.V. Browell, and S.P. Longmore, Meteorological conditions associated with vertical distributions of aerosols off the west coast of Africa, *J. Geophys. Res., 101*, 24105–24115, 1996b.

Garstang, M., P.D. Tyson, R. Swap, M. Edward, P. Kallberg, and J.A Lindesay, Horizontal and vertical transport of air over southern Africa, *J. Geophys. Res., 101*, 23721–23736, 1996.

Greenberg, J.P., and P.R. Zimmerman, Nonmethane hydrocarbons in remote tropical, continental, and maritime atmospheres, *J. Geophys. Res., 89*, 4767–4778, 1984.

Greenberg, J.P., P.R. Zimmerman, and P. Haagenson, Tropospheric hydrocarbons and CO profiles over the U.S. West Coast and Alaska, *J. Geophys. Res., 95*, 14015–14026, 1990.

Gregory, G.L., et al., Chemical characteristics of Pacific tropospheric air in the region of the ITCZ and SPCZ, *J. Geophys. Res.*, this issue.

Hao, W.M., and M.-H. Liu, Spatial and temporal distribution of tropical biomass burning, *Global Biogeochem. Cycles, 8*, 495–503, 1994.

Hoell, J.M., et al., Pacific Exploratory Mission in the tropical Pacific: PEM-Tropics A, August–September 1996, *J. Geophys. Res.*, this issue.

Hollingsworth, A., D.B. Shaw, P. Lonnberg, L. Illari, K. Arpe, and A.J. Simmons, Monitoring of observations and analysis quality by a data assimilation system, *Mon. Weather Rev., 114*, 861–879, 1986.

Horel, J.D., and J.M. Wallace, Planetary-scale atmospheric phenomena associated with the Southern Oscillation, *Mon. Weather Rev., 109*, 813–829, 1981.

Hurst, D.F., D.W.T. Griffith, and G.D. Cook, Trace-gas emissions from biomass burning in Australia, in *Biomass Burning and Global Change*, edited by J.S. Levine, pp. 787–792, MIT Press, Cambridge, Mass., 1996.

Justice, C.O., J.D. Kendall, P.R. Dowty, and R.J. Scholes, Satellite remote sensing of fires during the SAFARI campaign using NOAA advanced very high resolution radiometer data, *J. Geophys. Res., 101*, 23851–23863, 1996.

Kahl, J.D., A cautionary note on the use of air trajectories in interpreting atmospheric chemistry measurements, *Atmos. Environ., Part A, 27*, 3037–3038, 1993.

Lawrence, M.G., W.L. Chameides, P.S. Kasibhatla, H. Levy II, and W. Moxim, Lightning and atmospheric chemistry: The rate of atmospheric NO production, in *Handbook of Atmospheric Electrodynamics*, edited by H. Volland, pp. 189–202, CRC Press, Boca Raton, Florida, 1995.

Lelieveld, J., and P.J. Crutzen, Role of deep convection in the ozone budget of the troposphere, *Science, 264*, 1759–1761, 1994.

Loring, R.O., Jr., H.E. Fuelberg, J. Fishman, M.V. Watson, and E.V. Browell, Influence of a middle-latitude cyclone on tropospheric ozone distributions during a period of TRACE A, *J. Geophys. Res., 101*, 23941–23956, 1996.

McNeal, R.J., J.P. Mugler Jr., R.C. Harriss, and J.M. Hoell Jr., NASA Global Tropospheric Experiment, *Eos Trans. AGU, 64*, 561–562, 1984.

Merrill, J.T., Atmospheric long-range transport to the Pacific Ocean, in *Chemical Oceanography*, vol. 10, pp. 15–50, Academic, San Diego, Calif., 1989.

Merrill, J.T., R. Bleck, and L. Avila, Modeling atmospheric transport to the Marshall Islands, *J. Geophys. Res., 90*, 12927–12936, 1985.

Newell, R.E., Y. Zhu, E.V. Browell, W.G. Read, and J.W. Waters, Walker circulation and tropical upper tropospheric water vapor, *J. Geophys. Res., 101*, 1961–1974, 1996a.

Newell, R.E., W. Hu, Z.X. Wu, Y. Zhu, H. Akimoto, B.E. Andersen, E.V. Browell, G.L. Gregory, G.W. Sachse, and M.C. Shipham, Atmospheric sampling of supertyphoon Mireille with NASA DC-8 aircraft on September 27, 1991, during PEM-West A, *J. Geophys. Res., 101*, 1853–1871, 1996b.

Orville, R.E., E.J. Zipser, M. Brook, C. Weidman, G. Aulich, E.P. Krider, H. Christian, S. Goodman, R. Bakeslee, and K. Cummins, Lightning in the region of the TOGA COARE, *Bull. Am. Meteorol. Soc., 78*, 1055–1067, 1997.

Philander, S.G., *El Nino, La Nina, and the Southern Oscillation*, 293 pp., Academic, San Diego, Calif., 1990.

Philander, S.G., and E.M. Rasmusson, The Southern Oscillation and El Nino, in *Advances in Geophysics*. vol. 28, pp. 197–215, Academic, San Diego, Calif., 1985.

Pickering, K.E., A.M. Thompson, D.P. McNamara, M.R. Schoeberl, H.E. Fuelberg, R.O. Loring Jr., M.V. Watson, K. Fakhruzzaman, and A.S. Bachmeier, TRACE A trajectory intercomparison, 1, Effects of different input analyses, *J. Geophys. Res., 101*, 23909–23925, 1996a.

Pickering, K.E., et al., Convective transport of biomass burning emissions over Brazil during TRACE A, *J. Geophys. Res., 101*, 23993–24012, 1996b.

Rood, R.B., A.R. Douglass, M.C. Cerniglia, and W.G. Read, Synoptic-scale mass exchange from the troposphere to the stratosphere, *J. Geophys. Res., 102*, 23467–23485, 1997.

Sachse, G.W., G.F. Hill, L.O. Wade, and M.G. Perry, Fast-response, high-precision carbon monoxide sensor using a tunable diode laser absorption technique, *J. Geophys. Res., 92*, 2071–2081, 1987.

Sachse, G.W., J.E. Collins Jr., G.F. Hill, L.O. Wade, L.G. Burney, and J.A. Ritter, Airborne tunable diode laser sensor for high precision concentration and flux measurements of carbon monoxide and methane, *Proc. SPIE, Int. Soc. Opt. Eng.*, 1433, 145–156, 1991.

Schultz, M., et al., On the origin of tropospheric ozone and NO_x over the tropical South Pacific, *J. Geophys. Res.*, this issue.

Sinclair, M.R., An objective cyclone climatology for the southern hemisphere, *Mon. Weather Rev., 122*, 1139–2256, 1994.

Singh, H.B., and P. Zimmerman, Atmospheric distributions and sources of nonmethane hydrocarbons, *Adv. Environ. Sci. Technol., 24*, 177–235, 1992.

Stohl, A., G. Wotawa, P. Seibert, and H. Kromp-Kolb, Interpolation errors in wind fields as a function of spatial and temporal resolution and their impact on different types of kinematic trajectories. *J. Appl. Meteorol., 34*, 2149–2165, 1995.

Suhre, K., J.-P. Cammas, P. Nedelec, R. Rosset, A. Marenco, and H.G.J. Smit, Ozone-rich transients in the upper equatorial Atlantic troposphere, *Nature, 388*, 661–663, 1997.

Swap, R., M. Garstang, S.A. Macko, P.D. Tyson, W. Maenhaut, P. Artaxo, P. Kallberg, and R. Talbot, The long-range transport of southern African aerosols to the tropical South Atlantic, *J. Geophys. Res., 101*, 23777–23791, 1996.

Talbot, R.W., J.E. Dibb, E.M. Scheuer, D. R. Blake, N.J. Blake, G.L. Gregory, G.W. Sachse, J.D. Bradsahw, S.T. Sandholm, and H.B. Singh, Influence of biomass combustion emissions on the distribution of acidic trace gases over the southern Pacific Basin during austral springtime, *J. Geophys. Res.*, this issue.

Thompson, A.M., K.E. Pickering, D.P. McNamara, M.R. Schoeberl, R.D. Hudson, J.H. Kim, E.V. Browell, V.W.J.H. Kirchhoff, and D. Nganga, Where did tropospheric ozone over southern Africa and tropical Atlantic come from in October 1992? Insights from TOMS, GTE TRACE A, and SAFARI 1992, *J. Geophys. Res., 101*, 24251–24278, 1996.

Trenberth, K.E., Spatial and temporal variations of the Southern Oscillation. *J. Meteorol. Soc., 102*, 639–653, 1976.

Trenberth, K.E., Short-term climate variations: Recent accomplishments and issues for future progress, *Bull. Am. Meteorol. Soc., 78*, 1081–1096, 1997.

Tyson, P.D., M. Garstang, R. Swap, P. Kallberg, and M. Edwards, An air transport climatology for subtropical southern Africa, *Int. J. Climatol., 16*, 265–291, 1996.

Vay, S.A., B.E. Anderson, T.J. Conway, G.W. Sachse, J.E. Collins Jr., D.R. Blake, and D.J. Westberg, Airborne observations of the tropospheric CO_2 distribution and its controlling factors over the South Pacific Basin, *J. Geophys. Res.*, this issue.

Vincent, D.G., The South Pacific convergence zone: A review, *Mon. Weather Rev., 122*, 1949–1970, 1994.

D.R. Blake, Department of Chemistry, University of California, Irvine, CA 92717.

E.V. Browell, G.L. Gregory, and G.W. Sachse, NASA Langley Research Center, Hampton, VA 23681.

H.E. Fuelberg and S.P. Longmore, Department of Meteorology, Florida State University, Tallahassee, FL 32306-4520. (e-mail: fuelberg@met.fsu.edu)

R.E. Newell and Y. Zhu, Department of Earth, Atmospheric, and Planetary Sciences, Massachusets Institute of Technology, Cambridge, MA 02139.

D.J. Westberg, Science Applications International Corp., NASA Langley Research Center, MS 483, Hampton, VA 23681.

(Received October 7, 1997; revised March 6, 1998; accepted April 7, 1998.)